Essays on Directional-Change Intrinsic Time

Dissertation
submitted to the
Faculty of Business, Economics and Informatics
of the University of Zurich

to obtain the degree of
Doktor der Wirtschaftswissenschaften, Dr. oec.
(corresponds to Doctor of Philosophy, PhD)

presented by

Vladimir Petrov
from Russia

approved in August 2019 at the request of
Prof. Dr. S. Battiston
Prof. Dr. C. J. Tessone

The Faculty of Business, Economics and Informatics of the University of Zurich hereby authorizes the printing of this dissertation, without indicating an opinion of the views expressed in the work.

Zurich, 7.08.2019

Chairman of the Doctoral Board: Prof. Dr. Steven Ongena

Acknowledgements

Doing a PhD research is similar to leaving in a marvel fairytale. The main character departs to the great journey far away from his safe home. He is in search of great feats and rewards. Like the character from the fairytales, a PhD researcher does not know what he will encounter on the way of the journey. Numerous difficulties will test his immature skills and temper his character. The fairytale protagonist should never give up on solving the most challenging and unfamiliar problems, for embracing them, he transforms from a layperson to the wise master. He cultivates the skills and intelligence over the entire way by wading through thorn bushes of predicaments and escaping tricky traps routinely lied on his challenging way.

Not only the desire of the bright future brings the character through challenges. The regular support of accidental acquaintances eases his journey. The supporters always appear in the most hopeless situations, supply with wise advice, explain how to solve the most intricate issues, and provide warm shelter in the darkest nights of the journey. The protagonist would hardly finish his adventure without the assistance of the numerous patrons.

My protagonist has just finished the next chapter of his inspiring story. In contrast to fairytales, all his supporters were genuine. It is difficult to thank each encounter who assisted him. The following is just a short list of the most influential individuals whose grandiose help is indisputable.

First and foremost, a great thank you to my supervisor Prof. Stefano Battiston for the constant eye-keeping on all turns my protagonist made at every fork of the road. Thank you for generously shared academic experience cultivated through many years of victorious working in the research world. That experience will be brought much further than to the end of the just-completed chapter. It will pop up in mind throughout the entire life.

Big thank you to Richard Olsen and Anton Golub, the people whom I have been proudly calling "my mentors from industry". These kind people did not only walk with me throughout the entire challenging adventure. They have always been exceptional examples of marble nobility, wisdom, and persistence. I sincerely wish that I can also be considered as an occasional encounter on their own protagonists' journeys.

I am happy to express my highest gratitude to the great friend, philosopher, and writer James Glattfelder. Many hours were spent by admiring his talented writing skills while walking through the bible of knowledge embodied as his book on information, consciousness, and reality. The depth of knowledge discovered in every sentence of the book helped my protagonist to learn how to admire the surrounding world as the most magnificent wonder.

There were no people closer to me within the adventure than my colleagues, especially Chiara Perillo, Olga Briukhova, and Alan Roncoroni. Their diverse range of expertise and the wonderful sense of humour made the work on the complicated scientific problems simple and entertaining. There are no doubts that would they choose any summit they would conquer it at the click of the fingers.

The latest in the acknowledgement but the closest to the heart: my precious family. Family is the only supported who did not only illuminate the darkest deeps and provided the shade in the hottest days of the adventure. The family has been preparing the protagonist to the adventure since his very birth. It followed his every step and shared all his diverse range of emotions. To the family, I dedicate this thesis.

Contents

1 INTRODUCTION AND SUMMARY OF RESEARCH RESULTS 1

2 AGENT-BASED MODELLING IN DIRECTIONAL-CHANGE INTRINSIC TIME 13

2.1 Introduction . . . 14
2.2 Intrinsic Time . . . 17
2.3 Structure of the Model . . . 22
2.4 Benchmarks . . . 28
2.4.1 Traditional Benchmarks . . . 30
2.4.2 The Ultimate Benchmark . . . 32
2.5 Results . . . 33
2.5.1 The Entire Grid . . . 33
2.5.2 Asymmetric Regions . . . 39
2.6 Conclusion . . . 41
2.A Overshoot as the Function of Trend . . . 43
2.B Dissection Algorithm . . . 45
2.C Additional Experiments . . . 47

3 INSTANTANEOUS VOLATILITY SEASONALITY 53

3.1 Introduction . . . 54
3.2 Drawdowns and Drawups: An Introduction . . . 56
3.3 Directional-Change Intrinsic Time . . . 57
3.4 Seasonality . . . 59
3.4.1 Traditional Markets . . . 59
3.4.2 Bitcoin Seasonality . . . 61
3.5 Data . . . 63
3.6 Methods . . . 65
3.6.1 Waiting Time . . . 65
3.6.2 Number of Directional Changes . . . 67
3.6.3 Instantaneous Volatility . . . 70

3.7 Results . . . 71
3.7.1 Number of Directional Changes . . . 71
3.7.2 Realised Versus Instantaneous Volatility . . . 72
3.7.3 Discrete Price Effect . . . 77
3.7.4 Volatility Seasonality . . . 79
3.7.5 Volatility Autocorrelation and Theta Time . . . 85
3.8 Concluding Remarks . . . 89
3.A Daily Seasonality . . . 91

4 DIRECTIONAL-CHANGE METHODOLOGY IN HIGHER DIMENSIONS 95
4.1 Introduction . . . 96
4.2 One-dimensional Directional-Change Intrinsic Time . . . 99
4.3 Theoretical Background . . . 100
4.4 Multidimensional Directional-Change Intrinsic time . . . 102
4.4.1 Dissection Example . . . 105
4.4.2 Algorithm Coherence . . . 107
4.5 Extension of 1D Approaches . . . 109
4.5.1 2D Space . . . 110
4.5.2 3D and Higher Dimensions . . . 114
4.6 Experiments . . . 115
4.6.1 Expansion Validation Criteria . . . 115
4.6.2 Correlation Coefficient Impact . . . 116
4.7 Multidimensional FX Market . . . 119
4.7.1 Ticks in Multidimensional Space . . . 119
4.7.2 2D FX EUR Exchange Rates . . . 120
4.7.3 5D FX EUR exchange rates . . . 128
4.7.4 23D FX . . . 129
4.8 Concluding Remarks . . . 132
4.A 3D Price Move . . . 135
4.B 1D EUR Scaling Laws . . . 136
4.C Expected Waiting Time . . . 137
4.D Evolution of Directional Vector as Markov Chain . . . 139
4.E Pseudocode of Multidimensional Dissection Algorithm . . . 144
4.F Correlation coefficients of EUR exchange rates . . . 147

BIBLIOGRAPHY 149

1

Introduction and Summary of Research Results

On the History of Time in Science, Philosophy, and Economics

Time is a dimension that comes into use in all scientific and philosophical domains. In economic literature, the nature of time has not been the main focus of research, even though the question of how to define and specify time explicitly or implicitly is an issue in many areas of economics. The areas span from theoretical and applied macroeconomics to microeconomics. Economists and philosophers have made statements about the nature of time:

In the late nineteenth century, Alfred Marshall, wrote in the first edition of *Principles* (Marshall 1961):

> "The element of Time ... is the center of the chief difficulty of almost every economic problem."

In Karl Marx's *Capital* (Marx 1875) economic models are mathematically described by the variable "time", indicating that all parameters in the theories are expressed as a function of time. Nicholas Georgescu-Roegen considered time in economics as a plurichromatic concept (Georgescu-Roegen 1993), meaning that:

> "time ... enters in economics in multiple ways, both in production and in life enjoyment."

The Nobel Laureate Peter A. Diamond considered periods of different durations while focusing on modalities of micro- and macroeconomic equilibria (Diamond and Hausman 1994). Behavioural economists analysed concepts of financial agents' time preference and time discounting (Frederick, Loewenstein, and O'donoghue 2002; Andreoni and Sprenger 2012a, 2012b). Researchers found that time preferences are subject to variability according to socio-economic status, culture, and levels of development.

When Benjamin Franklin stated that "time is money" (and neither should be wasted) (Franklin 1750) he laid the ground for time as a value per se. Time as a form of currency appeared in political economy with David Ricardo's theory of relative prices based on embodied labour hours (Ricardo 1817). Today, real economical values can be inferred through computer-based

high-frequency trading where time is converted into the value (Easley, De Prado, and O'Hara 2012; Jarrow and Protter 2012; Golub, Glattfelder, and Olsen 2017; Bakhach et al. 2018).

The specific nature of time has always been a subject of continuing debates among economists. François Quesnay's *Tableau économique* (Quesnay 1894) introduced cyclical representation of calendar time. Theories of cyclical movements were later employed to represent developments based on recurrent economic booms and recession (Morgan et al. 1990; Klein and Klein 1997). Shackle (1967), Robinson (1980), and Georgescu-Roegen (1993) criticised neoclassical models of development and macroeconomic dynamics for disobeying historical time and only operating in logical time[1]. George Shackle criticised economists for not specifying the underlying notion of "time" which they were using in their studies. Neoclassical economists addressed time as just one more "space dimension". However, despite the criticism, neoclassical economics is not absolutely "timeless" (Boland 1978):

> "A model is not timeless if any of its parts is not a tautology."

In the majority of the works on economic philosophy, the concept of causality defines the flow of time (over a period spanning at least from Gossen (1854) to Cassel, McCabe, et al. (1923) and Hicks (1946)). Menger (1871):

> "The idea of causality, however, is inseparable from the idea of time. A process of change involves a beginning and a becoming, and these are only conceivable as processes in time. Hence it is certain that we can never fully understand the causal interconnections of the various occurrences in a process, or the process itself, unless we view it in time and apply the measure of time to it."

Thus, the historical course of events and the causal links among them is one of the most important topics to economists.

Aristotle, René Descartes, Isaac Newton, Roger Joseph Boscovich, Albert Einstein, and Felix Bloch studied time as an objective matter, while Plotinus, Augustine, Gottfried Wilhelm Leibnitz, Immanuel Kant, Martin Heidegger, Edmund Husserl, and Maurice Merleau-Ponty selected the consciousness approach (subjective approach). Some of philosophers found that time is an emergent feature of reality (Page and Wootters 1983; Moreva et al. 2014), that it is an illusion (Glattfelder 2019). In Newton's period, time was deemed to be absolute. Einstein changed this concept forever: neither time nor space is absolute, but rather spacetime (he outlined all details in his Special Theory of Relativity in 1905 (Einstein 1905) and the General

1 Logical time permits the reversibility of ordered events and, thus, for any of these to be arbitrarily considered as the starting point of the selected process or the beginning of an observation.

Theory of Relativity in 1915 (Einstein 1915)). Einstein inferred that space and time are relative and interchanging.

Has the economical society the classical, absolute notion of time from Newton's mechanics? Surprisingly, concepts of relative time were considered in economics too. As stated in Željko Rohatinski (2017):

> "[T]he appearance of dilation of time and the contraction of costs in economic systems and sub-systems that move relative to each other — are analogous to the ones in physics — dilation of time and contraction of lengths of subjects in the inertial reference frames that move relative to each other..."

In the same way, as it is postulated in the theory of relativity, economic agents experience time differently, based on the duration of their individual economic cycles. Paul Krugman analysed relative time in economics (Krugman 2010) by using interest rates on goods which he assumed travelling at close to the speed of light. According to Krugman, problems in economics can be explored considering systems that move relatively with respect to systems in space and time.

Alfred Marshall suggested that the span of an economic period is a function of the level of resiliency of a given supply in relation to the trends of demand. He underlines that the number of calendar periods is a redundant measure. Alfred Marshall (1890):

> "Of course, there is no hard and sharp line of division between "long" and "short" period. Nature has drawn no such lines in the economic conditions of actual life; and in dealing with practical problems they are not wanted."

There is a wide range of economics literature where the notion of time deeply penetrates the very essence of the economic theory. Nevertheless, the use of time in economics has always been controversial. Today, economists have practically stopped contemplating novel ideas on the origin of time in the financial world proposing alternative theories. Time is primarily defined as a sequence of fixed intervals in physical time. Physical time remains the only considered and adopted concept for studying economic and financial problems. Therefore, today's economic understanding of the nature of time is dominantly based on the prospects of classical physics: intervals are indistinguishable and inseparable, and the economic properties are constant between consecutive observations.

Using physical time, high-frequency financial data are typically historical time series where the time distance between entries is fixed. Elementary price changes, called ticks, are used to create time series which are irregularly spaced in physical time. However, referring to the

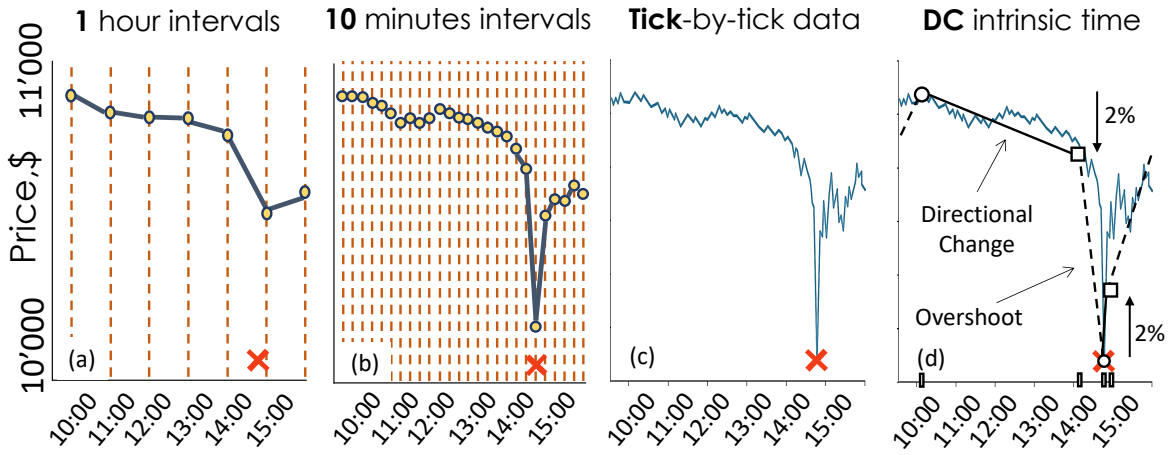

FIGURE 1.1: The Dow Jones Industrial Average on May 6, 2010 (10:00 AM - 4:00 PM EDT). Time series composed of one hour time intervals (where the most important information of the event, its depth, is not efficiently captured) **(a)**, ten minutes (where one of the records is close to the bottom of the crash, however, the substantial number of redundant measurements is performed when the market is relatively stable) **(b)**, tick-by-tick data (which is not convenient to work with as it is indicated in the text) **(c)**, and the price curve dissected by the directional-change framework with the threshold size equal to 2% (where only four records were enough to capture the bottom of the flash crash) **(d)**.

price behaviour over fixed and lengthy time intervals results in neglecting a large part of the information related to the market's microstructure (Bauwens and Hautsch 2009). Alternatively, too much noisy data is collected if the intervals are short (Ait-Sahalia, Mykland, and Zhang 2005; Hansen and Lunde 2006). The heterogeneity of the markets produces inconsistencies in the estimation of models in physical time. Figure 1.1 shows the aforementioned problem. The figure contains an example of a time series composed of high-frequency prices at the Flash Crash event[2].

It is important to highlight that the use of raw tick-by-tick data has substantial drawbacks too. Indeed, at tick frequencies, the size of the spread[3] is of the same order of magnitude as the size of the price changes. Also, the observed spread does not necessarily indicate the actual spread of the market (Goodhart, Ito, and Payne 1996). In the end, the information at the tick-by-tick level can be specific to the particular trading venue only. The synchronisation between different trading markets happens at significantly larger time intervals.

2 The financial phenomenon observed on May 6th, 2010. In a matter of minutes, the Dow Jones Industrial Average index lost nearly 9% of its value. The market rapidly balanced itself and eventually closed 3% below the opening price.

3 Spread is the difference between the best prices quoted for sale (ask) and for purchase (bid).

One example of side effects associated with the assumption of physical time driving the financial world is related to the stochastic volatility properties[4]. "Natural" volatility estimators, where returns are collected over predefined time intervals, were criticised with regards to the extent to which they overestimate the actual volatility (Gottlieb and Kalay 1985; French and Roll 1986).

Another problem related to physical time as the prime driver of economic processes concerns the capital asset pricing model (CAPM). A cornerstone of modern finance, CAPM states that the risk premium of an individual asset equals its beta[5] times the risk premium on the market portfolio (Sharpe 1964; Mossin 1966; Abdymomunov and Morley 2011). Many research studies (Fama and French (1992, 1993, 1996), among others) have considered constant betas while examining the CAPM. The studies reported low performance of the model and its inability to explain some asset pricing anomalies. The assumption of the constant betas over time (equivalence of the time stability itself) is one of the main reasons for the poor CAPM performance. Indeed, multiple papers find that betas are time-varying (Jagannathan and Wang 1996; Fama and French 1997; Lettau and Ludvigson 2001; Fama and French 2006; Lewellen and Nagel 2006; Ang and Chen 2007).

New Financial Time Paradigm

The challenge of the irregularity of financial properties (such as volatility stochasticity) could not be effectively addressed by leveraging physical time. New "event-based" measures were introduced, most notably by Benoit Mandelbrot. Now the sequence of entries in the time series are determined by the endogenous evolution of the time series' properties themselves. Mandelbrot and Taylor (1967), Allais (1974), Stock (1988), and Müller et al. (1993) proposed alternatives to physical time utilising event based frameworks. In Mandelbrot and Taylor (1967) a "transaction clock" ticks together with every financial transaction. Allais (1974) introduced a psychological time scale where the transformation of the time scale resembles physical time flow. Stock (1988) employed the information flows as the time scale of the aggregated market activity. Müller et al. (1993) define the event-based time through the accumulated market activity.

The directional change (DC) event-based intrinsic time framework, proposed by Guillaume et al. (1997), is an alternative way to describe the evolution of price changes beyond the limits of

4 Stochastic volatility enters the models in which the variance of a stochastic process is itself randomly distributed, that is, is not constant over time.

5 Beta measures the degree of co-movement between the asset's return and the return on the market portfolio.

physical time. Guillaume et al. divides the price curve into a sequence of alternating upturns (price rises) and downturns (price falls). In this approach, physical time is inessential, and only interchanging downturns and upturns form a sequence of events. According to the proposed framework, a downturn (upturn) event is an event at which price drops (rises) by a certain selected threshold from its highest (lowest) price since the moment of the latest event. The threshold is a percentage that the observer considers significant, e.g., for one 0.01% might be a meaningful change when another could tolerate price moves higher than 10%. Different thresholds result in different sequences of intrinsic events. An example of the directional-change framework applied to the flash crash tick-by-tick data is provided in Figure 1.1(d).

There are multiple examples of the added explanatory power obtained from financial markets by the introduction of directional-change intrinsic time. Guillaume et al. (1997) avoided the inconsistencies in the estimation of models in physical time induced by heterogeneity of the markets by employing this alternative intrinsic time scale. The directional-change framework was applied to develop an advanced measure of the risk through describing the price evolution as a sequence of directional-change events.

When markets are observed at short term intervals (intraday) or continuously, common approaches to measuring volatility such as the standard deviation cannot be applied due to the inhomogeneous data structure of the time series. Kablan and Ng (2011) disclosed a novel method of capturing realised volatility using the directional-change event approach. The authors directly employed the method for a trading strategy which outperforms standard strategies such as buy-and-hold or linear forecasting.

In finance, it is often hard to come by with frames of reference and fixed points. What moment should be selected as the beginning of the time series? Will the properties of the created time series vary together with the variations in the frequency of the entries in the time series? Glattfelder, Dupuis, and Olsen (2011) employed directional-change intrinsic time to circumvent these issues associated with the stiffness of physical time in finance. Glattfelder et al. enhanced our understanding of the behaviour of prices in financial markets by discovering novel stylised facts concerning the Forex market in directional-change intrinsic time. The author states:

> "The new [discovered] laws represent the foundation of a completely new generation of tools for studying volatility, measuring risk, and creating better forecasting and trading models."

Price changes are results of market reactions to the occurrence of events related to the financial sector. There are many ways of how the market, and hence the price, can react to

news. Some of the events can cause a substantial price increase, some a minor decrease, and some could result in an instant oscillation. Price moves happen at all different scales and time spans. Equally spaced intervals in physical time do not efficiently capture the essential information on the price evolution (see Figure 1.1, for example). Directional-change intrinsic time, in turn, is not sensitive to time, but the price changes directly. Bisig et al. (2012) used this property of the intrinsic time to define a framework called Scale of Market Quakes (SMQ). SMQ is aimed to quantify the FX market activity at major economic and political events announcements. The developed framework is simple and it does not imply any ad-hoc choices of functions and works on the tick-by-tick basis.

There are numerous approaches aimed at quantifying such important financial property as liquidity. The approaches mainly suffer from a specific choice of intervals in physical time, that does not reflect the correct and multi-scale nature of any financial market. At any time period, the evolution of price curve varies depending on the choice of the price move scales selected for the observation. Golub et al. (2014) employed the directional-change approach for a new tool designed to more efficiently monitor high-frequency market liquidity. The authors tested the tool on the empirical data and show that the new metric has the ability to detect and predict periods of disturbances in financial markets. Recently, Golub, Glattfelder, and Olsen (2017) described a successful trading strategy which exploits a collection of risk-management instruments built upon directional-change framework.

Contribution of the Thesis

In this thesis, we are changing the physical time paradigm by extending the intellectual legacy of Mandelbrot and Taylor (1967), Allais (1974), Stock (1988), Müller et al. (1993), and Guillaume et al. (1997). Directional-change event based time, the key concept in the presented research, redefines the notion of time as an activity measure. Building on the foundation of the dynamic understanding of time, we construct a new edifice extending the first attempts at re-conceptualising time and offer new insights and tools for analysing financial markets, performing risk management, market-making, and trading.

This thesis contains three papers. Each of the papers has been published or submitted to a peer-reviewed journal. In Paper 1, we describe an agent-based model where trades happen in directional-change intrinsic time and which is able to replicate the properties of sophisticated financial markets. In Paper 2, we propose a novel intraday instantaneous volatility measure which utilises sequences of drawdowns and drawups non-equidistantly spaced in physical time as indicators of high-frequency activity of financial markets. Finally, in Paper 3, we ex-

tend the intrinsic time directional-change methodology to multidimensional space and justify the accuracy of the updated directional-change framework.

Detailed Summary of Paper 1

Agent-Based Modelling in Directional-Change Intrinsic Time

Various market participants, such as traders, corporations, and governments, interact in financial markets. The traders continuously exchange goods with each other where the market price is agreed upon. Periodically occurring asymmetries between the amount of goods supplied and demanded result in price changes (Muth 1961; Cohen, Diether, and Malloy 2007). Market participants observe the change in price and adapt their set of trading decisions. The resulting decisions produce more demand-supply asymmetry that then triggers the next price change, et cetera. The question of how exactly market participants react to instant or aggregated price changes has been of great interest to the research community for as long as finance exists. A solid answer would substantially benefit the financial world.

Researchers considered a wide range of agent-based models in order to disentangle the empirically observed "price change - market participants reaction" phenomenon. The scholars attempted to replicate real markets by creating artificial agents that impact the market price according to some specified rules. Most of the models represent complex systems, populated by a large number of independent and heterogeneous actors competing with each other (NACIRI and TKIOUAT 2016). Agent-based models are aimed at reproducing and explaining the dynamics of real markets, such as bubbles, crashes, and regime switches (Samanidou et al. 2007; Ehrentreich 2007).

In most of the agent-based models, the agent's activity is synchronised with periodical intervals of physical time (see LeBaron (2006) for the surveys on agent-based models used in finance). As outlined, the use of physical time in finance is associated with the risk of incomplete or even erroneous perception of the market dynamics.

The first paper in this thesis introduces an agent-based model describing market participants' responses to price changes. The developed model is a system populated by a large number of independent agents characterised by heterogeneous trading strategies. These simulated agents follow the evolution of the price curve and trade only when intrinsic time events of a certain magnitude specific to the agent occurs. Every price change observed by a group of traders causes a sequence of intrinsic events. The agents, registering the intrinsic events, create the demand-supply asymmetry. The empirically observed squared root impact func-

tion (Bouchaud 2010) defines the size of the price changes, called returns, originating from the imbalance. The agents evaluate the new return, and the procedure continues. A price time series of arbitrary length is generated by the agent-based model.

We show that these time series are characterised by the same stylised facts which are typical for Forex markets. These stylised facts include: low auto-correlation of returns, a fat-tailed distribution of returns (Jondeau and Rockinger 2003; Rachev, Menn, and Fabozzi 2005; Koning, Cassidy, and Ouyed 2018; Michel M Dacorogna et al. 2001; Cotter 2005; Liu et al. 2017; Begušić et al. 2018), aggregational normality (Cont 2001), and a mean price move scaling law (Müller et al. 1990; Mantegna and Stanley 1995; Galluccio et al. 1997; Guillaume et al. 1997; Ballocchi et al. 1999; Gençay et al. 2001; Corsi et al. 2001; Di Matteo, Aste, and Dacorogna 2005). In finance, that scaling law is of the specific importance: it has been widely applied to risk management and volatility modelling (Ghashghaie et al. 1996; Gabaix et al. 2003; Sornette 2001; Di Matteo 2007). In addition, the agent-based model successfully replicates a scaling law observed in directional-change intrinsic time. This law uncovers the equality of the average overshoot[6] size and the size of the directional-change threshold at various scales. We demonstrate that the direction of the trend in the generated time series can be varied by tuning the set of directional-change thresholds driving the model.

The proposed agent-based model replicates the properties of sophisticated financial markets despite its simplicity. This fact strongly suggests that real market participants relate to their own intrinsic time frame while choosing when to perform trades. The obtained knowledge of the market participants' reaction to price changes improves the quality of inferences we can make regarding the observed traders' behaviour.

Detailed Summary of Paper 2

Instantaneous Volatility Seasonality of High-Frequency Markets in Directional-Change Intrinsic Time

Volatility is a measure of the dispersion of returns for a given market. High dispersion is typically associated with high risk. The majority of risk management tools utilise volatility as an input parameter. It is thus crucial to accurately estimate its value to minimise the errors resulting from such risk management techniques.

6 The part of the price trajectory between the local extreme observed prior to the directional-change and the preceding intrinsic event.

Traditional scientific methods estimate volatility by assessing the variance of price returns. The returns are typically collected over periodical time intervals. However, various political, natural, and social events, which result in market price changes, are rarely periodical. Moreover, the resulting impact can be as instantly manifested as a price change (for example, the EUR/CHF floor removal in 2015) or can emerge over an extensive interval (for example, Bitcoin's appreciation over the course of eight years). The events' irregularity and the varying rate of their impact result in non-equal realised volatility[7] values when returns over specific intervals are considered (Müller et al. 1997). A better volatility estimator, independent of any fixed time intervals, is proposed in our work.

In the second paper, we introduce volatility estimator agnostic to physical time. The estimator is based on the directional-change intrinsic time framework. The methodology introduced in the paper connects the number of observed directional-changes of a particular size to instantaneous volatility[8]. The size of the directional-change threshold is the only parameter needed to compute the volatility.

We show analytically how the size of instantaneous volatility depends on the threshold selected to compute the number of intrinsic events. Also, we demonstrate and explain how the estimated instantaneous volatility value decreases when the number of price changes per unit of time in the simulated time series decreases. Instantaneous volatility is equal to the realised one for a continuous process.

Various seasonality patterns characterise the evolution of financial markets Rozeff and Kinney Jr (1976), Gultekin and Gultekin (1983), Seif, Docherty, and Shamsuddin (2017), Fang, Lin, and Shao (2018), Keim (1983), De Bondt and Thaler (1987), and Zarowin (1990). The patterns emerge due to the market architecture and the geographical distribution of trading centres across the world. The seasonalities are "footprints" of a particular market structure. We contribute to the set of known seasonality patterns by reconstructing the instantaneous volatility seasonality on a weekly scale. Forex markets, S&P500, and Bitcoin/USD price time series have been considered. We show that the emerging patterns resemble the patterns of realised volatility. The seasonality of the Bitcoin/USD market is much weaker than that of Forex or S&P500. We also show that Bitcoin's volatility seasonality highs and lows are shifted towards American and European trading centre working hours.

Detailed Summary of Paper 3

7 The square root of the sum of squared returns.

8 The variance of a set or returns per unit time, as the time interval approaches zero.

Intrinsic Time Directional-Change Methodology in Higher Dimensions

Events in the global and interconnected world impact the evolution of financial markets (Gilpin and Gilpin 2001; Bauwens, Omrane, and Giot 2005). The events can occur at any instant in any location. National currencies can be disrupted by news originating from local or global events. However, the same news can have a varying impact on different national currencies (Evans and Lyons 2005). The financial world's interconnectedness and the varying degree of the influence news have on the exchange rates suggest that the global market should be analysed as a unified system.

In the third paper, we propose a method which can be used to study the concurrent and aggregated evolution of multiple exchange rates. For this, the directional-change intrinsic time framework has been extended to multidimensional space. The extended framework can be employed to perform the endogenous price curve analysis in a space where orthogonally arranged exchange rates form the dimensions.

We generalise the dissection procedure of a price curve into a set of directional-changes. The proposed multidimensional directional-change framework can efficiently cope with any space topology. The analytical equations derived for the data analysis of single exchange rates are adapted for the multidimensional case.

The extended framework was employed to perform an analysis of multiple Forex exchange rates in directional-change intrinsic time. We illustrate how the framework can be utilised to unveil the evolution of the changing cross-rate correlation coefficients.

Scaling laws based on the directional-change intrinsic time framework, and found in one-dimensional time series, are present in the higher-dimensional Forex data. We establish a connection between one of the scaling laws and the volatility of the examined process. The connection was employed as a novel approach for evaluating the volatility of multidimensional exchange rates.

Scaling laws are visually represented as simple linear dependencies of two values expressed in log-log space. Previous research works on directional-change intrinsic time applied to one-dimensional data did not report any substantial curvature of the relationship. We detail that the curvature appears in the range of small thresholds observed in multidimensional space. The curvature grows as the number of exchange rates forming the space increases. The scaling laws hold down to a certain threshold, which is significantly bigger than the smallest threshold used to uncover the scaling laws in one-dimensional space.

The extension of the original directional-change intrinsic time framework to multidimensional space creates a novel paradigm for high-frequency financial analysis. A wide range

of research papers on the novel methodology is expected to be produced in order to fully leverage its performance.

2

Agent-Based Modelling in Directional-Change Intrinsic Time

Who owns the information, he owns the world

Vladimir Petrov, Anton Golub, and Richard Olsen

A version of this paper has been submitted to *Quantitative Finance* (ISSN 469-7696).

I have presented it at:

- PhD Workshop on Quantitative Finance and Econometrics, July 2019, Manchester, UK;
- Quantitative Finance and Financial Econometrics 2018, June 2018, Marseille, France;
- Conference on Complex Systems 2017, September 2017, Cancun, Mexico;
- Winter School on Complex Financial Networks, January 2017, Zurich, Switzerland;
- Perm Winter School 2017, January 2017, Perm, Russia;
- Training Event on Data Science in Finance, August 2016, Tampere, Finland.

Abstract

We describe an agent-based model where trades happen in event-based time called directional-change intrinsic time. Events are defined as the reversal price moves of a directional-change threshold from a local extreme. The price impact of traded volumes is modelled according to the empirically observed squared root impact function. The time series generated by the agents is characterised by statistical properties typical for foreign exchange rates: low auto-correlation of returns, fat-tailed distribution of returns, aggregated normality, and the price jump scaling law. Furthermore, we introduce and use as a benchmark, the overshoot scaling law, which is an omnipresent feature of liquid markets and relates the expected length of price overshoots to the length of the corresponding directional-change threshold.

2.1 Introduction

According to the Bank for International Settlements, the daily trading volume in Foreign Exchange (FX) markets averaged $5.1 trillion per day in April 2016[1]. Such substantial volume can have a noticeable impact on the stability of the overall financial system. This volume is generated by the enormous number of transactions made by individual and institutional traders. Traders' behaviour is strictly connected to the flow of news related to the financial system (Ederington and Lee 1993; Bauwens, Omrane, and Giot 2005). Risk management tools capable of foreseeing and efficiently cope with the market impact of any political, environmental or technical change have to be built considering the characteristics and the origin of the market changes initiated by market participants. Due to the large trading volumes and the multitude of trading agents, the FX market is one of the biggest financial systems where agent-based models were extensively applied for its analysis (Aloud et al. 2017).

Market participants act on behalf of their perception and interpretation of the available information. Their consolidated behaviour is fully reflected in the prices of the traded financial instrument. This phenomenon is also known as the efficient-market hypothesis (Fama 1970). It encouraged scientists to look into historical time series to study the attributes of the aggregated activity of market participants involved in the trading. Multiple works have been done on the analysis of large amount of historical data in the search for fundamental properties of various financial markets. For example, Bollerslev and Melvin (1994) used more than 300 000 quotes for an empirical analysis of the bid-ask spread and its relation to the exchange rate uncertainty. Danielsson and Vries (1997) and Michel M Dacorogna et al. (2001) used high-frequency data to estimate the fat tails of exchange rate returns. Kozhan and Salmon (2012) employed the dataset of submitted market and limit orders to examine how the information contained in order books could be exploited in simple trading schemes.

A wide range of agent-based models was proposed to explore the observed changes in the market's dynamic. The changes are assumed to be the market's reaction to the actions of individual and aggregated groups of traders inhabiting the market. The models attempt to replicate the evolving behaviour of real market participants by creating artificial agents who impact the market in the same way as it happens in reality. Most of the models represent complex systems, populated by a large number of independent and heterogeneous actors competing with each other (NACIRI and TKIOUAT 2016). Agent-based models are aimed to reproduce and explain the phenomena of real markets, such as bubbles, crashes, and regime switches (Samanidou et al. 2007; Ehrentreich 2007).

1 https://www.bis.org/publ/rpfx16fx.pdf

There is a wide range of various designs of agent-based models characterised by specific properties intended to imitate phenomenon observed in reality. Despite the diversity of the models, one structural element is always present in their description: the definition of time and how the agents dynamically adapt themselves to its flow. Scientists used to rely on physical time where hours, days or even seasons are selected to measure elapsed periods and intervals between various events (see LeBaron (2006) for the surveys on agent-based models used in finance). Physical time is traditionally employed to describe the interaction between agents and the impact of their trading activity on the market prices. Equally spaced timestamps are assumed to be the points where the actions have to be considered. However, the real market is a complex system with its endogenous non-constant time stream. The activity of that stream is dependent on the inhomogeneous frequency of political, social or environmental events (Guillaume et al. 1997). The non-constant volatility typical for the FX market is the main aspect which helps to understand the disadvantages of physical time in agent-based modelling. The volatility of high-frequency markets is the proxy for the market participants' activity (Schwert 1989). At the same time, samples of equidistant time intervals of given lengths used to compute volatility can significantly affect its results (Müller et al. 1997). Therefore, financial instruments and agent-based models built upon physical time and designed to measure or replicate statistical properties of real time series are naturally limited by the stiffness of selected equidistant intervals.

The limitation of equidistant time periods applied to the financial data analysis can be overcome by applying the concept of directional-change intrinsic time proposed by Guillaume et al. (1997). In this intrinsic time representation, events are endogenously defined as reversal price moves measured from local price extremes. All reversals have to be of the size equal to the given directional-change threshold. The proposed measure dissects the real price curve into the sequence of alternating ascending and descending trends. Each elementary trend ends once a new price curve reversal is observed. Continuous price moves in the same direction of the latest reversal are called overshoots. Overshoots represent trend components of the price curve. Only price moves indicating the beginning of the new trend allow the system's clock tick. Thus, this intrinsic time is capable of dealing with the essential properties of price curves such as trends independently of the time intervals chosen to observe them. In other words, intrinsic time is agnostic of the scale and speed of the price evolution registered in physical time.

Trend changes are the primary indicators of the prevailed side of the aggregated behaviour of all market participants (Muth 1961; Cohen, Diether, and Malloy 2007). The agent-based

model, proposed in our work, employs the directional-change intrinsic time framework to monitor trends and dissect the price curve into a collection of directional-change points. These points and price overshoots are used by the agents as signals for their trading activity. Agents, operating in directional-change intrinsic time, judge the market conditions and make decisions on their actions employing prices as the only source of information.

A successful agent-based model should be able to reproduce statistical properties of real financial markets. These properties are mostly known as 'stylised facts' and are copiously discussed in numerous papers (Kaldor 1961; Pagan 1996; Kullmann et al. 1999; Gençay et al. 2001; Cont 2001; Chakraborti et al. 2009). In this work, we test the time series synthetically created by the model against a set of benchmarks. The main target of the test is to confirm that the created time series are characterised by the set of selected statistical properties. The following stylised facts are among the chosen tests: low autocorrelation of returns, fat-tailed distribution of returns, aggregational normality, the price jumps scaling law[2] and the overshoot scaling law. The latter statistical property was chosen in addition to the four stylised facts usually adopted as benchmarks of agent-based models. This scaling law was recently found in a wide range of real high-frequency time series from the FX market and even in arithmetic Brownian motion (Glattfelder, Dupuis, and Olsen 2011). It establishes a relation between the average length of overshoot and the corresponding size of the directional-change threshold. The relation states that on average, a directional change is followed by an overshoot of the same magnitude. The sovereignty of the directional-change concept of the flow of physical time makes the overshoot scaling law a very convenient tool for testing the performance of agent-based models. To the extent of our knowledge, it is the first research work where a stylised fact based on the directional-change intrinsic time is used to evaluate the time series generated by a group of heterogeneous agents.

The outline of the remaining paper is as follows. Section 2.2 illustrates the details of the directional-change intrinsic time framework. It also provides an example of a real price curve dissected into a collection of intrinsic events. Section 2.3 describes two main components of the agent-based model: the set of artificial agents and the market impact function. In Section 2.4 the collection of benchmarks used to validate the properties of the generated time series is discussed. In Section 2.5 we present all obtained results and observed statistical properties of generated time series. In Appendix 2.A the average length of overshoots is derived for the case of Brownian motion with the constant trend. In Appendix 2.B the pseudo-code of the

2 Scaling law (power law): the mathematical relationship between two variables that holds true over multiple orders of magnitude.

directional-change intrinsic time algorithm is provided. Appendix 2.C concludes the paper with a collection of graphics describing all auxiliary experiments.

2.2 Intrinsic Time

The number of transactions as well as traded volumes in liquid markets is much lower during holidays or weekends than during working days or after some unexpected but significant news (Chordia, Roll, and Subrahmanyam 2001). This evidence directly contributes to the continuous changes in the financial time series volatility over time (Blattberg and Gonedes 1974; Christie 1982; Scott 1987). Thanks to this non-homogeneous nature of financial markets, one can find drastically distinct price curve evolution within two separate historical time intervals of equal length. One period could be characterised by an instant price drop by several percents and not less instant recovery to the same level (for example, a flash crash) when the other could represent an absolute standstill. The latter often happens when the market is completely inactive due to holidays. Despite this well-known fact, the historical dynamics of financial markets have been mostly analysed using snapshots of market states equally spaced in time. Such snapshots are typically either too infrequent and do not allow capturing of all the available high-frequency information (Zhou 1996) or are too numerous which cause the excessive noisy details of the created set of data (Zhang, Mykland, and Aït-Sahalia 2005).

Mandelbrot and Taylor (1967) were one of the first researchers to propose an alternative event-based paradigm for modelling and analysing financial time series. Price changes over a fixed number of transactions were studied and compared to the price changes over fixed periods of time. Later, Guillaume et al. (1997) extended the early set of alternative data analysis techniques by introducing the directional-change intrinsic time concept. According to that concept, all ticks happen as a result of alternating rising and falling prices (returns) of a certain size. The size of returns can be arbitrary chosen. The latter allows independent monitoring of the trend changes at various scales. It is especially important taking into account that same price curve can be characterised by different directions of low- and high-scale trends. The phenomenon has been frequently exploited by traders. One specific trading strategy called 'Triple Screen Trading System' was proposed by Elder (2014).

The purpose of the directional-change intrinsic time is to register moments at which the price curve alternates its trend of the given scale. It also finds extreme prices which correspond to local maximum or minimum between two consecutive trend flips. The next paragraph contains a detailed description of the dissection procedure of tick-by-tick data by the

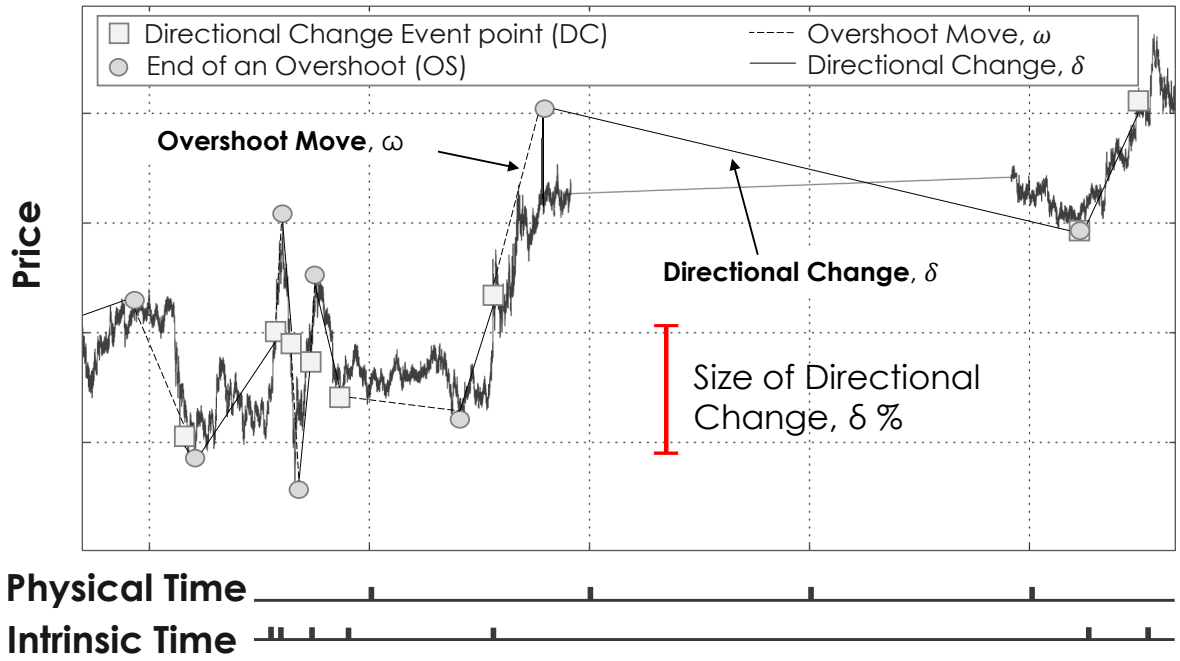

FIGURE 2.1: Example of a price curve dissected into a collection of directional changes using a threshold δ. Two types of sections are typical for each consecutive pair of intrinsic events: directional-change (marked by the solid line) and overshoot (dashed line). The direction of the initial mode is chosen to be downward. The first (left) grey square marks the first directional-change event which occurs when the price moves downward by δ percent from the local extreme. The local extreme for the given mode, coincides with the highest observed price (the first grey circle). The mode alternates (upward) as soon as a new directional-change point becomes registered. After this step, the local extreme coincides with the smallest observed price since the time of the latest directional-change. The next upward event is registered when a positive return of the size δ happens measured from the local extreme. After this, the mode alternates again and the dissection process continues.

directional-change algorithm. An example of a real price curve dissected into a collection of intrinsic events is shown in Figure 2.1.

The latest observed tick price should be taken as the starting point to initialise the dissection of a price curve into a set of directional changes. Then, the relative size of the directional-change thresholds δ and the initial direction of the trend should be selected. There are only two possible states of the trend which correspond to each given threshold δ: mode *up* for the upward or mode *down* for the downward trend. The initial value of the extreme price S_{ext} coincides with the first price used to initialise the algorithm. Each new tick has to be compared to the latest registered extreme. If the current mode is *up* (*down*) and the newest price S_{tick} is higher (lower) than the extreme price S_{ext}, then the S_{ext} takes the value of S_{tick}.

Alternatively, the distance between the latest price S_{tick} and the current local extreme S_{ext} should be compared to the size of the threshold δ. If the distance is bigger or equal to δ then the current price is a new directional-change point. At this moment, the mode should be changed to the opposite one and the local extreme reinitialised by $S_{ext} \leftarrow S_{tick}$. The overshoot part ω of the price curve corresponds to the price trajectory between the latest directional-change and the local extreme points.

Overshoot intrinsic events (overshoots events) are registered every time whenever the size of the overshoot ω becomes a multiple of the dissection threshold δ (Golub, Glattfelder, and Olsen 2017). We employ this category of intrinsic events in addition to the initially proposed in Guillaume et al. (1997) directional changes. The overshoot events will be connected to the empirically observed length of the overshoot section with the decision-making mechanism of the agent-based model. As the reader can see from Figure 2.1, the minimum size of overshoot is equal to zero. That can be observed when the price does not follow the trend and makes a reversal right after a new directional-change point. At the same time, there is no the upper bound on the size of the overshoot section. Therefore, there is no a limit on the number of overshoot intrinsic events between two consequent directional changes. The details on the expected length of ω will be provided in Section 2.4.2 where the overshoot scaling law is described. The pseudo-code of the dissection algorithm is provided in Appendix 2.B.

The recording of the price activity in directional-change intrinsic time does not rely on the exogenous evolution of physical time. Only endogenous price moves define the steps at which a measure should be taken. Interesting properties of the financial time series emerge in this case. Guillaume et al. (1997) presented a scaling-law discovered with the help of their new event-based concept. The scaling law establishes the relationship between the chosen thresholds δ and the number of the corresponding trend changes $N(\delta)$ registered within the given time period:

$$N(\delta) = \left(\frac{\delta}{C}\right)^{E}, \tag{2.1}$$

where $C \in (0, +\infty)$ and $E \in (-\infty, +\infty)$ are scaling law parameters. This scaling law states that the number of directional changes observed in a data sample of the fixed length relates to the size of the chosen threshold as a power law function. It is worth noting that although the size of the threshold δ can range from zero to infinity, the practically selected values depend on the volatility of the analysed process and the frequency of price changes. For example, Glattfelder, Dupuis, and Olsen (2011) selected the set of thresholds ranging from 0.01% to 5% to analyse scaling laws of foreign exchange rates. The typical annualised volatility of FX rates is about 20% which means that the selected range covers the majority of price trajectories

observed within several years. At the same time, the thresholds are practically bigger applied to the analysis of emerging markets such as their volatility is substantially higher (Petrov, Golub, and Olsen 2018).

The intrinsic time ticks more often during periods of high volatility and less often when the market is relatively quiet. The latter insures that no important information will be lost as well as no noisy points will enter the created data sample. The visualisation of the statement is provided in Figure 2.1 where the last two directional-change events are registered after a weekend (right part of the plot where the exchange rate does not move). There were no trades therefore no price moves and therefore no information which could enrich the collected recorded. Additionally, the directional-change intrinsic time allows capturing the most valuable moments represented by the local maximums and minimums indicating the end of each trend. All price ticks between the registered intrinsic events are considered as noisy at the scale given by the size of the threshold and become ignored. The prices, neglected by one threshold can at the same time play the role of tipping points at another scale. This multi-scale property of the directional-change intrinsic time can be used to decrease the signal to noise ratio in each specific experimental scenario sensitive to the scale of market moves.

There are various advantages of the event-based approach employed for high-frequency data analysis. They have been successfully applied and described in multiple papers. Among others:

1. The directional-change algorithm was used to discover numerous scaling laws hidden in the price curves from the FX market. The found properties are expected to improve the inferences we make on the price evolution through analysing liquid markets (Glattfelder, Dupuis, and Olsen 2011);

2. Several directional-change thresholds of various sizes can be initiated at the same time. The evolution of such multiscale system can be employed to describe prices of the given financial time series. This interpretation of the market dynamic leads to an efficient estimator of the price trajectory unlikeliness. This unlikeliness is later used as the indicator of the current and the forecasted liquidity of the market (Golub et al. 2014);

3. The number of directional-changes grows fast in periods of high volatility. The number stays small when the volatility is close to zero. Thus, the approach can be used as a volatility estimator of the given time series. The number of events as well as the magnitude of the trend components are the proxy for the volatility size (Petrov, Golub, and Olsen 2018).

A large number of directional changes can be registered if the size of the threshold δ is significantly smaller than the volatility of the analysed time series. The average numbers of overshoot intrinsic events observed in the upward and downward local trends is approximately equal to each other if the overall trend of the time series is equal to zero. Alternatively, if there is a persistent trend, the price curve tends to overshoot more often when the type of the directional-change mode coincides with the direction of the overall trend. Thus, the average numbers of overshoot events in upward and downward trends will not be equal to each other. However, it is possible to modify the original algorithm in such a way that the trend will have no impact on the balance of the overshoots number. A couple of distinct thresholds can be used to monitor two classes of directional-change modes independently: δ_{up} to register events which happen within the upward trend and δ_{down} for events within the downward trend. The theoretical analysis in Appendix 2.A demonstrates how the trend size affects the expected length of the overshoot sections. As it can be seen from equations (2.15) and (2.15), the expected size of an overshoot depends on the trend of the market μ and on its volatility σ. For example, if the trend is negative, then the expected upward overshoots $\omega(\delta_{up})$ are equal to downward overshoots $\omega(\delta_{down})$ only if $\delta_{up} < \delta_{down}$. It is important to note that the length of the overshoot section contributes to the number of overshoot intrinsic events. Therefore, the equations from Appendix 2.A can be used as the reference to the expected quantity of intrinsic events per given period of time.

Most of the analytical tools developed in finance were initially built using the assumption that the analysed market does not exhibit any particular trend. However, real price curves are collections of alternating trends of various scales. Therefore, parameters of some trading or risk-management algorithms require adjustments which can compensate nonzero trend typical for the given market and the selected period of time. The directional-change intrinsic time concept, equipped by the aforementioned asymmetric thresholds property, is one of the instruments capable to deal with that trend problem. A couple of directional-change thresholds $(\delta_{up}, \delta_{down})$ can be selected in such a way that the number of upward and downward overshoot intrinsic events will be always equal to each other. However, the price trend cannot be estimated ex-ante. Thus, it is impossible to say which pair of thresholds should be chosen to neutralise the drift expected in the near feature. An efficient solution of the problem was proposed in Golub, Glattfelder, and Olsen (2017). The authors describe an automated trading algorithm utilising a set of statistical properties accompanying the directional-change intrinsic time. The algorithm efficiently generates profit by capturing the price curve coastline and trading at the moments of expected alternating trends. The equal number of buy and sell

trades should happen within periods of the growing and the falling price sections to ensure stable positive returns. In other words, at any moment of time, the algorithm should have precisely tuned pair of upward and downward thresholds which corresponds to the currently present trend. The authors used the accumulated inventory of the trading bot as the proxy for the trend. The selected thresholds should be changed every time when the absolute size of the inventory crosses selected limits. In our work, we are creating a trivial agent-based model where the artificial agents do not keep track of their inventory. Instead, each of them has a unique ex-ante specified pair of non-modified thresholds. Such settings lead to the case when at any moment of time there is an agent whose couple of thresholds captures the current price trajectory in the best possible way (registering equal number of upward and downward overshoot events). The whole set of agents and their parameters will be described in the following section.

2.3 Structure of the Model

Financial markets can be schematically described as the interplay of two components. First, a group of trading agents characterised by the diverse range of behavioural patterns. Second, the exchange rate response on the aggregated agents' trades (see, for example, Delage et al. (2010)). We stick to this generalised representation to keep our model as simple as possible. Therefore, the agent-based model has: a set of agents buying and selling a fixed volume only at the moment when they register an intrinsic event; the volume impact function, a special algorithm which generates the next price move (return) as a reaction to the aggregated imbalance of the number of buyers and sellers. The latter will be described a few paragraphs below.

The demand and supply create equilibrium in any efficient financial system. In other words, the total buy and sell volumes over given period of time are equal to each other. Nevertheless, our agent-based model does not assume the complete equilibrium. Instead, we postulate that the excess volumes formed by all trading agents can be endlessly bought and sold to and from some external counterparties. The excess volume will be later connected to the price returns through the volume impact function.

The whole life cycle of each agent consists of only two actions: opening a long or short position and waiting for a moment to reverse it. The agents do not exploit each possible opportunity to perform trades (in the same way how it happens in the real world): they flip their positions with probability P_{flip} which makes the performance of the model more realistic. The moments when the agents try to open or flip the positions coincide with the

occasion when intrinsic events become observed. The sequence of such moments is unique for each agent since it is determined by the assigned directional-change thresholds δ_{up} and δ_{down}.

For simplicity, all agents trade identical volumes equal to one lot. To flip a position from long to short an agent shorts one unit to close its long position and shorts an additional unit to open a short position. In total two units should be sold. A similar procedure is in place for flipping from a short to a long position, whereas the agent buys two units. Thus, at any iteration there are always N_{long} agents who decided to flip their position from short to long after analysing the latest return and N_{short} agents who decided to become short instead of long. The value $\Delta N_n = N_{long} - N_{short}$ indicates the excess demand or supply at the step n. The variable ΔN_n, also called the net volume, is used by the model to determine the subsequent price change using the volume impact function. A simplified example of a sequence of intrinsic events registered by the trader with parameters $\delta_{up} = 3$ and $\delta_{down} = 2$ is visualised in Figure 2.2.

Real market participants have a diverse set of trading strategies: trading in working days or weekends, using technical or fundamental analysis, preferring high-frequency trading or holding long-term positions (see, for example, the survey of US market provided by Cheung and Chinn (2001)). Good agent-based models aimed to mimic real liquid markets should also be characterised by such varied behaviour. We emulate a complex system by creating a group of intrinsic event agents each of which has a unique set of parameters δ_{up} and δ_{down} which impact their trading patterns. The model does not have a pair of agents with completely the same settings. Each agent interprets a price curve from the point of view of the directional-change intrinsic time. The interpretation depends on the size of the assigned thresholds and their dissimilarity. Some of the simulated traders can register intrinsic events at each new price tick by operating with small enough thresholds (like real high-frequency traders). At the same time, traders with large thresholds register intrinsic time events significantly less frequently which makes their behaviour similar to the one of the long-term investors. Therefore, the selected diverse composition of the model makes the behaviour of individual traders exclusive and the whole range of strategies manifold. As a result, various trading activity patterns are reproduced.

The goal of the agent-based model is to generate a set of returns characterised by the same statistical properties found in the FX market. Each produced return is assumed to be defined in logarithmic terms (log-returns). This assumption makes it possible to directly compare aggregated returns and the size of the directional-change thresholds typically expressed in

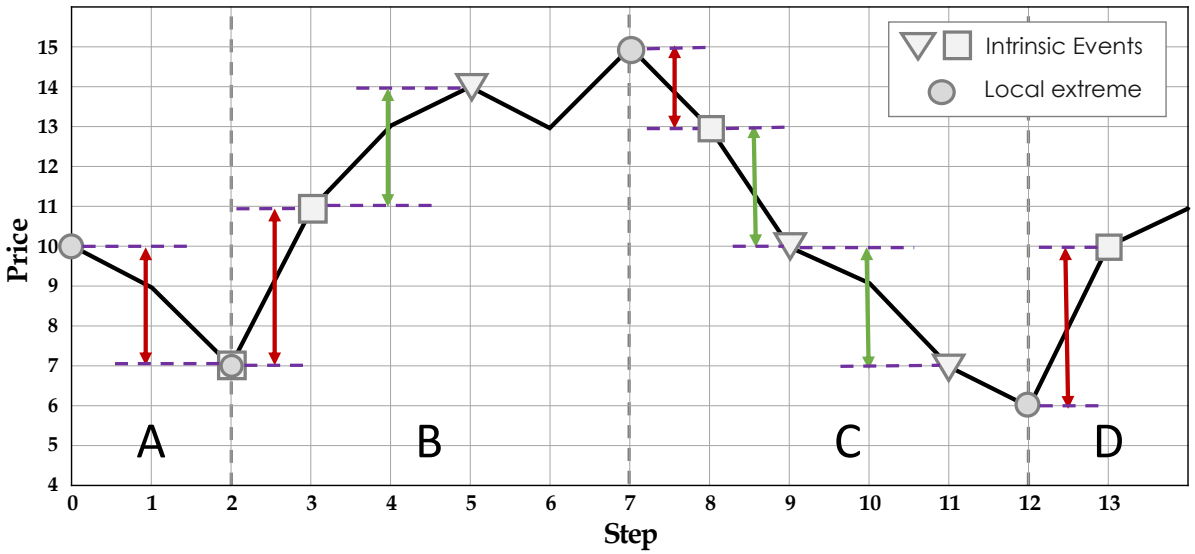

FIGURE 2.2: An example of a price curve dissected by a set of intrinsic events at which the agent with parameters $\delta_{up} = 3$ and $\delta_{down} = 2$ opens a position and makes trades. For simplicity, the chosen thresholds are expressed in the absolute price moves instead of the relative ones. The initial price is equal to 10 and the agent's initial mode is down. Red arrows mark the distance measured between local extremes and the following directional change points. Green arrows label price moves which lead to the next overshoot intrinsic event. Letters A, B, C and D are put here to tag four intervals of alternating modes. The agent registers its first directional-change intrinsic event as soon as the price goes down from the local extreme by at least two points (labelled by a circle). Since this is the first intrinsic event observed by the agent, it opens its first position at this point (step number 2). Then it is waiting for the next event which happens at step 3 after a big price move by four points up from the latest local extreme (coincides with the previous directional change intrinsic event, a grey square). Independently on its previous trading decision, the agent keeps analysing the price curve. At step 5 the price has made an overshoot move measured from the preceding directional-change point the size of which is equal to up (a grey triangle). This point marks the first overshoot intrinsic event. Though the price continues its overshoot move up, it does not go far enough to trigger another overshoot intrinsic event and the next tipping point becomes a directional change at step 8. The next two overshoot intrinsic events happen at steps 9 and 11. The last directional change concludes the example at step 13.

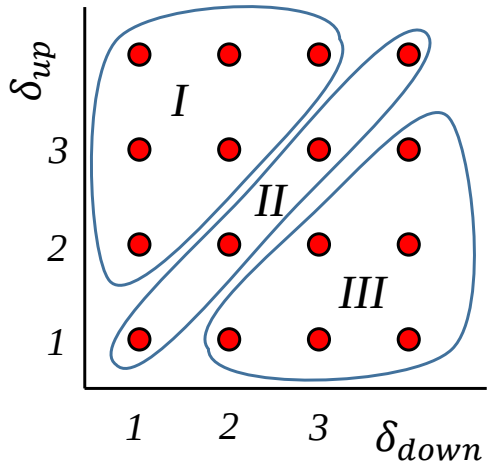

FIGURE 2.3: A part of the grid representing the collection of trading agents. Each point corresponds to an agent defined by a set of unique parameters (δ_{up}, δ_{down}). δ_{up} and δ_{down} are the size of upward and downward directional-change thresholds correspondingly. We mark regions with specific properties by numbers I, II and III. In the region I there are traders with the upward directional change thresholds larger than the downward ones ($\delta_{up} > \delta_{down}$). The region II contains 'symmetric' agents ($\delta_{up} = \delta_{down}$). Region III labels all agents with downward thresholds larger than upward ones ($\delta_{up} < \delta_{down}$).).

the percentage terms. In other words, returns between two given prices at steps m and n (x_n and x_m) are defined as $r(n,m) \approx \log(x_m) - \log(x_n) = S_m - S_n$ where S_m and S_n are sums of returns accumulated by the steps m and n. Thus, a new directional-change intrinsic event happens when the absolute distance between the latest price and the local extreme becomes bigger or equal to δ. This simplification significantly facilitates all computations and will be used in the rest of the article.

To simplify the model, we represent the whole set of agents as a collection of separate points on a square grid (Figure 2.3). Each point corresponds to a couple of thresholds assigned to one unique trader. Values δ_{down} are located along the horizontal side of the grid (x-axis) and all included in the model thresholds δ_{up} are placed along the vertical side (y-axis). It is worth mentioning that the given setup is built on the assumption that any price return should become a signal for a trade. Thus, the distance between two consecutive values on the same axis was selected to be equal to one price tick. This guarantees that any cumulative return will serve as a new signal for the agent-based model.

The geometrical size of the grid defines the extent to which the agents cover the diversity of various trading patterns. We split the grid by L points horizontally and vertically to assure the symmetry of the trading strategies. Figure 2.12a in Appendix 2.C demonstrates the number

of trades performed by all individual agents from the entire grid. As expected, agents with the smallest thresholds located in the left bottom corner make the biggest number of trades (high-frequency traders). The right top corner represents the rarely trading of agents who perform using the biggest thresholds (long-term holders).

The grid can visually be divided into three separate sections according to the types of agents' activity (Figure 2.3). Traders from section I have upward directional-change thresholds larger than the downward ones ($\delta_{up} > \delta_{down}$). These agents register the equal number of overshoot intrinsic events within local trends upward and downwards only when there is a persistent positive trend. Otherwise, the average number of overshoot intrinsic events registered within the directional-change mode downwards prevail over of the average number within the upward sections. These agents tend to exploit more trading opportunities when the trend is negative or equal to zero. Agents from the region II have equal upward and downward thresholds and are called diagonal agents. The absence of any global trend is the most stable condition for them. In that case, they witness the equal number overshoot intrinsic events within local trends in both directions. Region III marks all agents with upward directional-change thresholds smaller than the downward ones ($\delta_{up} < \delta_{down}$). Their behaviour is the opposite to the behaviour of traders from the region I. For each trader from the region I there is a corresponding opposite agent from the region III. Therefore, the complete set is fully symmetric and thus imitates the counterbalance of different traders in the real financial world. We will show later that one can simulate steady trends of given sizes by deactivating agents from specific parts of the grid.

The lack of demand motivates the supply side to reduce prices and the lack of supply affects the price rises (Walras 2013). This empirical observation was used in our work to define the volume impact function for the developed agent-based model. The function is committed to computing price changes caused by the imbalance between the total demand and supply. The exact shape of the function may depend on various factors (Lillo, Farmer, and Mantegna 2003). Among them: the selected time horizons where the impact is observed; the size of the traded volumes; the types of markets where the trades are performed and many others. Several research works have been done on this topic and different models were proposed. A stable and linear impact function was described by Kyle (1985). Huberman and Stanzl (2004) provided later the proof that permanent price impact must indeed be linear while the temporary one can be of a more general form. At the same time, more sophisticated non-linear functions were reported (Hasbrouck 1991; Hausman, Lo, and MacKinlay 1992; Kempf and Korn 1999). We decided to choose the model proposed in the relatively recent work

Bouchaud (2010) for our experiments. According to Bouchaud, the impact of trading volume is non-linear and one of the best approximations is the square root function. Therefore, we endow the market response to the agents' aggregated trades in the following way:

$$r_n(\Delta N_n) \equiv S_n - S_{n-1} = \left\lfloor \alpha \text{sgn}(\Delta N_n) \sqrt{|\Delta N_n|} \right\rfloor, \tag{2.2}$$

where: $r_n(\Delta N_n)$ is the price change (return) at the step n; α is the parameter limiting the minimum price shift; sgn(.) and $\lfloor . \rfloor$ are the sign and the floor functions correspondingly.

There is a situation among all possible scenarios when the number of agents deciding to flip short positions is less than the number of agents deciding to do the opposite just by one agent. This case leads to the imbalanced volume equal to the sum of the volume to close a position and the volume to open an opposite. Therefore, the smallest possible non-zero value ΔN_n is equal to two. The parameter α was chosen to guarantee that in such situation the market will respond to the smallest possible imbalance by changing the price by one unit: $\alpha = \sqrt{2}/2$. We use the floor function to simulate only discreet price changes typically observed in real markets.

Periods of economic equilibrium happen when demand meets supply (Debreu 1987). In this case, the sequence of trades happened at the market does not cause any price change, so the evolution of the price curve becomes temporarily stable. Such states do not last notably long. Even small market fluctuations enliven further asymmetric activity of the sell and buy sides. Eventually, the disturbance becomes portrayed in a sequence of substantial price moves. Similar to the reality, the proposed agent-based model is capable of producing zero difference between the number of all buyers and sellers which entails zero net volume. This volume being put into equation (2.2) does not cause any price change. The agents do not receive any new information and thus do not have a chance to make decisions on further trades without price changes. As a result, this puts the following evolution of the price curve on hold. To reactivate the trading, we add a small random price shift upward or downward with equal probability 0.5. The shift happens whenever the net volume ΔN_n is equal to zero. The size of the random move was chosen to be big enough to trigger a new intrinsic event for agents who have one or both thresholds equal to the size of the smallest price tick: $\delta = 1$. This way, these agents receive a new piece of information and try to flip their opened positions creating new demand or supply which leads to the consequent price change.

We used the next parameters for the main simulations: initial price level $S_0 = 0$; minimum price step (a tick) $r^{min} = 1$; $\alpha = \sqrt{2}/2$; smallest and biggest thresholds $\delta_{min} = 1$ and $\delta_{max} = 50$; the step between two consecutive thresholds on the grid equal to 1; total number of trading agents is 2500. Prices, produced by the model, are aggregated returns computed as responses

to all imbalanced volumes that happened in the past. Therefore, the zero initial price simply indicates that no returns happened before the model was initialised. The smallest threshold $\delta_{min} = 1$ guarantees that any elementary price move will trigger a new intrinsic event for agents operating at the minimal scale. The size of the probability to flip position P_{flip} coincides with the empirically and theoretically found probability to register a new overshoot event before the directional-change one (Golub et al. 2014):

$$P_{flip} = e^{-1} = \mathbb{P}(\omega(\delta) \geq \delta). \tag{2.3}$$

The maximum possible price move r^{max} can be observed only when all agents defined in the model decide to flip their positions simultaneously. Thus, the largest absolute price change is determined by the number of agents on the grid and is directly connected to its length L:

$$r^{max} = \alpha L\sqrt{2}. \tag{2.4}$$

To generate such big return, all agents should register intrinsic events at the same moment of time and their opened positions have to be of the same type. In the real markets, such significant returns with negative sign are usually interpreted as crashes. They do not happen on a daily basis and are observed when large numbers of market actors accidentally make similar trading decisions in one critical instant. In our model, the probability to observe the maximum price move of the size r^{max} is likewise possible but minuscule. It is guaranteed by the condition that the decision to flip positions should happen at the same time for all agents. The latter happens with the probability $P_{flip}^{L^2}$ which rapidly tends to zero with increasing the size of the grid L.

The schematic summary of the algorithm used to generate the synthetic time series is provided in Figure 2.4.

2.4 Benchmarks

The main goal of this research work is to check whether the agent-based model operating in the directional-change intrinsic time is capable of generating synthetic time series, statistical properties of which are coherent with the ones typical for foreign exchange market. Several benchmarks have been chosen to verify the accuracy of the model. The whole set of tests consists of four traditional methods often used in research with the same intent and a new approach wholly based on the directional-change intrinsic time. We propose that the latter is the best way of evaluating agent-based models. Further, we describe all selected benchmarks in details.

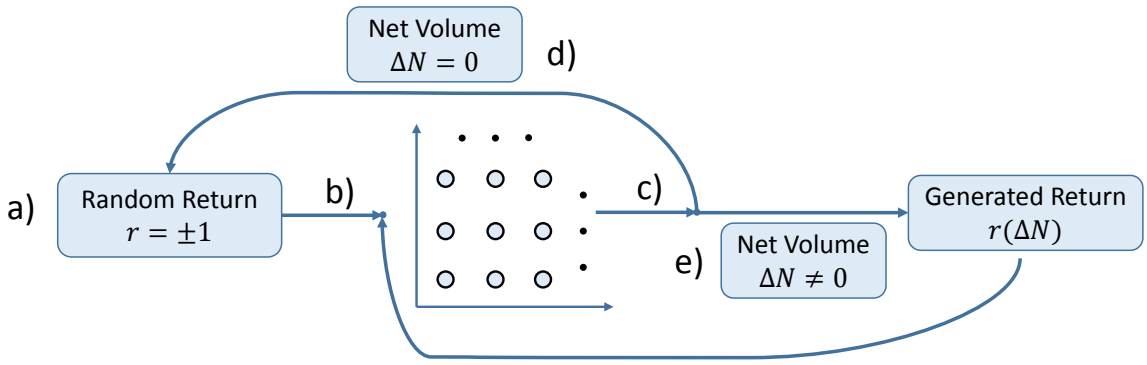

FIGURE 2.4: The schematic summary of the algorithm used to generate the synthetic time series. a) The model generates a random return in order to create the first signal for the group of agents represented by a grid of thresholds. b) All agents consider the latest price return as a signal in their local directional-change intrinsic time defined by the pairs of thresholds $(\delta_{up}, \delta_{down})$. Some group of the agents flip their opened positions reacting to the observed return. The generated net volume ΔN is expressed as the overall difference between the total number of agents decided to flip long and short positions. The net volume can be: d) equal to zero which means that no new signal is generated and a random price shift should happen to provide a new signal for the agents; e) not equal to zero which means the volume impact function (2.2) can generate a new return as the reaction to the aggregated traders' behaviour. The new return is the input for the grid of agents at the next step of the simulation.

2.4.1 Traditional Benchmarks

One of the well-known facts about the market microstructures is that price returns in any liquid market do not exhibit significant linear autocorrelation (Arneodo et al. 1996). This phenomenon is also formulated as the 'efficient market hypothesis': prices instantly and fully reflect all available information making it impossible to build a simple trading strategy based on the 'statistical arbitrage' (Basu 1977). Only at ultra-short time interval price curves could have slightly correlated historical returns. At this scale, the market, as a global multi-agent system, is still absorbing a new piece of information. According to Cont, Potters, and Bouchaud (1997), 'in a few minutes' the autocorrelation can be safely assumed to be equal to zero. Low autocorrelation of returns is one of the most popular stylised facts which regularly accompany liquid markets. Therefore, we selected that statistical property to be among our benchmarks. The autocorrelation function of the series of returns M with mean μ and variance $\sigma(\tau)$ computed using the given lag τ is defined as

$$R(\tau) = \frac{\mathbb{E}[(M_t - \mu)(M_{t+\tau} - \mu)]}{\sigma(\tau)^2}. \tag{2.5}$$

The second stylised fact chosen for the analysis is related to the fat-tailed distribution of returns at the frequency higher or equal to one day. This property, also known as excess kurtosis, is thoroughly discussed in the book Mandelbrot and Hudson (2010). The authors point out that there is the full range of theories build on top of the assumption that returns are normally distributed (including the famous work of Black and Scholes (1973)). Nevertheless, the processes in the real financial markets have always been different from Brownian motion and this assumption is a severe flaw of any related financial model. Therefore, it is important to create the model which is able to reproduce returns characterised by the fat-tailed distribution. We measure the excess kurtosis k in the following way:

$$k = \frac{\langle (r(t,\tau) - \langle r(t,\tau) \rangle)^4 \rangle}{\sigma(\tau)^4} - 3, \tag{2.6}$$

where $\sigma(\tau)$ is the variance of log-returns $r(t,\tau) = S(t) - S(t-\tau)$ computed with the lag τ. Excess kurtosis $k = 0$ means the absolutely normal distribution. Values bigger than zero indicate deviations from it. Brown and Warner (1985) demonstrated that in the stock market excess kurtosis is usually below 4; Cont (2001) mentioned that for S&P 500 futures the value is around 16; the kurtosis is equal to 60 for Dollar/Swiss Franc futures; in Gençay et al. (2001) one can find that for USD FX rates it is roughly 30 (through 10 minutes lag intervals).

Excess kurtosis is typically positive when time lag is relatively small and it tends to zero as the lag increases. This fact is called the aggregated normality or aggregational Gaussianity

and can be accounted for by the 'mixture of normals' (Antypas, Koundouri, and Kourogenis 2013). We select several increasing time lags to demonstrate that the distribution of returns produced by the agent-based model has distinct excess kurtosis. The values of the kurtosis are expected to be dependent on the selected scale. Thus, the aggregated normality is the third benchmark in our set.

The scale-invariance of the absolute price change (return) to the period of time when it occurs (Müller et al. 1990; Mantegna and Stanley 1995; Michel M Dacorogna et al. 2001) is the fourth selected benchmark. There is no agreement on the origin of this invariance called scaling law or power law and various assumptions can be found in the literature (Bouchaud 2001; Farmer, Lillo, et al. 2004; Joulin et al. 2008). Its omnipresence in finance incentivised scientists to apply it for real financial problems such as risk management and volatility modelling (Ghashghaie et al. 1996; Gabaix et al. 2003; Di Matteo 2007). We check whether the returns generated by the directional-change agent-based model are also characterised by this power law.

Most of the scaling laws found in financial markets rely on intervals measured in physical time. It is the essential fact to be aware of constricting any model of the real financial system. As it was discussed in Section 2.2, measures of the market's dynamic performed in physical time are not efficient in catching extreme events. Physical time does not adjust its flow to the speed of actions affecting the market. The extreme events, in turn, are the most critical information for statistical analysis. On the other hand, agent-based models are neither capable of 'feeling' the flow of physical time (they are a piece of code, after all). Therefore, it is not a trivial question of how one can connect the sequence of actions performed by simulated agents to real seconds, days and years. For example, the scale of volatility has a direct impact on the number of observed directional-change intrinsic events (see Figure 2.1). Each intrinsic event is a signal for the corresponding agent who registered it. Thus, the volatility clustering means compression and expansion of the inner clock used by the agent-based model. The exact way of how the agent's activity relates to the speed of physical time should be algorithmically predetermined. The assumption that the agents make decisions at equidistant moments of time, for example, every second, is the most popular approach used to bridge the gap between physical and intrinsic time in agent-based modelling. In this case, for instance, 20 000 000 steps in intrinsic time would correspond to 231.5 trading days (that is, close to a full trading year or 252 days). To validate the model by the traditional benchmarks, we follow the same principles and postulate that price changes can be observed only over discrete moments of time.

2.4.2 The Ultimate Benchmark

Scaling laws are ubiquitous properties of our world and are present in any domain of natural and social phenomena such as physics, biology and social sciences (Andriani and McKelvey 2007). The goal of the agent based model is the simulation of a collection of returns statistical properties of which coincide with the ones typical for the real financial markets. Therefore, it is also important to consider such omnipresent scaling properties while validating artificial sets of interacting agents.

The traditional benchmarks mentioned in the previous section can be successfully applied for describing processes and actions happening in the real world. Time is the universal measure of actions and interactions in such real environment. Therefore, all these benchmarks account for physical time as the factor of scale. Unfortunately, the artificial agents have no 'feeling' of elapsed periods and operate using the 'signal-reply' logic only. Therefore, applying these benchmarks as well as methods and tools where time plays the crucial role for interpreting the agents' automated actions is not fully correct. We consulted the work of Glattfelder, Dupuis, and Olsen (2011) in the search for a new omnipresent property of high-frequency markets which can be ultimately used to verify any agent-based model. The main criteria: it should be possible to employ the property as a benchmark independently on the relation of physical time and the sequence of agents' actions. Fortunately, there is one, out of 12, newly described scaling laws which perfectly fits the mentioned criteria: the 'overshoot scaling law'. It is fully based on the directional-change concept where only relative price moves dictate sequences of events dismaying time intervals between them. According to Glattfelder, Dupuis, and Olsen (2011) the average length of the overshoot section is approximately equal to the size of the directional-change threshold. Golub et al. (2014) analytically showed that in the continuous process with zero trend the probability of overshoot $\omega(\delta)$ reaching the length l equals to $\exp(-l/\delta)$, i.e.

$$\mathbb{P}(\omega(\delta) = l) = \exp\left(-\frac{l}{\delta}\right). \tag{2.7}$$

This dependence reveals the exponential relation between the length of a directional-change threshold δ and the expected length of the overshoot $\omega(\delta)$. From equation (2.7) it follows that the expected overshoot $\mathbb{E}[\omega(\delta)]$ is equal to the size of the directional change threshold δ:

$$\mathbb{E}[\omega(\delta)] = \delta. \tag{2.8}$$

Glattfelder, Dupuis, and Olsen (2011) have empirically shown that the average coefficients E_{OS} and C_{OS} of the overshoot scaling law $\langle\omega(\delta)\rangle = \left(\frac{\delta}{C_{OS}}\right)^{E_{OS}}$ across all 13 currency pairs analysed in the work are $E_{OS} = 1.04$ and $C_{OS} = 1.06$. Lowest and the highest registered

values specific for the pairs are: $C_{OS,low} = 0.98$, $C_{OS,high} = 1.17$; $E_{OS,low} = 0.98$, $E_{OS,high} = 1.08$. This statistical property is fully agnostic to the volatility and does not relate on any values defined in physical time. Its application as a benchmark to an agent-based model does not require any additional assumption on the connection of agents' activity and the flow of real physical time. Therefore, we call that scaling law as the main benchmark of our model.

We used the same notation proposed in Glattfelder, Dupuis, and Olsen (2011) to validate scaling laws mentioned above. We build log-log plots where on X- and Y-axis the base and dependent values of scaling laws are placed. We assume a linear relationship between the response variable Y (for example, the average size of price returns) and the fixed variables X (for example, a period of time): $Y = A + BX$, where A and B are unknown parameters to be estimated. Thus, B defines the slope of the line on the log-log plot and A is the intersection of Y-axis. In this way, a scaling law takes the following form:

$$y = \left(\frac{x}{C}\right)^E, \tag{2.9}$$

where $y = \exp Y$, $x = \exp X$, $E = B$ and $C = \exp(-A/B)$.

2.5 Results

In this chapter, we highlight the main findings of the research work and review how components of the agent-based model affect the properties of the generated time series.

All experiments have been performed in two steps. First, we analysed time series generated by the agents from the entire grid operating simultaneously; second, we examined the effects induced by I or III part of the grid being performing solely. The following two sub-chapters outline details of each experiment.

2.5.1 The Entire Grid

As the first step, we tested the performance of the whole grid of directional-change agents. Parameters of the experiment are specified in Section 2.3. An example of 10 price curves generated by the model with the help of the squared root impact function (2.2) is presented in Figure 2.5. The curves consist of various intervals with plateaus and sudden jumps thus mimicking features of the real FX market. At the same time, there is no any prevailing trend which would define the evolution of each given price curve. The red line represents the average aggregated return computed as the result of 1000 independent simulations. This line remains horizontal throughout all 10 000 steps. The latter confirms that the model where all agents participate in the trading does not possess any deterministic impact on the trend.

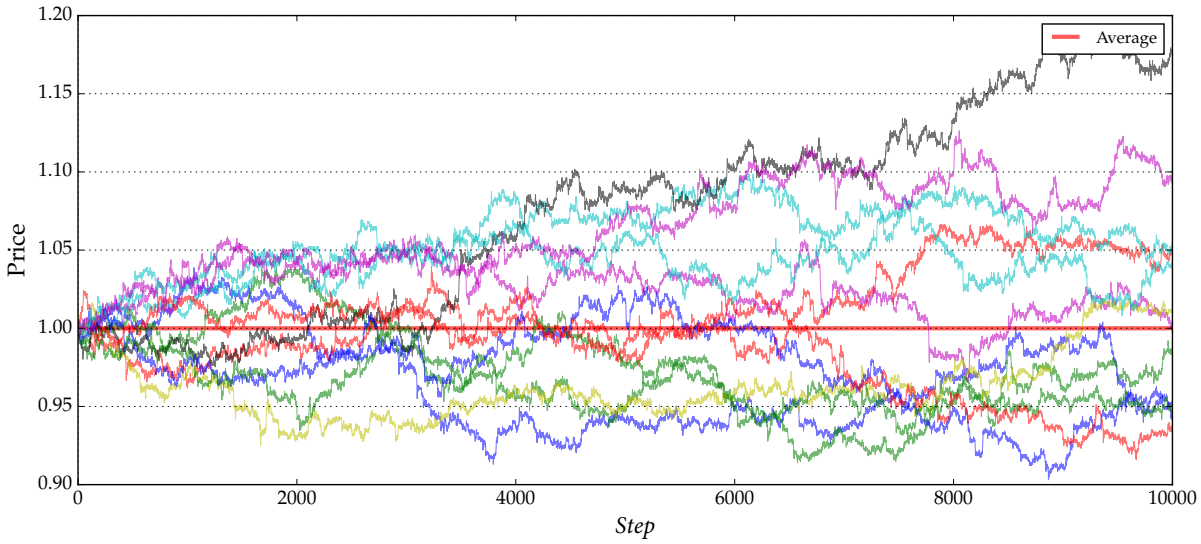

FIGURE 2.5: 10 time series generated by the agents from the entire grid of 50 by 50 equally distributed points (see Figure 2.3). The presented price curves were obtained by applying the exponential function to the set of logarithmic returns generated by the model: $Price = \exp(S_{log}/1000)$. Here 1000 is just a scaling factor.

Benchmarks introduced in Section 2.4 were applied to validate the synthetically generated data sets. Autocorrelation function (ACF) of a time series consisting of 10 000 000 simulated returns is shown in Figure 2.6a. The maximum negative correlation (-0.32) is observed for the lag size equal to one step. The rest of the autocorrelation values is significantly smaller. The autocorrelation function rapidly decays and becomes indistinguishable from zero after about ten steps.

Figure 2.6b shows slowly decaying autocorrelation functions of absolute returns computed over four different lag steps. The bigger the lag step, the lower the decline of the ACF. This effect confirms the ability of the agent-based model of replicating the slow decay of autocorrelation in absolute returns. That is, the aggregational normality has been successfully validated.

The absolute price change scaling law is shown in Figure 2.7a. C and E are the scaling parameters from equation (2.9) described in Section 2.4.2. R is the Pearson product-moment correlation coefficient. One can clearly observe the linear dependence of the absolute price change and the elapsed time interval expressed in logarithmic values. It is important to highlight that this scaling law employs physical time to measure the intervals between given prices of the time series. There is no academic agreement on the periodicity and intensity of trades assumed to be accomplished by artificial agents in physical time. Both these values are de-

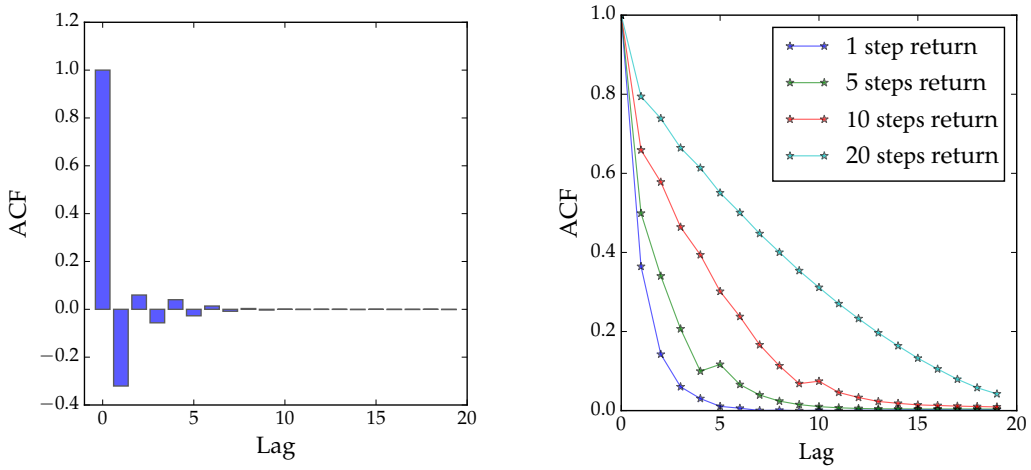

(a) (b)

FIGURE 2.6: **(a)** Autocorrelation function of the generated time series. Lags are measured in the numbers of elementary price moves. **(b)** Autocorrelation function of absolute returns computed on the same time series using four different lag steps.

termined by the assumption made in every particular model. High trades frequency induced big size of price changes over short periods of time. Low frequency results in the opposite. That is equivalent to the compression of time for the same agents' activity level. It leads to the increased or decreased volatility of the process and the bigger or lower slope of the log-log plot $Y = A + BX$ (see Section 2.4.2 for more details). The scaling parameters E and C are directly connected to the coefficients of the plot through equation (2.9). Therefore, the choice of the trade frequency in physical time directly affects the obtained scaling coefficients of the absolute price change scaling law. As results, it is not possible to compare the parameters observed in the FX markets with the ones generated by the model. Nevertheless, the fact that the absolute price change of generated returns depicted in Figure 2.7a is represented by a straight line on the log-log plot (described by a power law function) is enough to confirm the successful replication of the absolute price change scaling law.

Figure 2.8 shows distributions of returns generated by the model. The returns are computed over four gradually increasing lags: 10, 50, 100, and 1000 steps. As it can be seen from the figure, the distributions with lags up to the hundreds of steps (figures 2.8a, 2.8b, and 2.8c) are characterised by noticeable fat tails. The fat tails disappear around the lag level of 1000 steps (Figure 2.8d). Assuming that the agents generate a new return every minute, the observed effect is in line with empirical results found in real markets (for example, values from Kullmann et al. (1999)). Measured excess kurtosis k is equal to 2.73 at 10-steps lag and only 0.06 when the lag rises to 1000 steps. The excess kurtosis rapidly decreases together with the growing

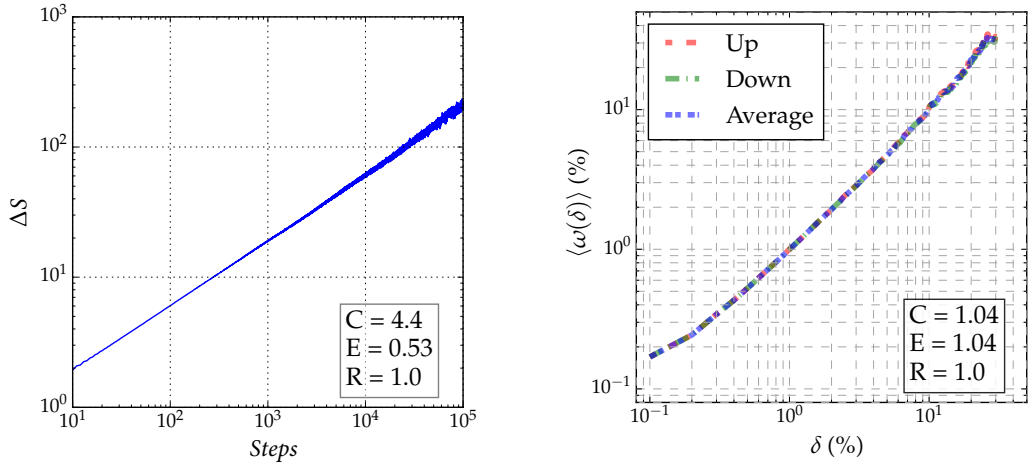

(a) (b)

FIGURE 2.7: **(a)** Average absolute price move as the function of the number of steps (the absolute price move scaling law). **(b)** Overshoot scaling law build from a time series generated by the agents from the entire grid. Parameters on the plot correspond to the average line. Approximation was done for $\delta > 0.3\%$. The same equation provided in the description of Figure 2.5 was used to transform thresholds from absolute values to relative ones (into percentage terms). Coefficients of the Up line: $C = 1.04, E = 1.05, R = 1.0$; of the Down: $C = 1.03, E = 1.03, R = 1.0$. The plot is based on 20 000 000 steps.

lag size confirming the empirically observed dependence. We present two probability plots for lags of 10 and 1000 steps in Figure 2.9. The probability plots confirm the aggregated normality once again. Nevertheless, the empirical analysis of Kullmann et al. (1999) shows that the excess kurtosis at such small lags is usually much higher ($k = 10$ and more). The intrinsic time agent-based model can also be used to generate returns characterised by the size of the kurtosis typical for the real price data. The size of the grid and thus the quantity and the diversity of trading agents directly contribute to the excess kurtosis. The grid 50 by 50 points produces returns with $k = 2.73$ at 10-steps lag; the grid 100 by 100 points result in $k = 3.46$; the grid 200 by 200 points generates time series with $k = 6.01$.

Finally, we validated the agent-based model using the properties of the overshoot scaling law. The log-log plot of the average overshoot length versus the size of the directional-change threshold was constructed (Figure 2.7b). The revealed dependence appears to be linear. The scaling parameters are $E = 1.04$ and $C = 1.04$. These values are exceedingly close to the ones observed in the real foreign exchange market (see Section 2.4.2). We also investigated two supplementary versions of the overshoot scaling law in addition to the one described in Glattfelder, Dupuis, and Olsen (2011): the dependence computed using only overshoots following upward directional changes (red dashed line in the figure) and only overshoots

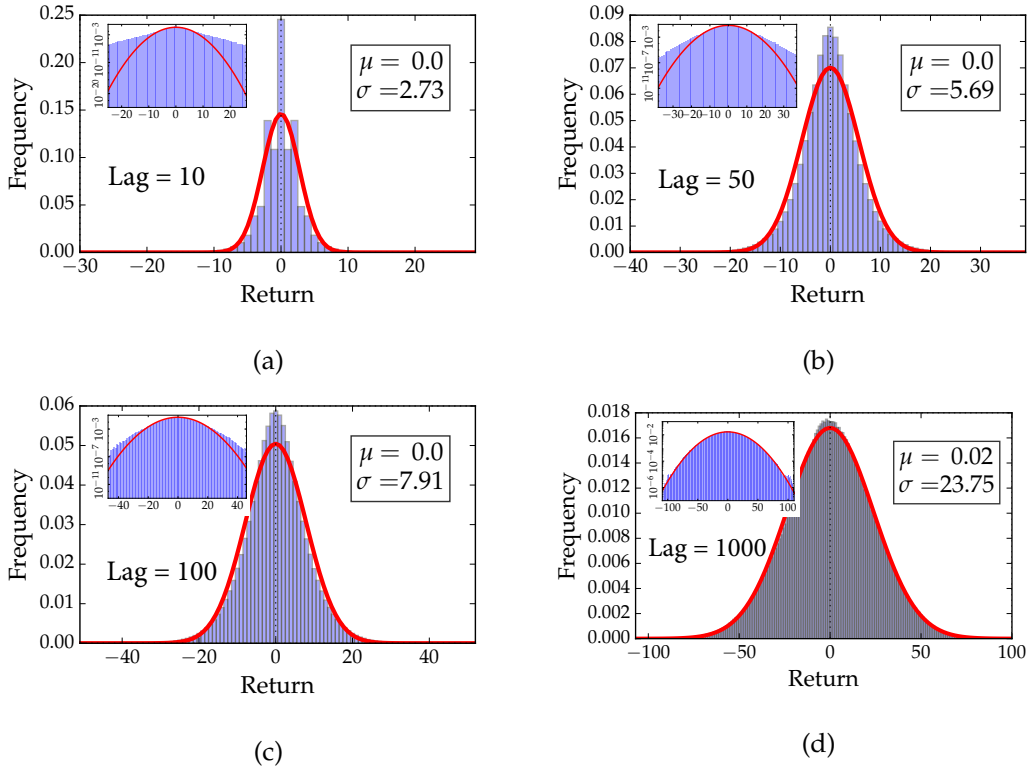

FIGURE 2.8: Distribution of returns generated by the agents from the entire grid and computed at four different lags. Their approximation by the Gaussian function is marked by red lines. Included sub-plots are the same distributions but presented in the logarithmic scale.

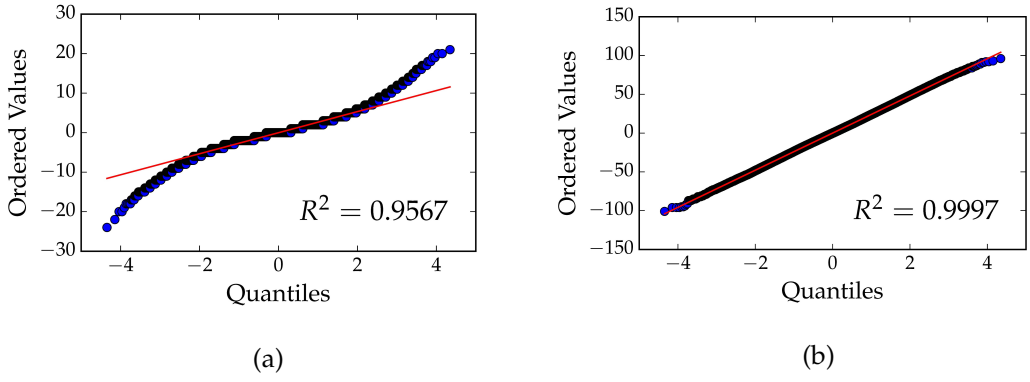

FIGURE 2.9: **(a)** Probability plots of returns computed with the lag equal to 10 steps. **(b)** Probability plots of returns computed with the lag equal to 1000 steps. The total number of prices in the generated time series is 10 000 000.

following downward directional changes (green dashed line). There is no noticeable difference between all three lines. This observation confirms that the directional-change agent-based model is able to reproduce the overshoot scaling law. Results of the experiment are also in line with the theoretical equations (2.15) and (2.15) provided in Appendix 2.A.

Markets react to exogenous shocks such as news in multiple ways (Frank and Sanati 2018). Positive and negative news could as permanently change the preceding price trend as well as make a short-term disturbance. The latter can become rapidly absorbed by the system or become pronounced in the corresponding price change. This sort of price change might be also observed as instantly after the respective event as well as over significantly longer period. We checked how the agent-based model operating in intrinsic time reacts to instant shocks of various amplitudes. Each shock was simulated by a small portion of extra volume on the sell or the buy side added to the net volume. The Monte Carlo simulation demonstrated that the extra volume added to the net volume at the arbitrary step has instant and permanent impact on the average return. The size of the impact is defined by equation (2.2). Results of the simulation can be requested from the authors.

Volume impact function connects the net volume generated by the set of agents at time t with the induced price change observed at $t + 1$. The square root dependence (2.2) was selected for the agent-based model although there is no scientific agreement on the universal form of the functions. Therefore, linear and logarithmic impacts have also been tested in our work. Statistical properties of time series generated with the help of these impact functions were considered. We found that the observed properties do not resemble stylised facts of FX markets better. The linear impact induces rapid price fluctuations around the initial level and none of the statistical properties become observed. In turn, time series generated using the logarithmic dependence expectantly have similar properties to the ones of time series produced with the help of the squared root. The fat-tailed distribution of returns is of the same scale for both functions. Nevertheless, scaling coefficients of the overshoot scaling law become noticeably worse in case of the logarithmic impact. The coefficients are: $C = 0.86$, $E = 0.95$, $R = 0.16$ for the linear impact; $C = 1.38$, $E = 0.99$, $R = 1.0$ for the logarithmic impact; $C = 1.04$, $E = 1.04$, $R = 1.0$ for the squared root function (2.2).

The linear distribution of thresholds and the squared shape of the grid are aimed to replicate the diversity of real groups of traders in FX markets. The selected parameters only approximately replicate the composition of the trading strategies existent in the real world. Nevertheless, we experimented with different sets of thresholds, such as their logarithmic distribution as well as the radial fit and the circular shape of the grid. The obtained performance of the agent-based model was close to the one offered by the simple squared grid whenever the number of agents remains substantial.

2.5.2 Asymmetric Regions

The entire grid of directional-change agents generate time series with zero average trend (Section 2.5.1). We claim that the reason of the observed phenomenon is the selected symmetry of the grid: to each agent from the region I with not equal thresholds δ^I_{up} and δ^I_{down} there is an agent in the region III with thresholds δ^{III}_{up} and δ^{III}_{down} such that $\delta^I_{up} = \delta^{III}_{down}$ and $\delta^I_{down} = \delta^{III}_{up}$. To confirm the statement, we performed a series of tests where the imbalance of trading agents was created. The imbalance is achieved by removing a part of agents from the initial grid. The effect observed in the test is the clearly pronounced non-zero average trend of the generated time series. We demonstrate results of two trivial experiments where only agents from the region I or region III have been selected to trade (Figure 2.10). The induced deviations of the average trend are upward and downward correspondingly. The permanent trend observed in both experiments is present due to the created imbalance between the number of agents supporting trends of opposite directions. Agents from the region I tend to trade more often when the price is going down while agents from the region III prefer the rising trend.

Several factors affect the average slope of all generated price curves: the total number of agents forming the initial grid, the section of the grid used to generate a time series, the selected time interval between two consecutive steps. We performed a set of experiments to visualise the impact of the created grid asymmetry on generated prices. An extra directional-change agent with the specific pair of thresholds was added to the initial set of agents forming the 50 by 50 points grid. This resulted in $2500 + 1$ agents trading simultaneously. We show in Figure 2.14 the distribution of final aggregated returns after 10 000 steps averaged over 1000 independent simulations. Additional agents with symmetric thresholds $\delta_{up} = \delta_{down}$ have no pronounced impact on the average aggregated return (parameter μ of the Gaussian distribution used for approximations) as well as on the standard deviation (parameter σ). Agents with asymmetric thresholds tend to deviate the average trend in the direction which coincides with the direction of their bigger thresholds. The deviation is bigger in case of smaller δ_{up} and δ_{down}. Agents with such thresholds are similar to high-frequency traders and eager to react to all trend changes. As result, they make more trades than the traders with substantially bigger directional-change thresholds (see Figure 2.12a). These facts explain the observed phenomenon. A set of overshoot scaling laws computed using the data generated in each experimental setup is presented in Figure 2.15. It is worth noting that lines related to the upward and downward overshoots are symmetrically shifted from the diagonal line.

The number of agents participating in the trading effects the excess kurtosis of generated returns (see Section 2.5.1). Grids of different sizes were tested to investigate whether there

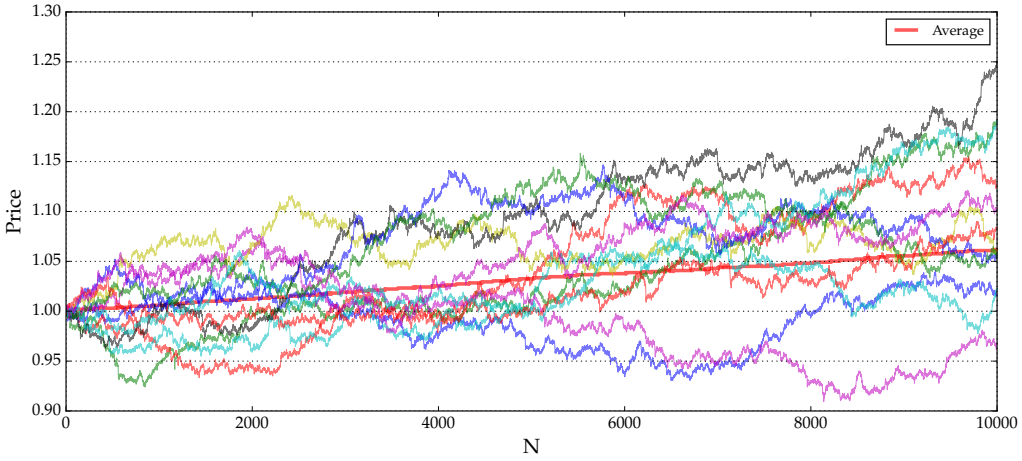

(a)

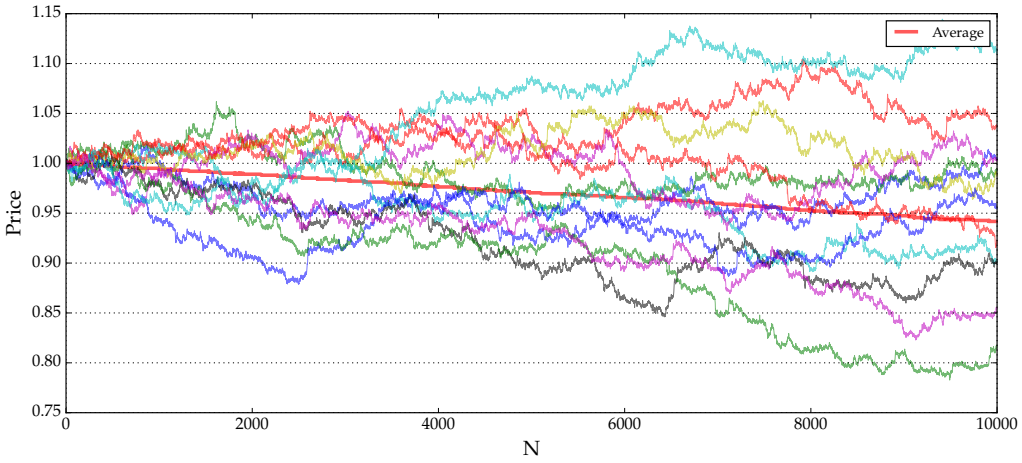

(b)

FIGURE 2.10: **(a)** Time series generated by agents from the region I of the initial grid and **(b)** by agents from the region III. Red lines represent average prices based on 1000 independent simulations. The initial grid size is 50 by 50 points.

is any other impact. Only agents from the I region were involved in the experiment. The average aggregated returns of 1000 independent simulations are shown in Figure 2.12b. As it can be seen from the figure, the bigger the size of the grid, the higher the deviation of the aggregated trend from the trend-less case. The net volume which is the only parameter of the impact function (2.2) is the reason of the observed deviation. Bigger number of agents creates higher standard deviation of the net volume. The latter induces the revealed in Figure 2.12b dependence of the grid size and the average trend. The dependence has been also confirmed in another experiment results of which are presented in Figure 2.16. The average positive and negative volumes generated by the model were computed as the function of the grid size. The

experiment proves the statement that the bigger the size of the grid, the higher the generated absolute net volume.

We would like to note that the stylised facts selected for this project are still reproduced even when a part of the agents from the grid is deactivated. In Figure 2.13 we include overshoot scaling laws computed using the data generated by two separate parts of the grid: by region I (Figure 2.13a) and region III (Figure 2.13b). The scaling coefficients C and E of studied dependencies insignificantly differ from the ones observed empirically in Glattfelder, Dupuis, and Olsen (2011). Therefore, we claim that the agent-based model operating in directional-change intrinsic time can be used to simulate financial time series with statistical properties closely related to high-frequency markets. Moreover, the trend of the collection of generated returns can be specifically predefined. The set of the directional-change agents is the parameter which can be used to setup the trend. A comprehensive analysis of its precise direction is a topic for an independent work which is beyond the scope of this research paper.

2.6 Conclusion

An agent-based model where trades happen in directional-change intrinsic time was tested in this work. A set of artificial agents mimics the behaviour of real market participants by buying/ selling one lot of the traded asset. All trades happen at the moments when the directional-change intrinsic time ticks. Two types of intrinsic events are considered: directional changes and overshoots. Directional changes are moments when the price curve makes reversals equal to the size of the selected threshold. Overshoot intrinsic events happen every time when the overshoot length is a multiple of the of the corresponding directional change threshold. The agents flip their opened positions from long to short and vice versa at times when they observe intrinsic events of given magnitude. They flip the positions with the empirically and theoretically found probability to register a new overshoot event before the directional-change one. The probability is aimed to mimic behaviour of real market participants who do not exploit every trading opportunity. Traders' decisions are not conditional on time intervals between registered intrinsic events. The agents are ignorant to the flow of physical time and consider prices as the only source of information about the market's activity needed to perform.

The agent-based model replicates a wide range of trading patterns observed in the real world. A unique pair of directional-change thresholds was assigned to each simulated trader. The size of the thresholds as well as their ratio define the scale of price trends analysed by each agent. The difference between the number of all agents decided to flip a long or short

position at each new price represented the net volume or imbalance between the supply and demand. The net volume was used to calculate the impact of the imbalanced decisions on the further price change. The empirically observed squared root function connects the net volume and the corresponding market return.

A set of benchmarks was chosen to test the performance of the constructed agent-based model. The model is assumed to be successful if it manages to reproduce 'stylised facts' discovered in the real financial world. The utilised benchmarks: low auto-correlation of returns, fat-tailed distribution of returns, aggregated normality, price jump and the overshoot scaling laws. The last benchmark is fully agnostic to the connection of the simulated agents' actions and the flow of physical time. We propose that the scaling law is the universal test for any agent-based model.

The presented agent-based model operating in the directional-change intrinsic time has successfully passed all chosen tests. The latter lets us make an educated guess that real market participants intentionally or unintentionally make trades using their own intrinsic time. In other words, they have preferences on the scale of price returns after which the traders reverse opened positions. The obtained knowledge can be used to substantially improve the quality of the inferences we make about the connection of the aggregated traders behaviours and observed price changes.

2.A Overshoot as the Function of Trend

The average length of an overshoot section is approximately equal to the length of the corresponding directional change threshold (Glattfelder, Dupuis, and Olsen 2011):

$$\langle \omega(\delta) \rangle \approx \delta. \tag{2.10}$$

This dependence was found not only in historical tick data but also in arithmetic Brownian motion. Nevertheless, the average length of overshoots does not resemble the length of the selected threshold if the time series has a constant trend. In turn, the average overshoot length depends on the size of the trend (Golub, Glattfelder, and Olsen 2017). To find the exact form of this dependence, we select an arithmetic Brownian motion with increments dS_t, trend μ, and volatility σ:

$$dS_t = S_t - S_{t-1} = \mu dt + \sigma dW_t. \tag{2.11}$$

Golub et al. (2014) derived the probability of the upward and downward overshoot to reach some fixed value x. The probabilities are the following:

$$\mathbb{P}(\omega(\delta_{up}) \geq x) = \exp\left\{ -\frac{x}{\sigma^2} \cdot \frac{(|\mu| - \mu) + (|\mu| + \mu) \exp\left\{ -\frac{2|\mu|\delta_{up}}{\sigma^2} \right\}}{1 - \exp\left\{ -\frac{2|\mu|\delta_{up}}{\sigma^2} \right\}} \right\}, \tag{2.12}$$

$$\mathbb{P}(\omega(\delta_{down}) \geq x) = \exp\left\{ -\frac{x}{\sigma^2} \cdot \frac{(|\mu| + \mu) + (|\mu| - \mu) \exp\left\{ -\frac{2|\mu|\delta_{down}}{\sigma^2} \right\}}{1 - \exp\left\{ -\frac{2|\mu|\delta_{down}}{\sigma^2} \right\}} \right\}, \tag{2.13}$$

where $\omega(\delta_{up})$ and $\omega(\delta_{down})$ stand for upward and downward overshoots correspondingly.

The expected value of the shown probability equations (2.12) and (2.13) $\overline{\mathbb{F}}(x) = \mathbb{P}(X \geq x)$ is

$$\mathbb{E}[X] = \int_0^\infty \overline{\mathbb{F}}(x) dx. \tag{2.14}$$

Using (2.14) one can find that:

$$\mathbb{E}[\omega(\delta_{up}, \mu, \sigma)] = \frac{\sigma^2 \left(1 - \exp\left\{ -\frac{2|\mu|\delta_{up}}{\sigma^2} \right\}\right)}{(|\mu| - \mu) + (|\mu| + \mu) \exp\left\{ -\frac{2|\mu|\delta_{up}}{\sigma^2} \right\}}, \tag{2.15}$$

$$\mathbb{E}[\omega(\delta_{down}, \mu, \sigma)] = \frac{\sigma^2 \left(1 - \exp\left\{ -\frac{2|\mu|\delta_{down}}{\sigma^2} \right\}\right)}{(|\mu| + \mu) + (|\mu| - \mu) \exp\left\{ -\frac{2|\mu|\delta_{down}}{\sigma^2} \right\}}. \tag{2.16}$$

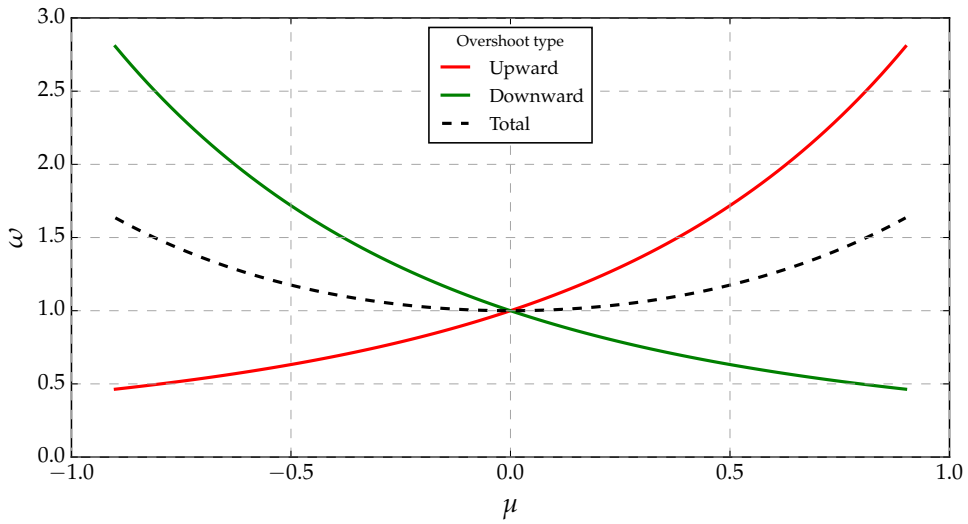

FIGURE 2.11: Expected length of the overshoot section ω as the function of trend μ computed using equations (2.15) and (2.16). The variance σ and threshold δ are fixed and equal to 1.

The expected length of the all overshoots is the average of upward and downward expected overshoots (equations (2.15) and (2.16)):

$$\mathbb{E}[\omega(\delta_{up}, \delta_{down}, \mu, \sigma)] = \frac{\sigma^2}{2}\left(\frac{1-\exp\left\{-\frac{2|\mu|\delta_{up}}{\sigma^2}\right\}}{(|\mu|-\mu)+(|\mu|+\mu)\exp\left\{-\frac{2|\mu|\delta_{up}}{\sigma^2}\right\}}+\right.$$
$$\left.+\frac{1-\exp\left\{-\frac{2|\mu|\delta_{down}}{\sigma^2}\right\}}{(|\mu|+\mu)+(|\mu|-\mu)\exp\left\{-\frac{2|\mu|\delta_{down}}{\sigma^2}\right\}}\right). \tag{2.17}$$

In Figure 2.11 we demonstrate the dependence of the overshoot length ω on various trends μ when volatility σ and the threshold size δ are fixed. The last two variables are assumed to be equal to one ($\sigma = 1$; $\delta = 1$). It is easy to notice that the lengths of upward and downward overshoots coincide with each other only in case of zero trend. One can observe significant divergence of the curves for any other value not equal to zero. The obtained result is quite intuitive: price tends to overshoot more after an upward directional-change event in case of the overall ascending trend. At the same time, it tends to make a directional-change reversal right after a downward directional-change event. This observation suggests that for each non-zero trend μ there are such thresholds δ_{up} and δ_{down} that the total number of overshoot intrinsic events registered in the given time series is equal to the number of overshoots observed within a time series of the same length and zero trend. This property was directly used in the proposed agent-based model to replicate the diversity of trading patterns (Section 2.3).

2.B Dissection Algorithm

By S_{tick} we mark the latest observed price, by S_{ext} the local extreme, mode is the current mode of the alternating trend which can be equal either up or $down$, δ_{up} and δ_{down} are upward and downward thresholds respectively, S_{IE} is the price at which the latest intrinsic event was observed. The algorithm returns 1 and -1 when the price curve hits levels of upward and downward directional-change events correspondingly. 2 and -2 will be returned in case of overshoot intrinsic events registered on ascending or descending trends.

Algorithm 1: Intrinsic Event

if *first tick* **then**
    $S_{ext} \leftarrow S_{tick}$
    $S_{IE} \leftarrow S_{tick}$
    return 0
else if *mode* is *up* **then**
    if $S_{tick} - S_{ext} \geq \delta_{up}$ **then**
        $mode \leftarrow down$
        $S_{ext} \leftarrow S_{tick}$
        $S_{IE} \leftarrow S_{tick}$
        return 1
    else if $S_{tick} < S_{ext}$ **then**
        $S_{ext} \leftarrow S_{tick}$
        if $S_{IE} - S_{ext} \geq \delta_{down}$ **then**
            $S_{IE} \leftarrow S_{tick}$
            return -2
        else
            return 0
else if *mode* is *down* **then**
    if $S_{ext} - S_{tick} \geq \delta_{down}$ **then**
        $mode \leftarrow up$
        $S_{ext} \leftarrow S_{tick}$
        $S_{IE} \leftarrow S_{tick}$
        return -1
    else if $S_{tick} > S_{ext}$ **then**
        $S_{ext} \leftarrow S_{tick}$
        if $S_{ext} - S_{IE} \geq \delta_{up}$ **then**
            $S_{IE} \leftarrow S_{tick}$
            return 2
        else
            return 0

2.C Additional Experiments

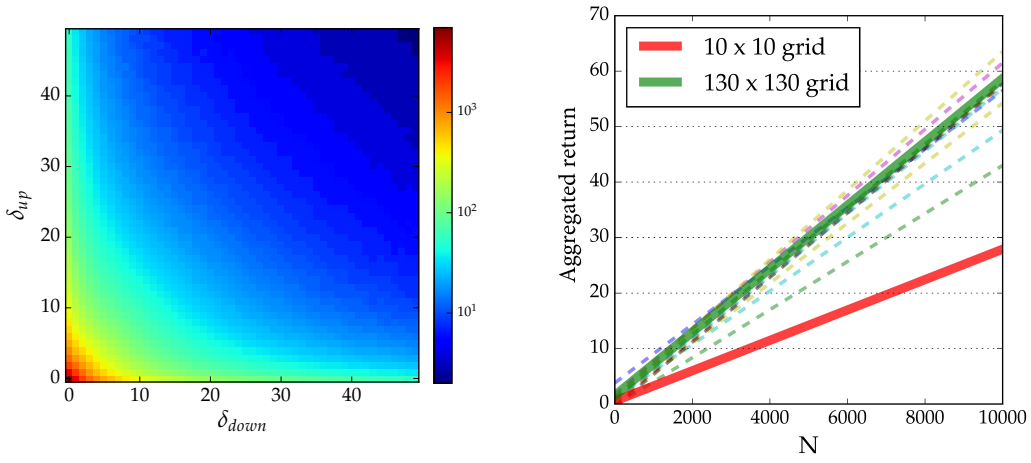

(a) (b)

FIGURE 2.12: **(a)** The average number of trades performed by directional-change agents with parameters δ_{up} and δ_{down} within 10 000-steps simulation. Parameters of the agents used for the simulation are provided in Section 2.3. **(b)** Average aggregated returns recorded within 10 000 steps (N) of 1000 independent simulation when only agents from the region I are active. 13 tests with grids of various sizes were performed. The smallest grid is 10 by 10 points. The biggest is 130 by 130. The applied increment is 10.

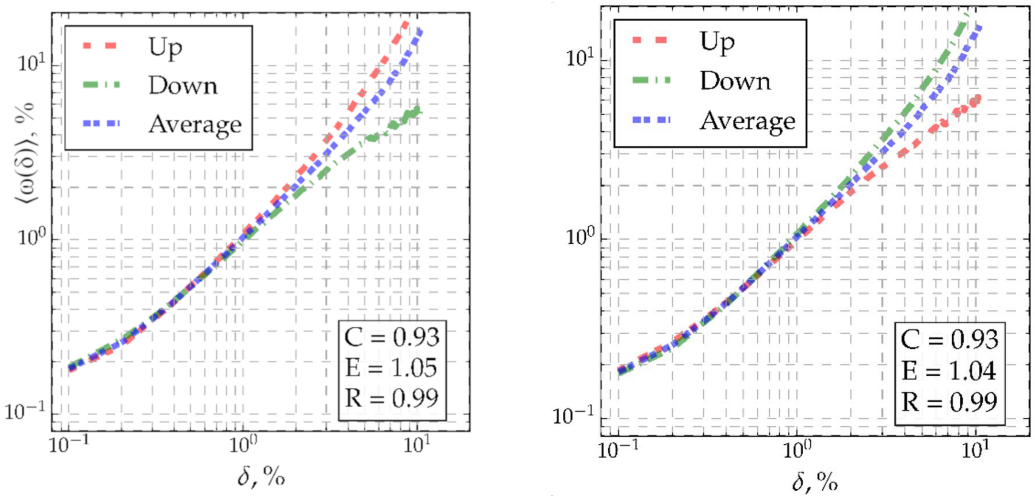

(a) (b)

FIGURE 2.13: Overshoot scaling laws computed using time series generated by the agents from **(a)** *I* and **(b)** *III* regions of the grid only. Red dashed line (Up) corresponds to the average overshoot computed after directional-changes upward. Green dashed line (Down) corresponds to the average overshoot measured after directional-changes downward. The scaling parameters *C*, *E*, and *R* are shown for the lines representing the average overshoot lengths (blue dashed line).

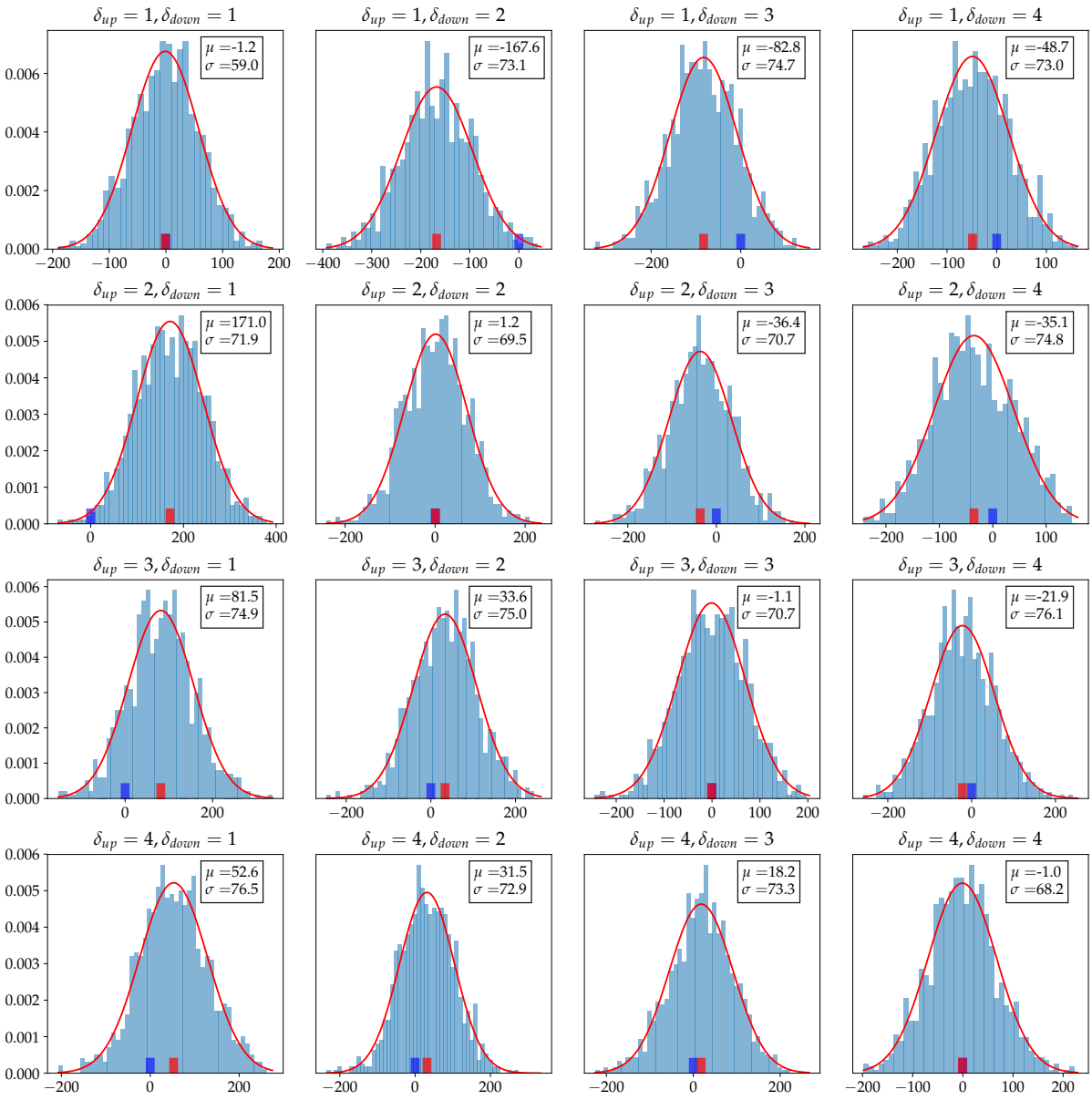

FIGURE 2.14: Impact of an additional intrinsic time agent on the average trend generated by the entire grid. $2500 + 1$ traders participate in each simulation. Parameters of the supplementary agents are put on top of each subplot. Experiment consists of 1000 independent simulations and 10000 steps. Normal distributions (red lines) approximate the final aggregated returns. Blue rectangular mark zero trend level. Red rectangular stand for the centre of the obtained distributions. The subplots are centred on the average aggregated return.

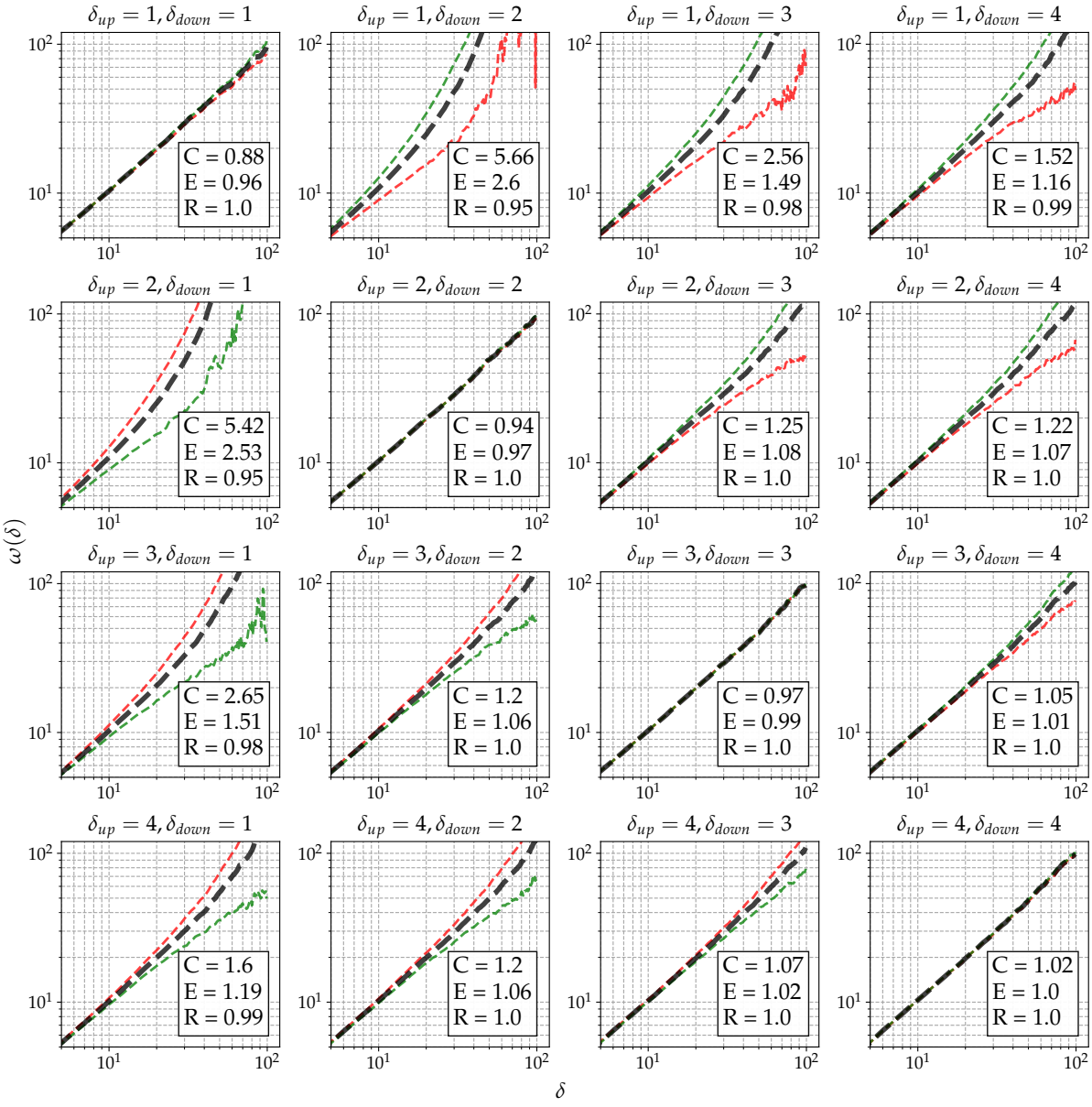

FIGURE 2.15: Overshoot scaling laws computed using the time series generated by the entire grid of agents plus one extra trader (see description of Figure 2.14). Green lines correspond to average overshoots computed on the downward trend and red lines to the average overshoots captured on the upward trend. The black line is the average of both lines. Scaling law coefficients C, E and the Pearson product-moment correlation correspond to the average (black) line.

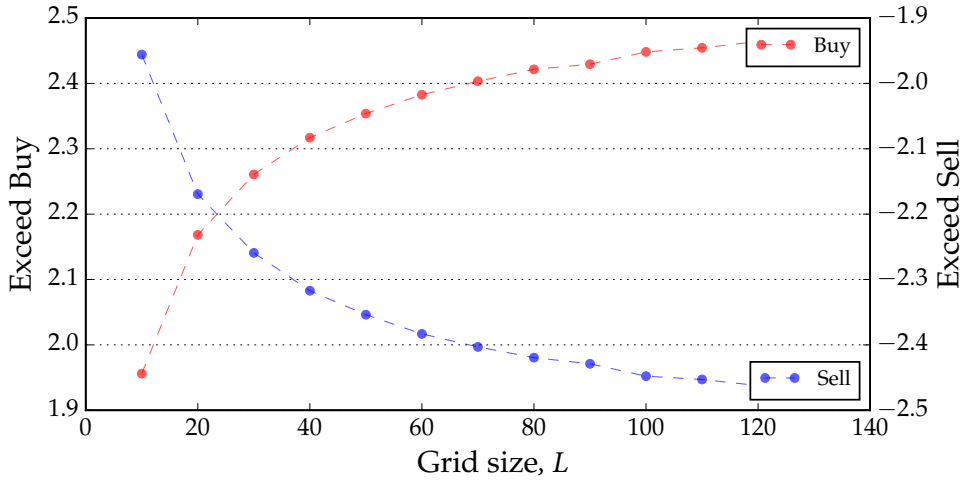

FIGURE 2.16: Positive (Exceed Buy) and negative (Exceed Sell) average net volumes as the function of the grid size. Average total net volume is equal to zero.

3

Instantaneous Volatility Seasonality of High-Frequency Markets in Directional-Change Intrinsic Time

---

Verweile doch! du bist so schön!

— Johann Wolfgang von Goethe

Vladimir Petrov, Anton Golub, and Richard Olsen

A version of this paper is published in: Vladimir Petrov, Anton Golub, and Richard Olsen. 2019. "Instantaneous Volatility Seasonality of High-Frequency Markets in Directional-Change Intrinsic Time." *Journal of Risk and Financial Management* 12 (2): 54.

I have presented it at:

- International Conference on Computational Finance, July 2019, La Coruna, Spain;
- 6th Paris Financial Management Conference, December 2018, Paris, France;
- Financial Econometrics Conference, September 2018, Lancaster, UK.

Abstract

We propose a novel intraday instantaneous volatility measure which utilises sequences of drawdowns and drawups non-equidistantly spaced in physical time as indicators of high-frequency activity of financial markets. The sequences are re-expressed in terms of directional-change intrinsic time which ticks only when the price curve changes the direction of its trend by a given relative value. We employ the proposed measure to uncover weekly volatility seasonality patterns of three Forex and one Bitcoin exchange rates, as well as a stock market index. We demonstrate the long memory of instantaneous volatility computed in directional-change intrinsic time. The provided volatility estimation method can be adapted as a universal multiscale risk-management tool independent of the discreteness and the type of analysed high-frequency data.

3.1 Introduction

All events relevant to the performance of the financial system such as political decisions, natural disasters, or economic reports rarely happen synchronously and are typically not equally spaced in time. A sequence of them has a non-homogeneous nature and is not characterised by any vital autocorrelation function. Ultimately, the change of days and nights, as well as seasons, is dictated by the natural structure of the physical world which is barely connected to the flow of financial activity. Human minds, with the whole diversity of peculiar and indescribable characteristics, are primal engines of all market's evolutionary shifts. The global market, where the majority of transactions happen online and where traders, dealers, and market makers are distributed all around the world, is completely blind and deaf to the periodicity of days and nights, as well as to the climate factors of any standalone region of the Earth. New statistical tools, agnostic to the flow of the physical time, should be employed in order to handle the inner periodicity of the financial activity efficiently. In this work, we explore a concept of the endogenously defined time in finance applied to evaluate seasonality in markets' activity.

Probabilities of price drops and price rises between the running price maxima and running price minima are one of the most well-known risk-factors in finance. These probabilities are also called drawups and drawdowns. Numerous research works have focused on the analysis of the size, periodicity, and the time of recovery associated with drawups and drawdowns in traditional markets. The joint Laplace transform was utilised by Taylor (1975) for deriving the expected time until a new drawup in a drifted Brownian motion occured (traditionally considered as the model for historical price returns). The joint probability of observing a drawup of a given size after a drawdown, during a given term, was analysed as a homogeneous diffusion process in Pospisil, Vecer, and Hadjiliadis (2009). Zhang (2015) derived the joint probability in the context of exponential time horizons (the horizons are exponentially distributed random variables). The authors also described the law of occupation times for both drawup and drawdown processes. These and other theoretical findings connected to the price trend reversals were successfully applied to real financial problems such as studding market crashes.

Market crashes, pronounced in the abnormal price decreases, might severely impact the long-term stability of markets. It is especially important to estimate the probability of the next crash occurrence within a given period of time. Many research works were done on studying the crash probabilities using the normal distribution of price returns as the proxy for the real process. However, extreme price drops occur more often in the real world than what should

happen when the distribution of returns coincides with the normal one. Fat-tailed distributions of returns ground the observed phenomenon. The distributions were discovered in the stock market (Jondeau and Rockinger 2003; Rachev, Menn, and Fabozzi 2005; Koning, Cassidy, and Ouyed 2018), in the Forex (FX) (Michel M Dacorogna et al. 2001; Cotter 2005), as well as in Bitcoin, prices (Liu et al. 2017; Begušić et al. 2018). The fat tails, accompanied by the extensive discontinuity of the price curve (jumps), make the equally spaced time intervals inconvenient for high-frequency market analysis. Research tools, capable of working independently to the price distribution, should be called to deal with the erratic price evolution. Prices, at which drawdowns and drawups of the given size are registered, are independent of the time component of the price progression. Thus, the drawdown and drawups are the concepts especially useful of handling the dynamics of high-frequency markets. A sequence of drawdowns and drawups, following each other, can describe the evolution of a time series purely from the price point of view. The efficient set of forecasting techniques aimed at identifying appropriate conditions for future market crashes should inevitably be supplied by risk-management tools managing sequences of drawdowns and drawups.

In this research work, we investigate the connection between the observed number of alternating drawdowns and drawups (directional-change intrinsic time measure) and the instantaneous volatility. Non-parametric estimation of instantaneous volatility is still a relatively new topic which, to the extent of our knowledge, has not been studied before from the point of view of directional-change intrinsic time. Obtained in the work, analytical expressions are employed to reveal the seasonality structure of instantaneous volatility typical for high-frequency exchange rates. The described tools and experiments contribute to the collection of existing literature on directional-change intrinsic time and the seasonality properties of high-frequency markets. The tools will benefit high-frequency traders whose computer algorithms primarily operate on ultra-short time intervals where the short-term properties dominate over the long-term statistical characteristics (Gençay et al. 2001; Hasbrouck 2018).

Three distinctive markets were considered in the work: FX (EUR/USD, EUR/JPY, and EUR/GBP), stocks (S&P500), and crypto (BTC/USD). All experiments are performed on the time series of the highest granularity: tick-by-tick data. That high granularity is essential considering the substantially growing interest in high-frequency trading after the 2008 financial crisis (Kaya, Schildbach, and Ag 2016). The data corresponds to the recent time period from 2011 to 2018 and is obtained from the largest trading venues (*JForex* and *Kraken*) opened for traders of any size. Each of the time series used in the empirical analysis is at least four years

long. Such an extended length allows us to claim that properties specific for any particular period of time should not be pronounced in the obtained results.

The outline of the remaining paper is as follows. Section 3.2 provides a brief overview of research works on the properties of drawups and drawdowns. Section 3.3 gives detailed reasoning on the need for directional-change intrinsic time and describes a set of literature where the concept was successfully applied. Existing studies on the volatility seasonality of high-frequency markets is provided in Section 3.4. Section 3.5 describes the data used in the experiments and Section 3.6 outlines how the number of directional changes is connected to the instantaneous volatility. In Section 3.7 we present all results obtained by the traditional, as well as the novel, volatility measurement techniques and also describe the application of theta time concept aimed to minimise the seasonality pattern. Section 3.8 concludes the main body of the paper and proposes the potential use of the developed technique. Appendix 3.A concludes the paper by presenting a set of experiments where the comparison of considered markets seasonality patterns is presented.

3.2 Drawdowns and Drawups: An Introduction

Probabilities of financial drawdowns and drawups were extensively studied and presented in multiple seminal research works. Drawdowns of extensive size are usually associated with market crashes. Carr, Zhang, and Hadjiliadis (2011) proposed a new insurance technique aimed to protect investors against unexpected price moves. The authors also covered a novel way of hedging liabilities associated with these risks. Zhang and Hadjiliadis (2012) employed statistical properties of drawdowns as an estimate of the stock default risk and also provided a risk-management mechanism affecting the investor's optimal cancellation timing. In Schuhmacher and Eling (2011) drawdowns are considered as one of 14 reward-to-risk ratios alternative to the widely known performance measures such as the Sharpe ratio. In Grossman and Zhou (1993) and Chekhlov, Uryasev, and Zabarankin (2005) the properties of drawdowns were also applied as an estimate of the portfolio optimisation problem. The latter can be personalised to match traders' or investors' expectations and their tolerance to the size and the length of the market disruption.

Drawdowns D_t and drawups U_t, also called rallies in Hadjiliadis and Večeř (2006), registered by the moment of time t, depend on the running price maxima $\overline{S_t}$ and the running price minima $\underline{S_t}$ (Zhang and Hadjiliadis 2012; Mijatović and Pistorius 2012; Landriault, Li,

and Zhang 2015; Dassios and Lim 2018). These reference points hinge on the set of historical prices S_s and are mathematically defined in the following way:

$$\overline{S_t} = \sup\{S_s : 0 \leq s \leq t\} \quad \text{and} \quad \underline{S_t} = \inf\{S_s : 0 \leq s \leq t\}, \tag{3.1}$$

where $t \geq 0$ and the interval $[0, t]$ is fixed. Drawdowns and drawups are the differences between the final price of the given time interval S_t and the registered local maxima and minima:

$$D_t = \overline{S_t} - S_t \quad \text{and} \quad U_t = S_t - \underline{S_t}. \tag{3.2}$$

The waiting time τ_a^D becomes measured once a price curve experiences a drawdown D_t of the size a. Similarly, τ_a^U is the waiting time associated with a drawup of the size a. In details:

$$\tau_a^D = \inf\{t \geq 0 : D_t \geq a\} \quad \text{and} \quad \tau_a^U = \inf\{t \geq 0 : U_t \geq a\}. \tag{3.3}$$

The waiting time τ_a measures the period of physical time which elapses before the first drawdown (potentially interpreted as a market crash) becomes registered.

3.3 Directional-Change Intrinsic Time

The existing literature on risk-management techniques primarily relies on physical time as a measure of the length and periodicity of financial events. In other words, the existence of a universal clock dictating the evolution of the market prices is assumed. However, the volatilities of different time resolutions behave differently (Müller et al. 1997). The volatility size depends on the scale of the entire time series as well as on the moment when the price activity started to be observed. More robust techniques which are beyond the limits of physical time are needed to handle this stochasticity.

The concept of directional-change intrinsic time (Guillaume et al. 1997) is one of the methods capable of replacing the universal physical clock with intrinsic one. This is an event-based framework which considers the activity of market prices as the indicator of the transition between its different states. The framework dissects a price curve into a collection of sections characterised by alternating trends of the arbitrary defined size. The essence of the concept is closely related to the meaning of drawdowns and drawups: the collection of directional changes following each other can be interpreted as the alternating sequence of drawdowns and drawups. The frequency of price changes in physical time does not play any role in the directional change dissection procedure.

The concept of trend directional changes provided by Guillaume et al. (1997) is capable of connecting the continuous flow of physical time with the endogenous evolution of price

returns. According to the event-based space proposed by Guillaume, only a sequence of price trends continuously alternating in direction has to be considered. The price curve gets dissected into a collection of alternating drawups and drawdowns or trend rises and trend falls correspondingly. Each elementary trend ends once a new price curve reversal is observed. Continuous price moves towards the direction of the latest trend change are called overshoots. The current state of the system changes only at the moments when the trend of the given size reverses its direction. Thus, the set of intrinsic events is decoupled from the flow of physical time. Instead, it depends only on the size of considered drawups and drawdowns labelled by the threshold δ. An example of a price curve dissected into a collection of directional changes is provided in Figure 3.1.

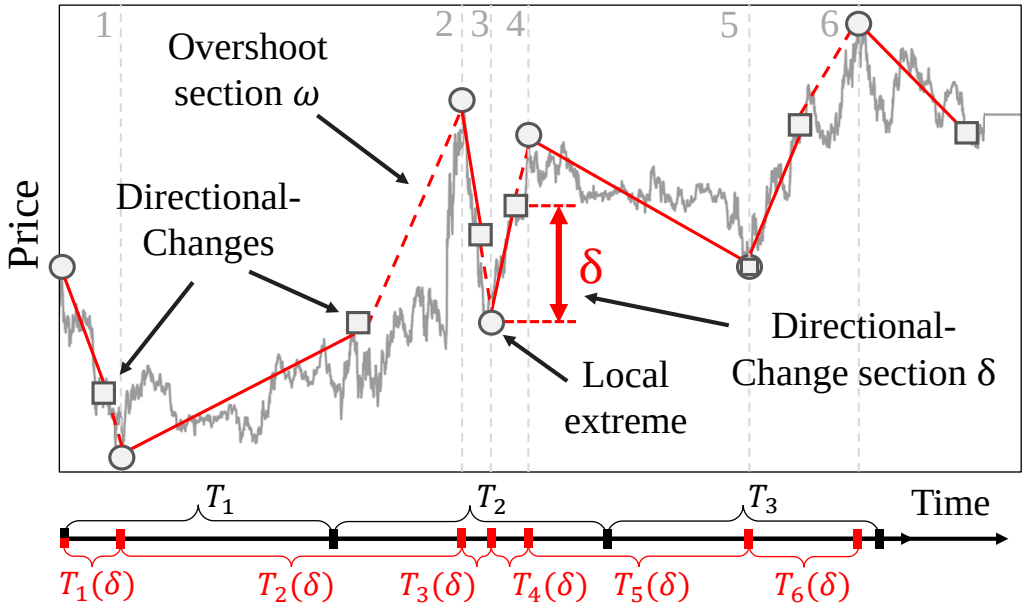

FIGURE 3.1: A part of EUR/USD price curve (grey) dissected into a set of directional-changes (grey squares) using a directional-change threshold δ. The size of the arbitrary chosen threshold is presented in the middle of the figure. Grey circles mark local extremes between two consecutive directional changes. The vertical distance between each directional-change and preceding extreme price is bigger or equal to the size of the threshold δ. Vertical dashed lines indicate the end of each trend section (identified only after the next event becomes observed) and go through the local extremes (circles). The timeline below the plot contains equal time intervals T_1, T_2, T_3 and length of each directional-change section $T_1(\delta), \ldots, T_6(\delta)$.

The density of directional-change intrinsic events depends only on the price curve evolution and the considered trend size. The stochastic nature of price evolution results in the phenomenon depicted in Figure 3.1: non-equal number of intrinsic events (empty squares)

correspond to the equal periods of physical time. The physical interval T_1 contains only the end of the section 1 (sections coincide with the intrinsic events and are separated by the dashed vertical lines) while the equal interval T_2 hosts three segments, namely $2, 3, 4$. This property of directional-change intrinsic time can be engaged as the efficient noise filtering technique: the intrinsic time ignores price changes between directional change. At the same time, it allows us to efficiently capture the most relevant to risk management information: precise moments of all trend changes. The equally spaced time intervals typically employed in the financial analysis are not capable of doing anything of the above: price timestamps, evenly spaced through periods T_1, T_2, and T_3, do not contain information on the extreme price curve activity located in the period T_2. This disability of the traditional price analysis techniques over stochasticity of the market's activity develops into volatility estimators that are too stiff and biased.

The concept of directional-change intrinsic time, applied for studying historical price, returns reveals multiple statistical properties of high-frequency markets. Guillaume et al. (1997) were the first researchers to uncover a scaling law[1] relating the expected number of directional-changes $N(\delta)$ observed over the fixed period to the size of the threshold δ. Mathematically:

$$N(\delta) = \left(\frac{\delta}{C_{N,DC}} \right)^{E_{N,DC}}, \tag{3.4}$$

where $C_{N,DC}$ and $E_{N,DC}$ are the scaling law coefficients. Glattfelder, Dupuis, and Olsen (2011) employed the directional-change framework to discover 12 independent scaling laws which hold across three orders of magnitude and are present in 13 currency exchange rates. Later Golub, Glattfelder, and Olsen (2017) described a successful trading strategy exploiting a collection of tools build upon directional-change intrinsic time. The proposed strategy is characterised by the annual Sharpe ratio greater than 3.0. The persistence of revealed scaling laws became the base elements for the tools designed to monitor market's liquidity at multiple scales (Golub et al. 2014).

3.4 Seasonality

3.4.1 Traditional Markets

The returns seasonality is the well-known statistical characteristic of developed markets such as FX and stocks. Rozeff and Kinney Jr (1976) studied the comprehensive set of historical stock data which spans from 1904 to 1974 and found a higher mean of return in the January distribution of returns compared with most other months. They also underline noticeably

1 A basic polynomial functional relationship where a change in input results in a proportional change in output.

high mean returns in July, November, and December, and low mean returns in February and June. Gultekin and Gultekin (1983) empirically examined stock market seasonality in major industrialised countries. They aimed at investigating the existence and the shape of the stock market seasonality pattern in foreign securities markets. The confirmed seasonal patterns in the stock returns supplied the further understanding of the seasonality anomaly. Seif, Docherty, and Shamsuddin (2017) studied seasonal anomalies in advanced emerging stock markets and provides re-examination of the markets efficiency. The authors did not find the confirmation of the January effect but confirmed the month of the years, the day of the week, the holiday, and the week of the year effects. The recent work Fang, Lin, and Shao (2018) presents a strong link between school holidays and market returns across 47 countries. The authors demonstrate that the returns in the month after major school holidays are 0.6% to 1% lower than at other times. The provided evidence states that post-school holiday small returns are explained by the investors' inattention during these periods. The reduced attention results in news effects being incorporated noticeably slower into prices than within the active trading periods. We also underline the relevance of other research works on the stock market seasonality: Keim (1983), De Bondt and Thaler (1987), and Zarowin (1990), among others.

Daily, weekly, and annually seasonality patterns are also inevitable components of the set of FX stylised facts. Müller et al. (1990) analysed four foreign exchange spot rates against the USD over three years. Authors' intra-day and intra-week analysis show that there are systematic variations of volatility present even within business hours. They also discovered daily and weekly patterns for the average bid-ask spread. Michael M Dacorogna et al. (1993) studied daily and weekly FX seasonality patterns from the geographically distributed trading point of view. The trading activity divided in three general components (East Asia, Europe, and America) was approximated by a polynomial activity function during business hours. The combined model was closely fitted into the empirical volatility (activity) seasonality data. The authors found that strongly seasonal activity autocorrelation can be approximated by the hyperbolic function. Bollerslev and Domowitz (1993) examined behaviour of quote arrivals and bid-ask spreads for continuously recorded deutsche mark-dollar exchange rate data over time, across locations, and by market participant. The authors find the relation of the considered information to the seasonality patterns typically observed in the deutsche mark-dollar exchange rate. Ito and Hashimoto (2006) showed U-shaped intra-day activities of deals and price changes as well as return volatility for Tokyo and London participants of USD/JPY and EUR/USD markets. The authors also note that the U-shape was not found for New York participants. A set of well-known seasonality factors was confirmed: the high activities at the

opening of the markets, high correlations between quote entries and deals, and higher trading activities associated with narrow spreads.

The seasonality of the rapidly evolving cryptocurrency domain is still insufficiently studied in the financial world. The next section unwraps some of the facts about cryptocurrencies and presents outcomes of the previous studies which have to be considered in the current work.

3.4.2 Bitcoin Seasonality

Bitcoin is the first successful pioneer in the crypto domain. It is also the most famous representative of the cryptocurrency markets. Bitcoin was described by Nakamoto (2008) and created in 2008 as an alternative to the classical financial system. The cryptocurrency was rapidly tagged as the "peer-to-peer version of electronic cash". Bitcoin and its underlying technology, blockchain[2], swiftly gained attention from the technologically savvy community and media. The peer-to-peer payment systems soon became one of the most debatable topics at all levels of modern society. Over a thousand alternative cryptocurrencies, based on the similar cryptography concept (Roy and Venkateswaran 2014), emerged since the time Bitcoin was invented. Some part of them became accessible for trading at various electronic venues also known as crypto-exchanges[3].

In contrast to the traditional FX market, cryptocurrency trades happen 24 h per day and seven days per week, independently of the holidays and seasons. Additionally, cryptocurrency trading activity is more uniformly distributed across the globe. There are not many big geographically segregated financial institutions where trades happen according to the working schedule (in contrast to the global FX trading centres described in Michael M Dacorogna et al. (1993)). There is still the limited acceptance of this new financial instrument by international organisations with access to sizable funds[4]. As result, the seasonality patterns prevalent in the world of cryptocurrencies could be incomparable with the ones typical for the FX or stock markets.

High volatility has been one of the most pronounced characteristics of the Bitcoin markets (see, for example, Dyhrberg (2016)). Bitcoin's trend drastically changes and their persistence indicates the aggregated expectations and trading actions of all market participants. Unstable trends also reveals the Bitcoin price sensitivity to exogenous stress factors. The high scale of

2 A growing list of records containing information on the ownership of all existing Bitcoins.

3 Information on all cryptocurrencies and trading venues can be found at Coinmarketcap.com.

4 At the moment of writing the paper, Wall Street and other big financial hubs are considering trading cryptocurrencies, which will potentially result in the higher segregation level.

Bitcoin trend changes attracts researchers to employ modern technologies in order to foresee the future price dynamics (Shintate and Pichl 2019).

There are a few research works concerned with the statistical properties of cryptocurrency markets. Sapuric and Kokkinaki (2014) analysed realised volatility of Bitcoin returns within a 4-year time interval to understand what the prime characteristics of its price activity are. They confirmed Bitcoin's high volatility, but emphasised that traded volume should be taken into account when computing the precise value[5]. The authors compared Bitcoin with conventional financial instruments, including gold, and several national currencies. They demonstrated that the calculated volatility significantly decreases when the traded volumes are included in the model.

Haferkorn and Diaz (2014) studied seasonality patterns of the number of payments performed in three cryptocurrencies: Bitcoin (classified as a worldwide payment system), Litecoin (open source software project), and Namecoin (decentralised name system). Their research confirmed that the monthly or yearly seasonality is not typical for the crypto market. The only robust weekly pattern was found in Bitcoin prices. Litecoin and Namecoin had weak or no patterns at all. The authors state that there is also no significant correlation between the returns of observed exchange rates. Authors speculate about the reason of this phenomenon. They say that these cryptocurrencies have similar core architecture, but they all have been created to serve specific needs.

JE de Vries and Aalborg (2017) made another attempt to discover Bitcoin seasonality patterns. They analysed daily traded volume, daily transaction volume, and Google trends (the number of searches for the word "bitcoin"). The author also inspected the seasonality of the number of transactions performed from individual blockchain accounts. All of the measurements demonstrated no particular periodicity.

Eross et al. (2017) gave a more positive answer on the existence of the most famous cryptocurrency intraday seasonality. The authors investigated Bitcoin returns, volume, realised volatility, and bid-ask spreads to reveal several intraday stylised facts. A significant negative correlation was found between returns and volatility. Volume and volatility were shown to have a considerably positive correlation. The authors attribute such patterns to the European and North American traders, as well as the insufficient number of market makers in the whole crypto space.

5 According to the Bank for International Settlements the daily average FX trading volume in April 2016 was $5.1 trillion (BIS 2016) when the highest registered volume in the crypto market is to the date only $45.8 billion (`https://coinmarketcap.com/charts/`).

The seasonal heteroscedasticity affects the results of statistical studies of intraday and intra-week price properties. The rapidly evolving electronic high-frequency trading is highly affected by the exchange rate seasonality properties too (Cont 2011). Therefore, the returns' seasonality has to be treated at the first priority.

More information on order patterns in time series can be found in the work Bandt and Shiha (2007). The authors determine probabilities of order patterns in Gaussian and autoregressive moving-average processes, which can be directly applied to the financial time series analysis.

3.5 Data

Three FX exchange rates were used in the work: EUR/USD, EUR/JPY, and EUR/GBP. The covered time interval is from January 2011 to January 2016 and includes 109069357, 134737397, and 88704676 ticks correspondingly. The source of the data is the *JForex* trading platform developed by the Swiss bank and marketplace *Ducascopy*, which provides various types of market data in the highest resolution[6].

Bitcoin price changes observed at the *Kraken* crypto-exchange were downloaded from the *Bitcoincharts* online platform supplying financial and technical data related to the Bitcoin network[7]. The studied time interval is from January 2014 to April 2018 and includes 4 778 429 ticks.

The stocks market is represented in this work by the index that currently comprises 505 common stocks listed by 500 large-cap companies on the US stock market: S&P 500 (with the ticker SPX500). The high-frequency data has been downloaded from the *JForex* platform too. The selected dataset spans from January 2012 to January 2017. The total number of ticks is 38931943.

There is a substantial difference in the number of ticks in time series used in the work. The difference reflects the distinct activity in the selected traditional and novel markets. That discrepancy does not undermine the further results since our goal is to apply the novel volatility measurement techniques, which is agnostic to the number of ticks per period of time (see Section 3.3). Moreover, the discrete price impact on the instantaneous volatility will be described in Section 3.7.3. The same is correct for the slight time-span shifts. The compatibility of the results is not affected: the designed experiments aim to depict the statistical properties of the volatility seasonality and not to compare price behaviour at any particular historical moment of time.

6 https://www.dukascopy.com/swiss/english/forex/jforex/.

7 http://api.bitcoincharts.com/v1/csv/.

The fully functional code used in the project can be downloaded from the author's GitHub repository[8].

Inner Price

Any collection of historical prices typically assumes two values: the best bid (buy) and the best ask (sell). These prices are collected from the complete order books specific for the given exchange. The order books contain all clients orders submitted in the market at the given moment. The non-zero price difference between the best offers on the sell and buy sides, called spread, indicates the level of a market's liquidity (Bessembinder 1994; Menkhoff et al. 2012; Dyhrberg, Foley, and Svec 2018). It also has a direct connection to realised volatility (Bollerslev and Melvin 1994), and is an indicator of the transaction cost (Hartmann 1999). Another role of the spread is to show the extent of uncertainty the market has on the fair price of the traded asset. The size of the spread constantly changes over time, together with the level of uncertainty. This fact does not allow us to employ only bid or ask prices to study properties of the whole market at the micro level since some part of the information is in the risk to be lost while analysing intraday data. The average of these two values (mid-price) is also not the best alternative since it does not keep the knowledge on the size of the current spread. Therefore, an alternative measure should be chosen to apply the directional-change algorithm to the real data analysis.

The trend-dependent concept of inner price was selected to resolve the spread issue. Inner price, specific for the given moment of time, is defined as the bid or the ask price depending on the direction of the current trend. In other words, it is the price where the spread is deduced. The following example demonstrates details of the concept. According to the directional-change algorithm, one should wait for the price increase by δ percents from the local price minimum to register a new directional change if the current trend is downward. In this case, the value of the inner price coincides with the best price on the offer side of the order book, that is, the ask price. A new intrinsic event will tick only when the distance between the latest bid price and the inner price reaches the size of the chosen directional-change threshold δ. Alternatively, the inner price takes the value of the best bid price, and the distance is measured between the newest ask and the extreme if the current mode is upward.

8 https://github.com/VladUZH/VlPetrov.

3.6 Methods

Theoretical researchers mostly rely on the Brownian motion as the proxy for price returns of real financial markets (one of the most famous examples is the work of Black and Scholes (1973)). The analogy between historical price moves and changing coordinates of an ensemble of molecules in thermodynamics is the motive behind this common approach. Osborne (1959) shows in the classical work that the steady-state distribution of log-returns in the stock market is the probability distribution for a particle in Brownian motion. It is important to emphasise that at the telegraph-driven time of Osborne's publication (1959) the structure and the dynamic of the market was very different from the ones typical for our modern digital world. The present-day trading has almost completely moved to the digital online space instead of the physical trading floors where all deals happened more than a half a century ago (see Harris (2003) for the historical endeavour on the evolution of trading and exchanges). In this space, a signal can easily propagate through international borders with the speed of light. It stipulated the majority of trades to happen in a fully automated way. The significantly bigger diversity of the market participants and the ability of the high-frequency trading made the financial stylised facts more important today than ever. The stylised facts describe the deviations of real price returns from the theoretical Brownian motion (see Cont (2001) for the set of stylised empirical facts). Nevertheless, in our work, we will operate with Brownian motion as the core for the analytical part of the research.

The choice of Brownian motion, employed in this work, is justified by two reasons. First, the statistical properties of the number of directional-change intrinsic events, studied in this work, is agnostic to the flow of physical time. Second, the divergence of empirical results from the properties of the selected model, if any, helps in understanding the features of the real markets better.

3.6.1 Waiting Time

We model the set of prices $\{S_t : t \geq 0\}$ as an arithmetic Brownian motion with trend μ and volatility σ:

$$dS_t = \mu dt + \sigma dB_t. \tag{3.5}$$

In terms of the directional-change intrinsic time framework, $T_{up}(\delta_{up})$ denotes the time for an upward directional change of the size $\delta_{up} > 0$ to unfold. In other words, it is the time

interval which passes until the price increases by δ_{up} percents from the local minimum m_t. Technically:

$$T_{up}(\delta_{up}) = \inf\{t > 0 : \frac{S_t - m_t}{m_t} \geq \delta_{up}\}, \tag{3.6}$$

where

$$m_t := \inf_{\epsilon \in [0,t]} S_\epsilon. \tag{3.7}$$

Similarly, $T_{down}(\delta_{down})$ is the time of a downward directional change of the size $\delta_{down} > 0$:

$$T_{down}(\delta_{down}) = \inf\{t > 0 : \frac{M_t - S_t}{M_t} \geq \delta_{down}\}, \tag{3.8}$$

where

$$M_t := \sup_{\epsilon \in [0,t]} S_\epsilon. \tag{3.9}$$

Both of these equations are also known in the literature as waiting times of drawups and drawdowns (see Section 3.1). It is shown in Landriault, Li, and Zhang (2015) that expected times of a drawup δ_{up} and a drawdown δ_{down} depend on the volatility and the trend of the drifted Brownian motion. It can be mathematically expressed as

$$\mathbb{E}[T_{up}(\delta_{up})] = \frac{e^{-\frac{2\mu}{\sigma^2}\delta_{up}} + \frac{2\mu}{\sigma^2}\delta_{up} - 1}{\frac{2\mu^2}{\sigma^2}}, \tag{3.10}$$

and

$$\mathbb{E}[T_{down}(\delta_{down})] = \frac{e^{\frac{2\mu}{\sigma^2}\delta_{down}} - \frac{2\mu}{\sigma^2}\delta_{down} - 1}{\frac{2\mu^2}{\sigma^2}}. \tag{3.11}$$

Using the Taylor expansion $e^{\pm\frac{2\mu}{\sigma^2}\delta} = 1 \pm \frac{2\mu}{\sigma^2}\delta + \frac{(\frac{2\mu}{\sigma^2}\delta)^2}{2!} + \mathcal{O}(\mu^3)$ and letting $\mu \to 0$, one can recover that in the case with no trend the equation simplifies to

$$\mathbb{E}[T_{up}(\delta)] = \mathbb{E}[T_{down}(\delta)] = \frac{\delta^2}{\sigma^2}. \tag{3.12}$$

These equations establish a scaling law dependence between waiting times of a directional change, volatility, and the selected size of the directional-change threshold. Indeed, in the analysis of Glattfelder, Dupuis, and Olsen (2011) it was empirically found that in the FX market the average waiting time is proportional to the second power of the directional-change threshold δ used to identify alternating trends:

$$\langle T(\delta) \rangle \sim \delta^2. \tag{3.13}$$

The closeness of Equations (3.12) and (3.13) confirms the assumption that the evolution of high-frequency prices expressed in terms of the directional-change intrinsic time has similar properties to the random walk.

3.6.2 Number of Directional Changes

Let $N(\delta_{down}; \sigma, \mu, [0, T])$ denote the number of drawdowns of the size δ_{down} observed within the time interval $[0, T]$ in Brownian motion process with parameters μ and σ. Since the sequence $T_{down}(\delta_{down})_1$, $T_{down}(\delta_{down})_2$,... is the sequence of non-negative, independent, and identically distributed random variables, the sequence $\{\psi_n; n \in \mathbb{N}\}$ where $\psi_n = T_{down}(\delta_{down})_1 + \ldots + T_{down}(\delta_{down})_n + \ldots$ is the renewal point process. Thus, $N(\delta_{down}; \sigma, \mu, [0, T])$ can be considered as the renewal counting process and its values can be found applying the Theorem 6.1.1 of Rolski et al. (2009) (Landriault, Li, and Zhang 2015) to the waiting time Equation (3.11):

$$\lim_{T\to\infty} N(\delta_{down}; \sigma, \mu, [0, T]) = \mathbb{E}[T_{down}(\delta_{down})]^{-1} T = \frac{T\frac{2\mu^2}{\sigma^2}}{e^{\frac{2\mu}{\sigma^2}\delta_{down}} - \frac{2\mu}{\sigma^2}\delta_{down} - 1}. \tag{3.14}$$

Correspondingly, the expected number of drawups $N(\delta_{up}; \sigma, \mu, [0, T])$ takes the form

$$\lim_{T\to\infty} N(\delta_{up}; \sigma, \mu, [0, T]) = \mathbb{E}[T_{up}(\delta_{up})]^{-1} T = \frac{T\frac{2\mu^2}{\sigma^2}}{e^{-\frac{2\mu}{\sigma^2}\delta_{up}} + \frac{2\mu}{\sigma^2}\delta_{up} - 1}. \tag{3.15}$$

Equations (3.14) and (3.15), combined together, give the estimate of the number of directional changes consequently following each other:

$$\mathbb{E}[N(\delta_{up}, \delta_{down}; \mu, \sigma, [0, T])] = \frac{2T\frac{2\mu^2}{\sigma^2}}{e^{-\frac{2\mu}{\sigma^2}\delta_{up}} + e^{\frac{2\mu}{\sigma^2}\delta_{down}} + \frac{2\mu}{\sigma^2}(\delta_{up} - \delta_{down}) - 2}. \tag{3.16}$$

The expression is simplified in the trend-less case ($\mu \to 0$) to the following form:

$$\mathbb{E}[N(\delta_{up}, \delta_{down}; \sigma, [0, T])] = \frac{2T\sigma^2}{\delta_{up}^2 + \delta_{down}^2}. \tag{3.17}$$

The theoretical dependence of the number of directional changes and the properties of underlying process resemble the empirical observations of Guillaume et al. (1997). The authors mention there that $N(\delta) \sim \delta^{-2}$ (for $\delta = \delta_{up} = \delta_{down}$).

Monte Carlo statistical tests were performed to numerically verify the accuracy of Equations (3.10), (3.11), and (3.16). Results of the tests are provided in Table 3.1. We selected only positive trend values μ since the equations are symmetrical with respect to the direction of the trend. Values in Table 3.1 exhibit high similarity of both empirical and theoretical results.

The meaning behind the provided equations is that the absolute size and the ratio of directional-change thresholds used to dissect a price curve into a sequence of upward and downward trends affect the frequency and the total number of events registered within a given time interval. It follows from Equations (3.14) and (3.15) that the combination $\gamma = \frac{\mu}{\sigma^2}$

is the crucial factor affecting the expected number of intrinsic events[9]. We check the number of directional changes registered by a couple of thresholds in three extreme scenarios: $\frac{\mu}{\sigma^2} = 0$ (Figure 3.2a), $\frac{\mu}{\sigma^2} \ll 0$ (Figure 3.2b), and $\frac{\mu}{\sigma^2} \gg 0$ (Figure 3.2c). A diverse set of dissection procedures was applied to the randomly generated time series defined by the parameters γ. All results were composed as a heatmap where each point corresponds to the number of directional changes observed by a pair of thresholds $\{\delta_{up}, \delta_{down}\}$ (Y- and X-axis of the plots) in a time series of the given length (Figure 3.2).

TABLE 3.1: Waiting times and number of directional changes in a Monte Carlo simulation. μ and σ are parameters of the Brownian motion used for the test. There are 10^9 ticks in the simulated time series. N_{DC}^{MC}, $\langle T_{up}^{MC} \rangle$, and $\langle T_{down}^{MC} \rangle$ are the numbers of directional changes and the average waiting times registered in the Monte Carlo simulation. $\mathbb{E}[N_{DC}]$, $\mathbb{E}[T_{up}]$, and $\mathbb{E}[T_{down}]$ are theoretical values dictated by Equations (3.16), (3.10), and (3.11) correspondingly. Values $\sigma^{-}_{T_{up}^{MC}}$ and $\sigma^{-}_{T_{down}^{MC}}$ are standard deviations of empirical and theoretical waiting times.

μ, %	σ, %	$N_{DC}^{MC}/\mathbb{E}[N_{DC}]$	$\langle T_{up}^{MC} \rangle/\mathbb{E}[T_{up}]$	$\sigma^{-}_{T_{up}^{MC}}$	$\langle T_{down}^{MC} \rangle/\mathbb{E}[T_{down}]$	$\sigma^{-}_{T_{down}^{MC}}$
1	10	1.028	0.968	2.54×10^{-5}	1.019	2.53×10^{-6}
	20	1.009	0.989	2.78×10^{-6}	1.012	3.32×10^{-7}
	30	1.001	0.995	8.79×10^{-7}	1.033	9.58×10^{-8}
6	10	1.021	0.971	2.29×10^{-5}	1.043	2.59×10^{-6}
	20	1.005	0.993	2.94×10^{-6}	1.019	3.29×10^{-7}
	30	0.987	1.011	8.84×10^{-7}	1.034	9.98×10^{-8}
11	10	1.029	0.968	2.20×10^{-5}	1.011	2.78×10^{-6}
	20	0.994	1.006	2.72×10^{-6}	0.997	3.30×10^{-7}
	30	0.986	1.014	8.82×10^{-7}	1.017	1.02×10^{-7}

9 The expression γ is known in the insurance industry as "adjustment coefficient" or "the Lundberg exponent" (Asmussen and Albrecher 2010). It finds its application in the ruin theory dating back to 1909 (Lundberg 1909). It is also described as the optimal information theoretical betting size called Kelly Criterion (Kelly Jr 2011).

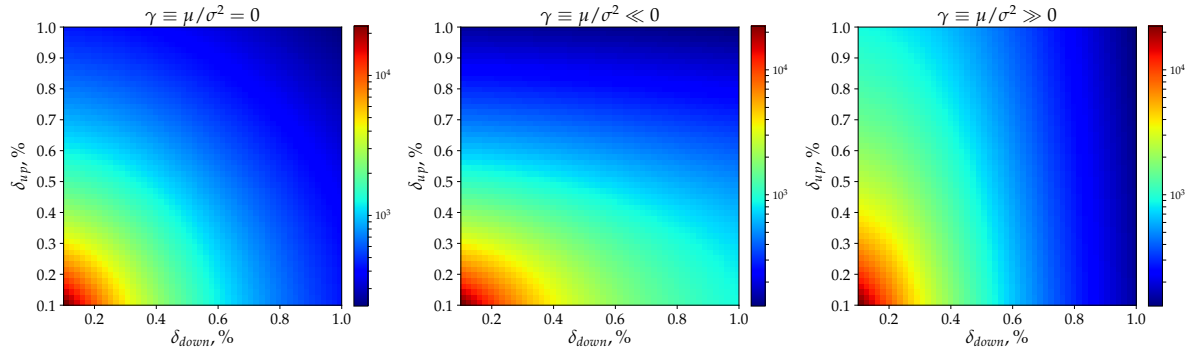

(a) (b) (c)

FIGURE 3.2: Heatmaps of the number of directional changes observed by the pair of directional-change thresholds $\{\delta_{up}, \delta_{down}\}$ (Y- and X-axis of the plots) in a timeseries of the given length (Geometrical Brownian Motion (GBM), 10^9 steps in each simulation). Selected trend and volatility values: (**a**) $\mu = 0$, $\sigma = 0.15$; (**b**) $\mu = -3$, $\sigma = 0.15$; (**c**) $\mu = 3$, $\sigma = 0.15$. The values on the plots coincide with the ones computed using Equation (3.17).

Panel 2a in Figure 3.2 corresponds to the set of experiments where the Brownian Motion trend is equal to zero. It follows from Equation (3.17) that in such conditions the value $\mathbb{E}[N(\delta_{up}, \delta_{down}; \sigma, [0, T])]$ should be constant along circular contours $\delta_{up}^2 + \delta_{down}^2 = \delta^2$ for $\delta > 0$. The colour gradient in the provided picture confirms the noted dependence. It is shown in panels 2b and 2c of Figure 3.2 that the circular contours transform into ellipses when the "adjustment coefficient" γ is significantly smaller or significantly bigger than zero. This phenomenon can be interpreted in the following way: if $\mathbb{E}[N(\delta_{up} = \delta_{down}; \gamma = 0, [0, T])]$ is the expected number of directional changes registered in the drift-less time series of given length and characterised by the fixed σ then for any γ greater or smaller than zero there is always such a couple of non equal thresholds $\{\delta_{up}, \delta_{down} | \delta_{up} \neq \delta_{down}\}$ that

$$\mathbb{E}[N(\delta_{up}, \delta_{down} \mid \delta_{up} \neq \delta_{down}; \gamma \neq 0, [0, T])] = \mathbb{E}[N(\delta_{up}, \delta_{down} \mid \delta_{up} = \delta_{down}; \gamma = 0, [0, T])]. \tag{3.18}$$

In other words, any process characterised by a certain degree of persistent trend could be treated as the one without the trend by tuning the size and the ratio of selected directional-change thresholds. The property is essential for risk management techniques constructed on top of directional-change intrinsic time approach. An example of real application of this fact is provided in Golub, Glattfelder, and Olsen (2017). The authors employed asymmetric thresholds to design an optimal inventory control function sensitive to the significant price trend changes.

3.6.3 Instantaneous Volatility

The volatility size of the financial time series is an inevitable component of any financial risk analysis. Therefore, a clear understanding of the way how volatility changes over time is particularly important for risk management and inventory control problems. Classical volatility estimation methods, also called "natural" or "traditional" estimators (Cho and Frees 1988)[10], primarily rely on physical time as the persistent measure of the intervals when the price returns should be computed. The fact that the variance of returns on assets tends to change over time creates obstacles on the way of employing the "traditional" volatility estimators. The changing variance, also known as the stochastic volatility, became a cornerstone for multiple research works (for example, Andersen and Lund (1997), Barndorff-Nielsen and Shephard (2002), A1, Kimmel, et al. (2007), and Campbell et al. (2018) and many others).

Values, computed by "natural" estimators, dominantly correspond to the integrated volatility of the studied process. The integrated volatility describes the averaged price activity over non-zero time intervals. Alternative estimators, designed to reveal the size of the volatility as the time interval approaches zero (instantaneous volatility), are mostly based on Fourier analysis[11] and require extensive computation efforts (see Chapter 3 in Mancino, Recchioni, and Sanfelici (2017)). Therefore, new methods, capable of describing the price evolution independently of the flow of the price in physical time, should be employed to overcome the existing volatility estimation difficulties.

The directional-change intrinsic time concept is by design agnostic to the speed of the price change. Risk-management tools, based on top of the concept, automatically adapt their performance to treat the changing price activity better. This property of directional-change intrinsic time, together with analytical Equations (3.16) and (3.17), bring the idea of a new volatility estimator devoid of the shortcomings of the equidistant time in finance. It follows from Equation (3.17) that the volatility can be estimated for a trendless time series by counting the number of directional changes within the time interval $[0, T]$:

$$\sigma_{DC} = \delta \sqrt{\frac{N(\delta)}{T}}. \tag{3.19}$$

10 The work Cho and Frees (1988) is particularly interesting due to the analysis the authors did to compare volatilities computed by "natural" and "temporal" estimators. The latter employs time intervals measured between consequent and alternating price moves of fixed relative size and thus is very close to the approach presented in the current paper.

11 The type of mathematical analysis applied to identify patterns or cycles in a normalised time series data.

We use the superscript DC to distinguish the volatility computed through the directional-change intrinsic time from volatility computed by the traditional estimators. The latter we will mark by σ_{trad}.

Equation (3.19) solely computes the volatility part σ of the Brownian proces. That contrasts the "natural" volatility estimation techniques where the entire stochastic σdW_t part is typically measured. That stochastic factor includes the noise component dW_t. Therefore, the directional change approach employed for volatility measurements can be classified as the true estimator of the instantaneous volatility. Further, we apply Equation (3.19) to study changing dynamic of financial time series throughout one week. We reveal volatility seasonality patterns of three FX exchange rates, crypto market BTC/USD, and the stock index S&P500.

3.7 Results

Empirical properties of three distinct markets will be discussed in this section. We omit the EUR/JPY, and EUR/GBP exchange rates in some of our experiments due to the fact that their properties are greatly similar to the properties of the most traded FX rate EUR/USD. In this case, EUR/USD is selected as the representative exchange rate of the entire FX domain.

3.7.1 Number of Directional Changes

Equations (3.16) and (3.17) connect the expected number of directional changes with parameters of the underlying Brownian motion process. The evolution of real historical returns have properties similar to the Brownian motion. The evolution sometimes compared to the sequence of the free particle moves (see Section 3.6). Thus, similar counters shown in Figure 3.2 should be found in heatmaps depicting the number of directional changes empirically registered in real data conditional that the assumption of the normal distribution of real returns is true. EUR/USD, BTC/USD, and SPX500 exchange rates were taken to verify the statement by replicating the same experiment done with the Brownian motion before (Figure 3.3). A collection of 40 directional-change thresholds ranging from 0.1% to 4.1% defines the scale of the heatmap grid. Colour schemes, used for the plots, have different scales due to the significantly bigger number of directional changes per a period of time in the BTC/USD case. Yellow solid lines indicate the examples of the areas where the number of direction changes is constant. The selected for the examples deltas are $\delta_{up} = \delta_{down} = \{1.15\%, 2.8\%\}$ (EUR/USD, Figure 3.3a), $\delta_{up} = \delta_{down} = \{1.4\%, 3.0\%\}$ (BTC/USD, Figure 3.3b), and $\delta_{up} = \delta_{down} = \{1.1\%, 2.9\%\}$ (SPX500, Figure 3.3c).

Curves in Figure 3.3a have an almost circular shape and are only slightly shifted towards the bigger δ_{down} values. This shift is present due to the downward trend experienced by the exchange rate from 2011 to 2016 (from \$1.4 to \$1.1 per EUR). BTC/USD exchange rate was much more unstable considering that the EUR/USD time series exhibited relative stability with no noticeable regime switches apart from the slow constant price depreciation. The price of Bitcoin grew with accelerating pace by more than 20 times in the second half of 2017 and then lost nearly 70% of its value at the beginning of 2018[12]. These significant trend changes are pronounced in Figure 3.3b by yellow contours notably deviated from the circular shape. The price roller-coaster caused considerable disparity of the number of registered directional changes and the ones predicted by Equation (3.17) (relevant to the trend-less case). As result, the solid price curves can be decomposed into two parts of independent ellipses similar to the ones observed for Brownian motion with non-zero "adjustment coefficient" γ (Figure 3.2b,c).

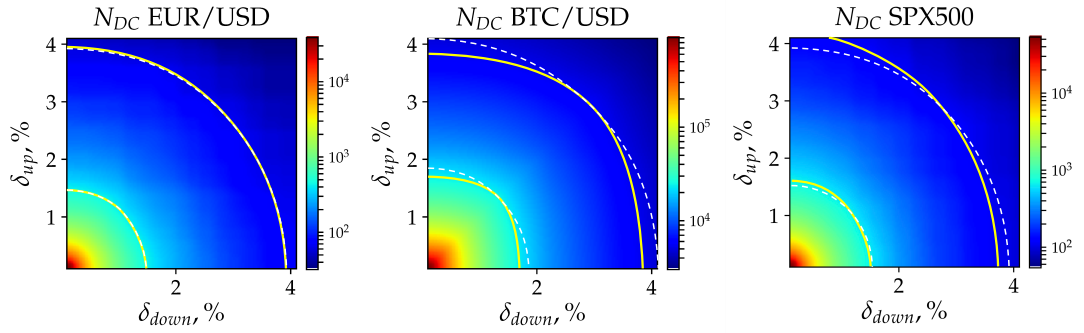

(a) (b) (c)

FIGURE 3.3: Heat map of the number of directional changes calculated in (**a**) EUR/USD, (**b**) BTC/USD, and (**c**) SPX500 time series. Each point on the grid represents the number of directional changes registered by a unique pair of thresholds $\{\delta_{up}, \delta_{down}\}$. Heatmaps have different scales. Yellow solid lines, specific for each heatmap, label the examples of the areas along which the number of intrinsic events is constant. The dashed lines represent the theoretical areas of the equal number of intrinsic events observed in case of the trend-less time series. White dashed lines are parts of circles centred around the left bottom corner of each picture. The lines go through the intersection of the solid yellow lines and the diagonal of each picture.

3.7.2 Realised Versus Instantaneous Volatility

In the second experiment, we compared the annualised volatility computed by the traditional method (Equation (3.20)) and the volatility based on the observed number of directional changes (Equation (3.19)).

12 It had a minimum at \$230 per Bitcoin, temporary maximum at about \$20 000, and then a drop to \$6000.

Returns R_t are defined as logarithms of the price change between S_t and S_{t-1} measured over equal periods of time. The number of returns n depends on the selected time interval Δt and equal to $n = T/\Delta t$ where T is the length of the entire tick-by-tick sample. Thus, the length of a sample can be computed ex-ante.

The whole set of returns was used to find the standard deviation of the time series. The measure is also known as realised volatility σ_{trad}:

$$R_t = \ln(S_t/S_{t-1}), \quad R_{avg} = \frac{\sum_{t=1}^{n} R_t}{n}, \quad \sigma_{trad} = \sqrt{\frac{\sum_{t=1}^{n}(R_t - R_{avg})^2}{n-1}}. \tag{3.20}$$

The directional-change method does not define the number of observations ex-ante in contrast to the traditional approach. According to Equation (3.19), the size of the directional-change threshold δ determines only the expected number of measures (or timestamps) in the data sample of the given length. It is also worth saying that the price moves of the highest frequency, tick-by-tick, do not appear over any predefined period. They occur together with the flow of new orders in the market. The flow, initiated by thousands of independent traders' demands, not synchronised with any periodical process. Thus, the time distance between two consecutive ticks can be represented by a fraction of a second as well as by several minutes. The equally spaced timestamps used to calculate returns for the "natural" estimators have a high chance to happen not at the moment of a new price change. The additional decision should be made on whether the historical price located before the timestamp or right after it should be selected to compute the corresponding return. The directional-change intrinsic time, in turn, directly reacts to the changes of the price levels. This flexibility of the intrinsic time makes it possible to use the data of the highest frequency: tick-by-tick prices.

Specifications of tools used to estimate volatility can affect the experiments results (Müller et al. 1997). Four increasing time intervals Δt_k, where $k = \{1, 2, 3, 4\}$, were selected to define the distance between each pair of consecutive prices S_t and S_{t-1} used for the "natural estimator": $\Delta t_1 = 1$ min, $\Delta t_2 = 10$ min, $\Delta t_3 = 1$ hour, and $\Delta t_4 = 1$ day. The set of thresholds employed to investigate the directional-change approach can also be arbitrarily chosen. However, we selected them with the intent to compare the results of both experiments. For this reason, we used the number of returns in the data sample corresponding to each time interval Δt_k as the target for the number of directional changes registered in the same data set. That is, the collection of four thresholds δ_k was selected in such a way that in the given time series the number of directional changes is approximately equal to the number of time intervals n_k of the length Δt_k. We utilised one of the scaling properties described in Glattfelder, Dupuis, and Olsen (2011) to find the precise thresholds size. The scaling property

has the name "time of total-move" scaling law (law 10 in the article). The total-move is composed as the sum of the directional-change (DC) and overshoot (OS) parts. The law connects the size of the threshold δ with the waiting time $T_{TM}(\delta)$ between two consecutive intrinsic events:

$$T_{TM}(\delta) = \left(\frac{\delta}{C_{t,TM}}\right)^{E_{t,TM}}, \tag{3.21}$$

where $C_{t,TM}$ and $E_{t,TM}$ are the scaling coefficients. Equation (3.21) can be used to express the threshold δ in terms of the waiting time T_{TM}:

$$\delta(T_{TM}) = T_{TM}^{1/E_{t,TM}} C_{t,TM}. \tag{3.22}$$

The currency average scaling parameters $E_{t,TM}$ and $C_{t,TM}$ computed in Glattfelder, Dupuis, and Olsen (2011) are 2.02 and 1.65×10^{-3}, correspondingly. Putting these coefficients into Equation (3.21), one can calculate that thresholds reciprocal to the selected time intervals $\Delta t_1, \ldots, \Delta t_4$ are: $\delta(\Delta t_1) = 0.013\%$, $\delta(\Delta t_2) = 0.039\%$, $\delta(\Delta t_3) = 0.095\%$, and $\delta(\Delta t_4) = 0.458\%$. It is worth mentioning that applied scaling parameters are relevant only to the FX market which was the object of the research in Glattfelder, Dupuis, and Olsen (2011). To the extent of our knowledge, parameters specific to Bitcoin prices, as well as to the S&P500 index, were not mentioned in the scientific literature before. Therefore, as the first step, we obtained the parameters by studying the "time of total-move" scaling law of historical Bitcoin, and SPX500 returns. The log-log plot of waiting times $T_{TM}(\delta)$ versus the directional-change threshold size δ is provided in Figure 3.4. The red line marks BTC/USD scaling law and is shown together with black, yellow, and green lines computed for EUR/USD, SPX500, and Geometrical Brownian Motion (GBM) correspondingly. Settings of the latter are chosen to mimic returns typical for the FX market.

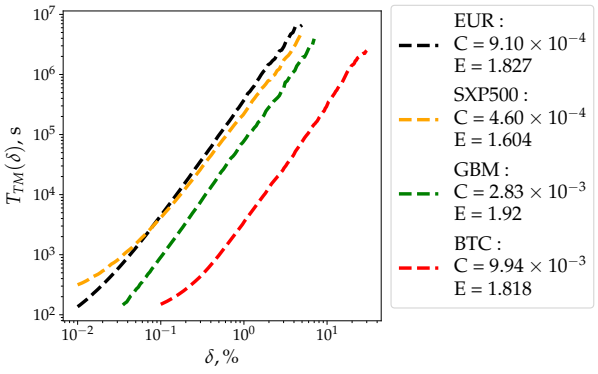

FIGURE 3.4: hlTime of total-move scaling laws computed for BTC/USD, EUR/USD, SPX500, and Geometrical Brownian Motion (GBM). GBM's parameters are $S_0 = 1.3367$, $\mu = 0$, $\sigma = 20\%$, $T =$ 1 year, and 10 million ticks in total. Scaling parameters C and E correspond to the coefficients of Equation (3.21).

Total-move scaling law parameters, obtained in the experiment, exhibit distinct resemblance of the stylised properties of the traditional FX and SPX500, as well as the emerging Bitcoin markets. Scaling factors $E_{t,TM}$ of EUR/USD, BTC/USD, and SPX500 are 1.827, 1.818, and 1.604, correspondingly. The coefficient specific for the BTC/USD pair is approximately 0.5% smaller than the one of EUR/USD. The coefficient of the SPX500 index is, in turn, is substantially smaller: by 9.9%. The same scaling factor of the GBM is the biggest among others: 1.920 ($\approx$ 5.6% difference with EUR/USD). The parameter is noticeably distant from the parameters of the analysed exchange rates. We account the divergence to the non-normal distribution of real returns at ultra-short timescales (fat tails). The fat tails effect is pronounced in Figure 3.4 as the upward bend of the curves towards the beginning of the X-axis. The bends are read as the longer time needed for a total-move to unwrap than it is predicted by the linear part of the plot in the range of higher thresholds values. Linear regressions, built in the range of straight parts of the curves, are characterised by the scaling coefficients $E_{t,TM}$, which are close to the ones observed in GBM. The observed evidence is an additional confirmation of the "Aggregational Gaussianity" stylised fact[13] typical for high-frequency markets (Cont 2001). Scaling parameters $C_{t,TM}$ of EUR/USD, BTC/USD, and SPX500 are 9.07×10^{-4}, 9.94×10^{-3}, and 4.60×10^{-4}, correspondingly. These values are significantly different due to the unlike scale of the corresponding volatility. This volatility dependent scaling parameter is not critical for the current analysis and will be discussed in the future research works.

The goal of the experiment is to compare the volatility computed using the "traditional" approach to the volatility based on the directional-change intrinsic time concept. Scaling law parameters $E_{t,TM}$ and $C_{t,TM}$ of historical BTC/USD returns were used to find the size of the directional-change thresholds, which would result in the average number of registered intrinsic events in the entire data-sample equal to the number of evenly spaced periods n_k. Expressing the parameter δ_k from the Equation (3.21) we find that for BTC/USD the thresholds are: $\delta(\Delta t_1) = 0.09\%$, $\delta(\Delta t_2) = 0.33\%$, $\delta(\Delta t_3) = 0.89\%$, $\delta(\Delta t_4) = 5.13\%$. The values are about ten times bigger than the ones related to the FX market (mentioned above) because of the proportionally larger realised volatility.

The same procedure, described in the previous paragraph, was performed in order to find the corresponding thresholds for the SPX500 time series. The obtained values: $\delta(\Delta t_1) = 0.006\%$, $\delta(\Delta t_2) = 0.025\%$, $\delta(\Delta t_3) = 0.076\%$, $\delta(\Delta t_4) = 0.55\%$.

The set of selected time intervals $\Delta t_{k=\{1,\dots,4\}}$ and the complementary thresholds $\delta_{\Delta t_1}, \dots, \delta_{\Delta t_4}$ specific for each considered market were used to calculate realised and instantaneous volatil-

13 The evidence that the distribution of returns approaches the normal one measured over longer timescales.

ity by traditional and the novel approach. We present in Table 3.2: average value of the realised volatility $\langle \sigma_{trad} \rangle$ computed as the sum of all four measurements ($k = \{1, 2, 3, 4\}$) divided by the number of experiments; its standard deviation σ^{-}_{trad}; average value of the instantaneous volatility computed by the novel approach $\langle \sigma_{DC} \rangle$; the corresponding standard deviation σ^{-}_{DC}; ratios of both measures $\langle \sigma_{trad} \rangle / \langle \sigma_{DC} \rangle$ and $\sigma^{-}_{trad} / \sigma^{-}_{DC}$. The last column of the table demonstrates the difference in the stability of results obtained by two measures.

The size difference of the realised and the instantaneous volatility is significant and is pronounced across all tested exchange rates (column $\langle \sigma_{trad} \rangle / \langle \sigma_{DC} \rangle$). The realised volatility computed in the "natural" way persistently exceeds the instantaneous volatility discovered via the novel approach. Only the two types of Bitcoin's volatility appear to be 5% different whenever the divergence grows up to 99% in the case of SPX500. The striking difference is partially explained by the various discreteness of the employed data (which will be elaborated in the next section), and partially by the phenomenological properties of the selected markets (more on it in Section 3.7.4). This phenomenon is captivating especially taking into account that Bitcoin is particularly famous due to its oversized price activity. Its activity is clearly pronounced as the large standard deviation of the instantaneous volatility of BTC/USD pair (column σ^{-}_{DC}). Three FX exchange rates, having noticeably smaller realised volatility, are characterised by the wider range of the standard deviation values (column σ^{-}_{trad}). The ratio $\sigma^{-}_{trad} / \sigma^{-}_{DC}$ reaches the 0.02 level computed for EUR/USD. In other words, the standard deviation of the EUR/USD instantaneous volatility is 50 times bigger than the realised volatility value.

TABLE 3.2: Volatility of the considered time series computed using the "traditional" (Equation (3.20)) and the directional-change (Equation (3.19)) approaches. Provided values $\langle \sigma_{trad} \rangle$ and $\langle \sigma_{DC} \rangle$ are the average of four measurements performed with specific parameters: in the "traditional" case time intervals between observations S_n and S_{n-1} are $\Delta t_1 = 1$ min, $\Delta t_2 = 10$ min, $\Delta t_3 = 1$ h, and $\Delta t_4 = 1$ day. In the case of the directional-change intrinsic time approach, the thresholds δ are $\delta(\Delta t_1) = 0.013\%$, $\delta(\Delta t_2) = 0.039\%$, $\delta(\Delta t_3) = 0.095\%$, $\delta(\Delta t_4) = 0.458\%$ (FX prices), $\delta(\Delta t_1) = 0.09\%$, $\delta(\Delta t_2) = 0.33\%$, $\delta(\Delta t_3) = 0.89\%$, $\delta(\Delta t_4) = 5.13\%$ (BTC prices), and $\delta(\Delta t_1) = 0.006\%$, $\delta(\Delta t_2) = 0.025\%$, $\delta(\Delta t_3) = 0.075\%$, $\delta(\Delta t_4) = 0.545\%$ (SPX500).

Name	$\langle \sigma_{trad} \rangle$, %	σ^-_{trad}	$\langle \sigma_{DC} \rangle$, %	σ^-_{DC}	$\langle \sigma_{trad} \rangle / \langle \sigma_{DC} \rangle$	$\sigma^-_{trad} / \sigma^-_{DC}$
EUR/USD	9.72	0.03	7.53	1.38	1.29	0.02
EUR/JPY	11.93	0.12	8.55	2.07	1.40	0.06
EUR/GBP	8.04	0.23	5.81	1.43	1.38	0.16
BTC/USD	84.76	8.67	80.87	22.21	1.05	0.39
SPX500	13.19	0.67	6.63	3.24	1.99	0.21

3.7.3 Discrete Price Effect

The instantaneous volatility standard deviation computed for four different directional-change thresholds has an extremely high value (column σ^-_{DC} in Table 3.2). This indicates that in contrast to the realised volatility capable of the scaling, together with the time interval Δt, the instantaneous one does not scale together with the threshold size δ.

The price discontinuity typical for all real markets is the cause of the high standard deviation of the instantaneous volatility computed by the directional-change approach. Conventional exchange architecture restricts the price quotations to be a multiple of some constant, for example, 0.001 of a USD. This discreteness caused substantial debates in the scientific literature with regards to the accuracy of the "natural" estimators and on the extent to which they overestimate the actual volatility of the studied process (Gottlieb and Kalay 1985; French and Roll 1986). Equation (3.19) connects the number of directional changes observed per period of time and the instantaneous volatility and is built on the assumption of the continuous Brownian process. It has no adjustment factors to the discreteness of the analysed data. In reality, the directional-change intrinsic time does not precisely tick at the level where the size of the return is equal to the size of the threshold δ. Instead, in most cases, a new directional-change event becomes registered when the price has already jumped over the expected level. This discreteness effect becomes more pronounced when the size of the elementary price move

(tick) is relatively big. That is, two factors contribute to the size of the instantaneous volatility of the discrete data-sample computed by the novel approach: the scale of the selected threshold δ and the tick size in the given sample (discreteness). Further, we provide results of a set of experiments where the impact of the price discreteness and the threshold size δ on the computed instantaneous volatility is observed.

Three time series were generated by GBM with the various density of ticks per period of time. Variation of the number of price changes in the simulation is equivalent to changing the simulated tick size having fixed a one-year time interval and volatility of the generated process fixed to be 15%. Forty gradually increasing directional-change thresholds were applied to all three GBMs. The thresholds range from 0.01% to 0.29%. We provide the plot of the computed instantaneous volatility of simulated time series in Figure 3.5. Two particular properties can be noticed. First, one brings the generated time series closer to the continuous process by making the size of a tick smaller (increasing the number of price changes per period in the sample). In this case, the values of the estimated instantaneous volatility σ_{DC} become closer to the volatility σ embedded in the model. Second, bigger thresholds are less sensitive to the discreetness of the given set of prices. The slippage effect of the price jump over the expected intrinsic time level becomes less pronounced, and the obtained result also approaches the value σ when the tick size represents a small fraction of the directional-change thresholds. A more comprehensive analysis should be performed in further research works to bridge the gap between the realised and instantaneous volatilities.

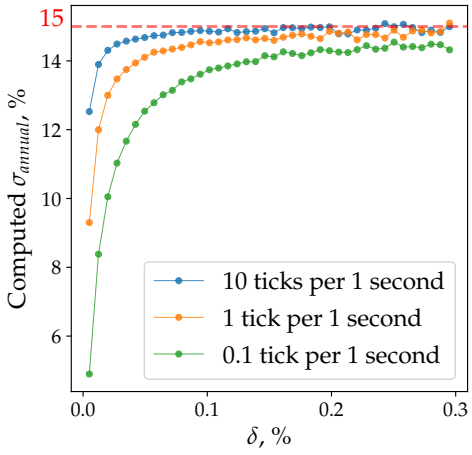

FIGURE 3.5: Instantaneous volatility of three time series generated by GBM with various tick frequencies and fixed volatility (15%). The volatility is computed by the directional-change approach (Equation (3.19)). Sizes of the directional change thresholds, used to calculate the volatility values, are put on the X-axis. Red dashed line marks the 15% level.

3.7.4 Volatility Seasonality

Michael M Dacorogna et al. (1993) presented a weekly seasonality pattern of price activity in the FX market. The authors' analysis is based on the assumption that worldwide trading happens at strictly separated time zones with several dominated cores and operates within specific trading hours. Such a physical distribution of traders is embodied in geographical components of the market activity and eventually becomes pronounced as the weekly volatility seasonality. We do not build a similar assumption in our work. Instead, the collection of observed historical returns is treated as the only source of information available for the analysis. Further, we discover and describe the seasonality pattern of instantaneous volatility typical for FX exchange rates, Bitcoin prices, and S&P500 index.

We divide a whole week into a set of 10-minute time intervals (bins). There are 1008 equally spaced points located at the fixed distance from the beginning of each week. This is a significantly larger number than the one used in the work Michael M Dacorogna et al. (1993) (168 points spaced by one hour intervals). We can afford this decreased granularity thanks to the more detailed historical time series employed for the experiment: instead of 12 million ticks for 26 exchange rates, we have on average 100 million ticks for each of the FX pairs. For each bin, the average number of directional changes will be computed.

The following series of steps allowed to construct the seasonality pattern. First, we run all historical tick-by-tick prices through the directional-change algorithm with the specified threshold δ. As soon as a new intrinsic event becomes registered, we check within which out of 1008 bins it happened. We add $+1$ to the number of directional changes corresponding to that time interval. When there are no prices left in the historical time series, we find the average number of intrinsic events per each bin. Equation (3.19) is then applied to compute the corresponding instantaneous volatility. Considering the five-year-long historical data, the obtained average is based on nearly 250 observations. Calculated instantaneous volatility values should be later normalised by the number of years and the length of a bin to get the annualised volatility specific for each bin of the week.

We select the threshold $\delta = 0.01\%$ for the first experiment with FX exchange rates. The average number of directional changes in a week registered by a threshold of this size is approximately equal to the number of 10-minute long bins in it (1008). The reconstructed instantaneous volatility seasonality pattern of the FX pairs is shown in Figure 3.6. The pattern is notably stable across all tested exchange rates and is similar to the one demonstrated in Michael M Dacorogna et al. (1993).

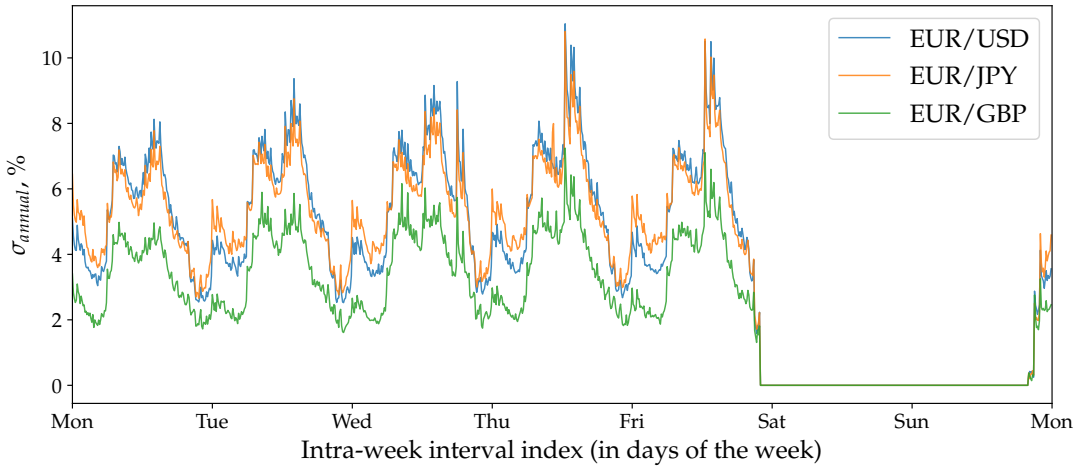

FIGURE 3.6: Instantaneous volatility seasonality of three Forex (FX) exchange rates computed using the directional-change approach (Equation (3.19)). Applied directional-change threshold $\delta = 0.01\%$. The whole week is divided by equally spaced time intervals $T = 10$ min (1008 bins in total).

We provide results of the same experiment where the "traditional" volatility estimator (Equation (3.20)) was employed to reveal the seasonality patterns of the FX exchange rates in Figure 3.7 and of BTC/USD in Figure 3.8. In contrast to the volatility seasonality pattern computed using the directional-change approach (Figure 3.6), the "traditional" pattern is less affected by the frequency of ticks per period of time specific for each studied time series. The difference between the average realised volatility across a week of the most active pair (EUR/JPY) and the least active (EUR/GBP)[14] is equal to 46%. The same difference of the instantaneous seasonality (Figure 3.6) is 10% bigger and equal to 56%. The "traditional" estimator of the realised volatility seasonality demonstrates more rapid changes in the consecutive bins values. Local maximums at the beginning and the end of a day are considerably abrupt. The reason for this is that the directional-change intrinsic time captures the part of the volatility of the underlying process free of the noise component by ignoring the overshoot part of each trend move. The exact form and scale of the noise component and its connection to the overshoot section of the directional-change intrinsic time is a topic for future research work.

Assets traded in the crypto market have several specific properties which make them noticeably different compared to the traditional financial instruments such as FX exchange rates. Among the characteristics are: open trading within weekends and holidays; the absence of isolated physical trading centres where working hours are fixed; still low acceptance of the

14 According to Table 3.2.

emerging market among professional traders. The outlined differences are endorsed by the history of technologies employed in the traditional FX and the emerging crypto worlds. The first one has originated in times when the trading happened in person and the settlement assumed the actual physical assets delivery. The trading organically evolved over time and became digital thanks to the internet expansion. Nevertheless, old properties, such as the governmental and the middle-man controls, have never been removed from the list of the accompanying FX markets design features. Bitcoin, in turn, has been designed as the alternative of the traditional financial system. It benefits from the blockchain technology by endorsing the principles of equality, openness, and accountability. We studied the historical prices of Bitcoin to investigate whether these specialities have any considerable impact on the BTC/USD instantaneous volatility seasonality pattern.

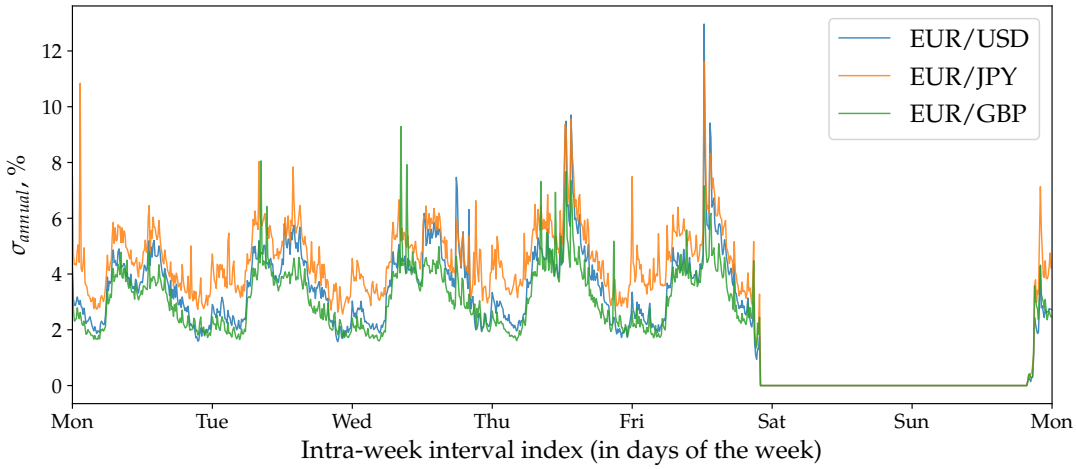

FIGURE 3.7: Realised volatility seasonality patterns of three FX exchange rates computed using the traditional approach (Equation (3.20)). Time intervals of 1-min have been used to calculate returns. The size of each bin is 10 min, 1008 bins in total.

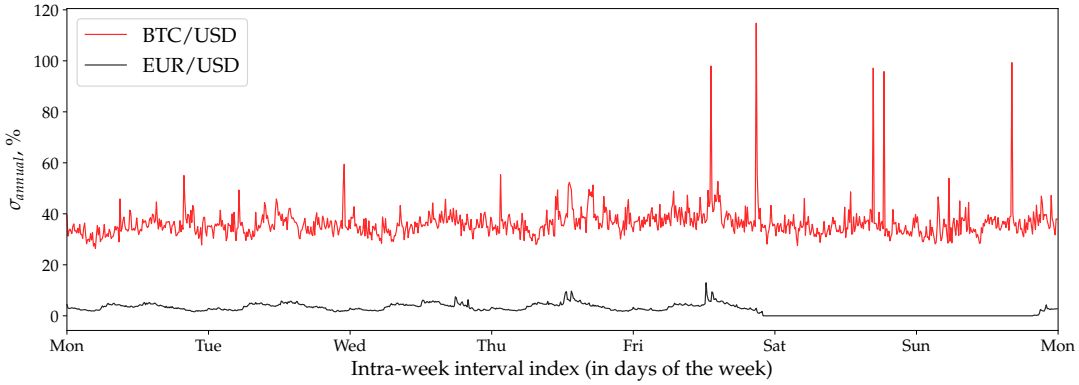

FIGURE 3.8: Realised volatility seasonality patterns of BTC/USD and EUR/USD exchange rates computed using the traditional approach (Equation (3.20)). Time intervals of 1-min have been used to calculate returns. The size of each bin is 10 min, there are 1008 bins in total.

We apply the same threshold size $\delta = 0.01\%$ used in the FX experiment to compare the seasonality patterns of Bitcoin and EUR. The obtained seasonality pattern put on top of the EUR/USD seasonality is presented in Figure 3.9. As can be seen from Figure 3.9, the periodical shape of Bitcoin's curve is much less pronounced in contrast to EUR/USD. Its standard deviation computed within a week is 0.5%. It is roughly four times smaller than the standard deviation of the EUR/USD pattern (equal to 1.9%). Surprisingly, the intra-day maximums and minimums of Bitcoin seasonality do not precisely coincide with those observed in the traditional market. They are shifted towards the time intervals where European and American markets contribute the most to the geographical pattern (as disclosed in Michael M Dacorogna et al. (1993)). This observation confirms the one provided in Eross et al. (2017). That is particularly interesting since Asian markets are known for their substantial contribution to the cryptocurrency trading volumes. The fact that China has ruled that financial institutions cannot handle any Bitcoin transactions could be the reason of the observed phenomenon (Ponsford 2015). Instantaneous volatility over weekends is slightly lower than within the middle part of the week and is practically equal to Monday's activity. We attribute the observed facts to the mentioned above non-traditional characteristic of the cryptocurrency market.

As it was shown before, the instantaneous volatility computed by the novel approach directly depends on the size of the selected directional-change threshold δ (Figure 3.5). To examine the threshold size impact on the seasonality pattern of the real data, we arbitrarily selected the following set of values: $\delta = \{0.01\%, 0.04\%, 0.10\%\}$. The same algorithm described above was applied to reconstruct the volatility seasonality pattern for the FX pair EUR/USD (Figure 3.10) and SPX500 (Figure 3.11). The seasonality patterns shift toward higher volatility values when the size of the threshold is bigger. The observation is in line with the results of the experiments on GBM (Figure 3.5). Average values of EUR/USD seasonality curves computed with thresholds δ equal to 0.10% and 0.04% are correspondingly 1.71 and 1.57 times higher than the values computed with $\delta = 0.01\%$. The dependence of the seasonality smoothness on the size of the directional-change threshold become vividly pronounced: the seasonality curve constructed with the smallest threshold in the set is much sleeker (less wander) than the rest of the curves. This phenomenon should urge researchers and practitioners to select directional-change thresholds according to their needs very carefully while employing the directional-change technique.

According to Table 3.2, realised volatility of Bitcoin returns computed in the "traditional" way is about nine and six times bigger than the analogous volatility of the FX and SPX500 exchange rates (column $\langle \sigma_{trad} \rangle$). Besides, the retrieved sample of historical BTC/USD prices has

1.2 million ticks per year, which is 16.7 times smaller than the number of ticks per year in the EUR/USD case (about 20 million). As a result, the choice of the directional-change threshold δ has a much more significant effect on the average BTC/USD instantaneous volatility. We demonstrate results of four experiments where different threshold sizes were employed to reveal the seasonality patterns in Figure 3.12. The same $\delta = 0.01\%$ was used as the reference for the set of all arbitrary selected thresholds: $\delta = \{0.01\%, 0.03\%, 0.10\%, 0.20\%\}$. As it can be seen from Figure 3.12, the increase in the size of δ causes the corresponding increase in the volatility level around which the seasonality patterns oscillate. The levels of the seasonality distribution for $\delta = \{0.03\%, 0.10\%, 0.20\%\}$ are 1.5, 4.0, and 11.1 times bigger than the value corresponding to the smallest threshold $\delta = 0.01\%$. The biggest $\delta = 0.20\%$ lifts the value up to the level of $\sigma_{annual} = 68.5\%$ (which is still smaller than the realised volatility presented in Table 3.2 ($\sigma_{annual} = 84.76\%$)).

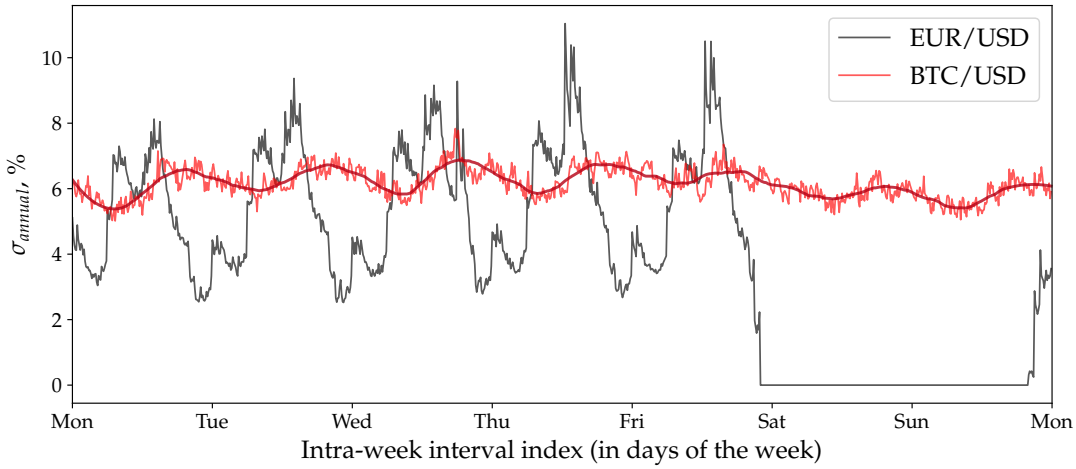

FIGURE 3.9: Instantaneous volatility seasonality of BTC/USD compared to the seasonality pattern of EUR/USD computed using the directional-change approach (Equation (3.19)). The dark-red curve approximates the Bitcoin seasonality pattern using the Savitzky–Golay filter (number of points in the window is 101, the order of the polynomial is 2). The directional-change threshold $\delta = 0.01\%$ was used in both experiments. Each discrete time interval (bin) is $T = 10$ min. There are 1008 bins in total.

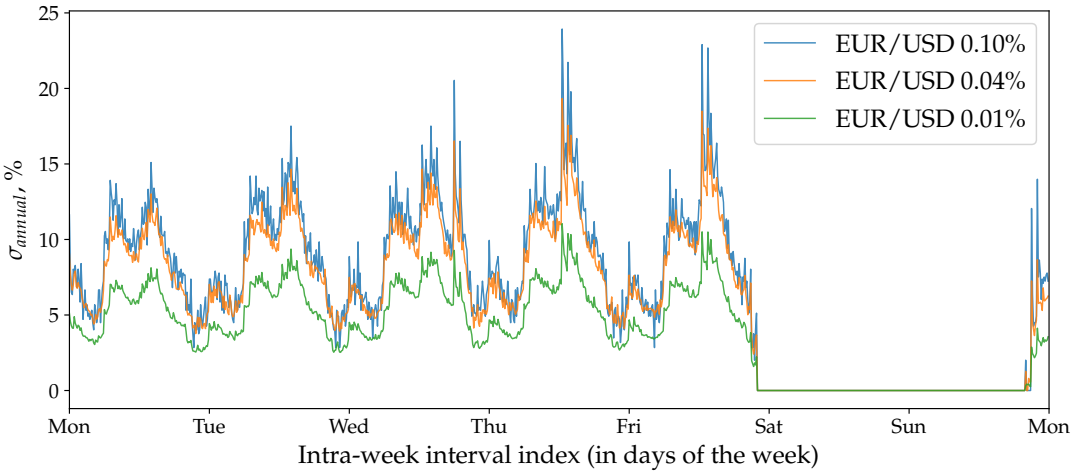

FIGURE 3.10: Volatility seasonality of EUR/USD computed using the novel approach (Equation (3.19)) and three different thresholds: $\delta = \{0.01\%, 0.04\%, 0.10\%\}$. The size of a bin is 10 min, there are 1008 bins in a week.

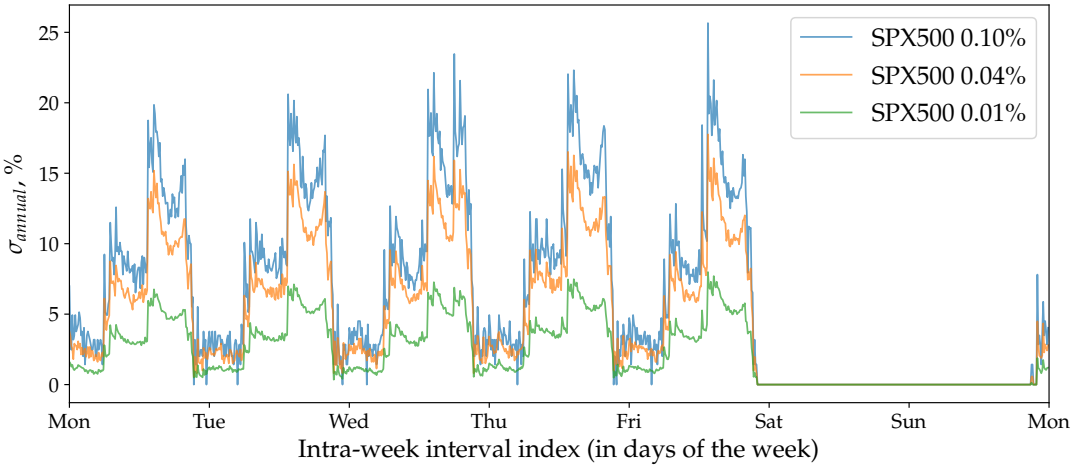

FIGURE 3.11: Volatility seasonality of SPX500 computed using the novel approach (Equation (3.19)) and three different thresholds: $\delta = \{0.01\%, 0.04\%, 0.10\%\}$. The size of a bin is 10 min, there are 1008 bins in a week.

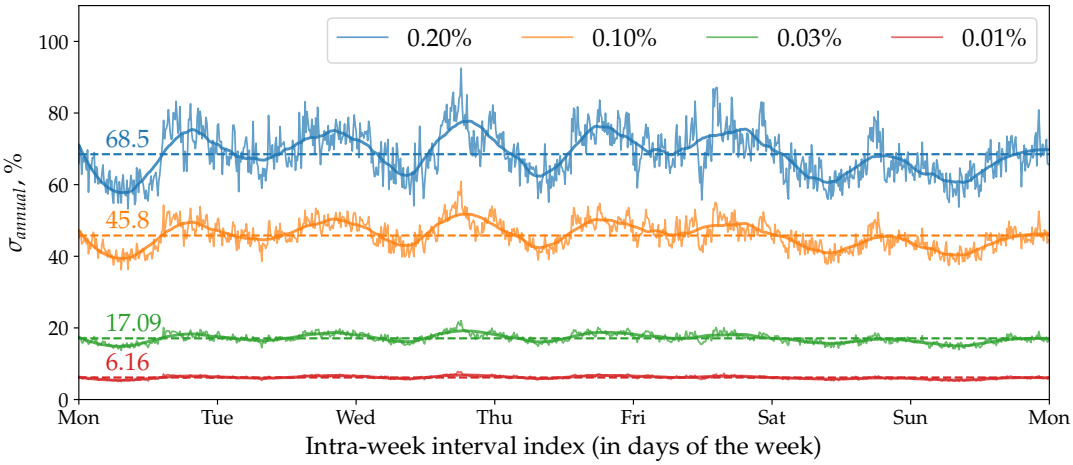

FIGURE 3.12: Instantaneous volatility seasonality of BTC/USD exchange rate computed using the directional-change approach (Equation (3.19)) and four different thresholds. Applied thresholds, from top to bottom: $\delta = \{0.20\%, 0.10\%, 0.03\%, 0.01\%\}$. The dark solid curves approximate the Bitcoin seasonality patterns using the Savitzky–Golay filter (number of points in the window is 101, order of the polynomial is 2). Bin size $T = 10$ min was chosen in all cases (1008 bins in a week). Dashed lines and the numbers over them represent the average level of each seasonality pattern across a week.

More information on the daily instantaneous and realised volatility seasonality ratio is provided in Figures 3.15–3.18 and Table 3.4 in Appendix 3.A.

3.7.5 Volatility Autocorrelation and Theta Time

The shape of the persistent instantaneous volatility seasonality patterns computed for the FX and SPX500 exchange rates changes with clear daily periodicity. This observation suggests that there should be a strong autocorrelation of the instantaneous volatility over time. The connection of the number of directional changes and the volatility value (Equation (3.19)) translates into the autocorrelation of the number of directional changes. We examined the autocorrelation function (ACF) of the number of directional changes observed within each bin of a week to check the assumption. The results of the experiment made for the FX exchange rates are provided in Figure 3.13. The same size of the directional-change threshold used to reveal the seasonality distribution $\delta = 0.01\%$ was employed. A remarkably stable pattern was found where daily and weekly seasonality is easily recognisable. The ACF function of FX exchange rates discovered in our work is highly similar to the results provided by Michael M Dacorogna et al. (1993). Nevertheless, there are clear differences between the FX autocorrelation patterns in our work and in the work of Michael M Dacorogna et al. (1993). The ACF of the number of directional changes computed through time lags defined in physical time does

not cross the zero level for a much more extended period. It is consistently positive with lags even greater than several weeks. The curve representing the ACF of EUR/JPY has the smallest amplitude (smallest variability). In contrast, curves of EUR/USD together with EUR/GBP invariably follow the same pattern shifted up in the case of EUR/USD.

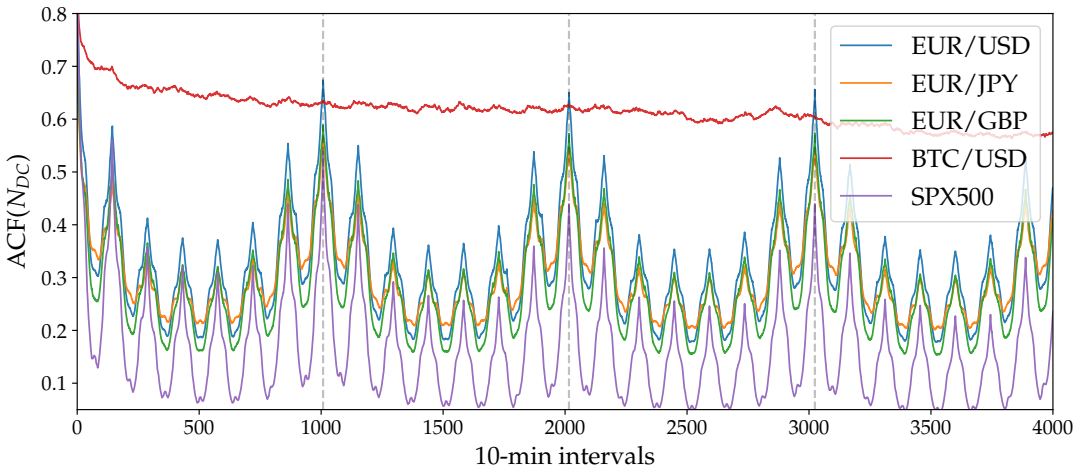

FIGURE 3.13: Autocorrelation function of the number of directional changes per 10-minute long bins computed in physical time. Vertical dashed lines label weekly intervals. Applied threshold $\delta = 0.01\%$.

The SPX500 time series ACF has a similar shape to the shape of the FX market ACF. Two distinct properties can be noticed: the higher ACF amplitude and the faster decay. The exact level of decline of all exchange rates will be discussed a few paragraphs later.

The BTC/USD exchange rate seasonality pattern, characterised by much less pronounced instantaneous volatility, has also been tested in order to get the shape of the autocorrelation function. The results are presented in Figure 3.13. The amplitude of the ACF curves is the main difference in the values computed for the traditional FX and the emerging BTC/USD markets: the variability of the BTC/USD curve is 10 times lower than the variability of the EUR/USD one. We note that significantly bigger thresholds than the one used in the experiment ($\delta = 0.01\%$) have also been tested. All results confirmed that they reveal less accurate patterns due to the data insufficiently frequent for the statistical analysis.

A certain level of decline characterises the ACFs of all exchange rates as it can be seen from Figure 3.13. Large seasonal peaks of the autocorrelation functions drawn against of physical time do not allow to measure the level of decline precisely. A measure capable of converting the stochastic price evolution process to the stationary one should be applied to estimate the level of the downturn better. We minimise the seasonality pattern by employing the concept of theta time (Θ-time) proposed by Michael M Dacorogna et al. (1993). Θ-time

is designed to eliminate the periodicity pattern by defining a set of non-equal time intervals within which the measure should be performed. The length of each Θ interval in physical time depends on the historical activity of the market. The theta time concept states that the average cumulative price activity (or volatility) between each consecutive couple of Θ steps is constant. Therefore, the distance between Θ timestamps, measured in physical time, is dictated by the shape of the volatility seasonality pattern. The periods of high price curve activity are equivalent to increasing the speed of physical time. The frequency of Θ stamps increases when the volatility rises too. In contrast, periods of low activity are identical to stretching the flow of the physical time, and the lower number of Θ intervals appears. As a result, active parts of the seasonality pattern, coinciding with the middle of the trading day, have the higher density of Θ timestamps per a unite of the physical time than the standstill sections overnights. Mathematically:

$$\Theta(t) = \int_{t_0}^{t} \sigma(t')dt', \tag{3.23}$$

where t_0 and t are the beginning and the end of the considered period of physical time and $\sigma(t')$ is the value of the instantaneous volatility corresponding to each moment of the interval. Equation (3.23) can be transformed into the sum of elements $\sigma_{\Delta t'}$ between the beginning and the end of the observed interval Δt_n in the case of a non-continuous seasonality pattern where the values are discretely defined in periods Δt (as in our experiment):

$$\Theta(t) = \sum_{\Delta t_0}^{\Delta t} \sigma_{\Delta t_n}. \tag{3.24}$$

It should be noted that the number of bins in a week is always constant in both physical and Θ times. This is achieved through the assumption that the integral (or the sum) of the weekly activity is the constant value.

The autocorrelation function of the number of directional changes computed in Θ-time is shown in Figure 3.14. Curves are approximated by the logarithmic function $y = A_{ACF} \log x + B_{ACF}$. The logarithmic coefficients A_{ACF} and B_{ACF} are presented on Figure 3.14 and in Table 3.3.

Major weekly fluctuations of the volatility seasonality pattern have been successfully eliminated for all three FX and BTC/USD exchange rates. Nevertheless, Θ-time does not completely remove the seasonality shape of ACF in the same way it happened in the work Michael M Dacorogna et al. (1993): noticeable peaks are still present in the final part of each business day. Moreover, the SPX500 curve is characterised by vividly pronounced daily seasonality pattern despite being run through the theta time algorithm. The phenomenon, observed in the original paper (Michael M Dacorogna et al. 1993), was explained by the non-optimal setup

of the chosen model. The assumed same activity for all working days is indeed not fully correct (see Figure 3.6). However, we do not use any analytical expression postulating equal daily activity to describe the seasonality pattern. Instead, components $\sigma_{\Delta t'}$ of real empirically found volatility seasonality patterns depicted in Figures 3.6 and 3.9 were utilised to define the timestamps in Θ-time. Therefore, we eliminate the inefficiency connected to the assumption mentioned above. Thus, the alternative interpretation for the remained seasonality should be provided.

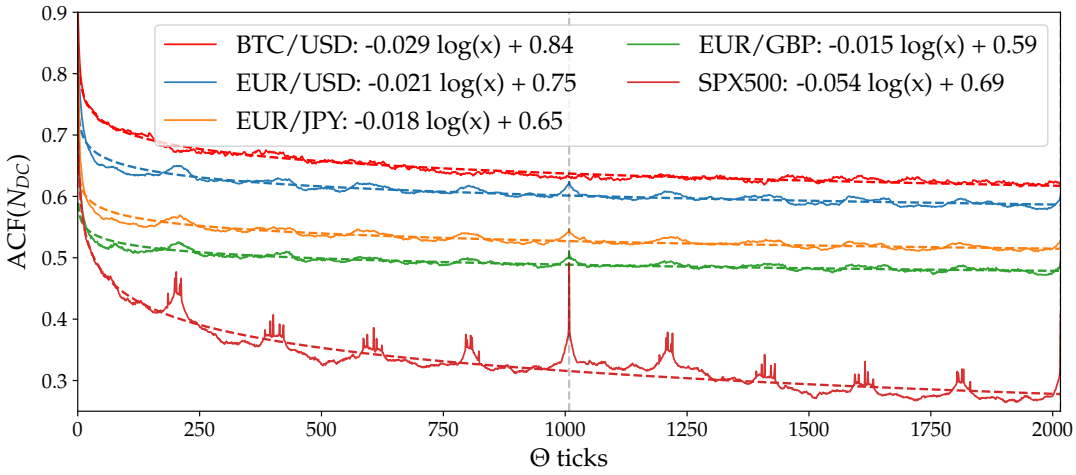

FIGURE 3.14: Autocorrelation function (ACF) of the number of directional changes per a bin in Θ-time. Vertical dashed line labels one week interval. There are 1008 bins in a week.

TABLE 3.3: Parameters of the logarithmic decay $y = A_{ACF} \log x + B_{ACF}$ used to fit the autocorrelation function (ACF) of the number of directional changes in Θ-time (Figure 3.14).

Name	A_{ACF}	B_{ACF}
BTC/USD	−0.029	0.84
EUR/USD	−0.021	0.75
EUR/JPY	−0.018	0.65
EUR/GBP	−0.015	0.59
SPX500	−0.054	0.69

We attribute the remaining fluctuations to the selected directional-change algorithm, which dissects the price curve into a collection of alternating trends. We also claim that the choice of the frequency of bins in a week used for the experiments affects the shape of the autocorrelation function in theta time. According to the directional-change algorithm (see Section 3.1), the dissection procedure has to be initialised only once and then it performs unsupervised.

The evolution of the price curve dictates the sequence of intrinsic events. This fact leads to a certain dilemma: once registered, to which bin of a week should the intrinsic event be assigned? The following example illustrates the preditacament. A couple of prices, at which two subsequent directional changes become registered, could belong to different bins. Let us say these are the intervals Δt_{n-1} and Δt_n. This means that the beginning of the price move that triggered the latest intrinsic event had started within Δt_{n-1}. But the end of this price trajectory finishes within the interval Δt_n. The crucial point is at what part of the Δt are the beginning and the end located. In the extreme case, the whole price trajectory before the directional change could be fully placed inside of the interval Δt_{n-1}. The latest tick that eventually triggered the new directional-change event can be at the very beginning of Δt_n. Should such an event be assigned to the bin Δt_{n-1} or to Δt_n? The answer to this question is particularly important considering the effect the threshold size has on the seasonality patterns (Figures 3.10 and 3.11). The patterns constructed by using different thresholds have not only different average value over a week but also characterised by slightly shifted regions of local maximums and minimums (see, for example, the curves for $\delta = 0.01\%$ and $\delta = 0.10\%$).

A better way of associating locations of intrinsic events with bins of a week is another question related to the transition from the physical to intrinsic time and vice versa. This topic should be discussed in more details in further research works. Until then, the use of smaller thresholds and bigger time intervals is the strategy capable to impact the localisation problem positively.

3.8 Concluding Remarks

The language of traditionally considered drawdowns and drawups has been translated into the language of the directional-change intrinsic time. This translation made it possible to interpret the evolution of a price curve as a sequence of alternating trends of the given scale. The observed number of directional changes per period of time has been connected to the properties of the studied time series characterised by the instantaneous volatility σ_{DC} and the trend μ. The choice of directional-change thresholds δ_{up} and δ_{down} used to dissect the historical price curve is arbitrary but affects the results of the experiment. Bigger thresholds tend to register higher instantaneous volatility than the smaller ones. Equations (3.10), (3.11), and (3.16), connecting the observed number of directional changes to the properties of the studied process, have been validated by a Monte Carlo simulation. The simulation confirmed the robustness and accuracy of the obtained analytical expressions.

We extended the work of Michael M Dacorogna et al. (1993) by discovering the instantaneous volatility weekly seasonality pattern. One representative of the emerging cryptocurrency markets, Bitcoin, as well as of the traditional and widely accepted FX (EUR/USD, EUR/GBP, EUR/JPY) and stock (S&P500) markets, were considered. The connection of the number of directional-change intrinsic events to the instantaneous volatility has been employed to perform the computation. BTC/USD and SPX500 "total-move scaling laws" were computed for the first time to facilitate the seasonality discovery.

Similar patterns of the realised and the instantaneous volatility were obtained. Several noticeable differences between the results demonstrated in the work Michael M Dacorogna et al. (1993) and the ones presented in the current paper have been highlighted. First, the method based on the directional-change intrinsic time concept significantly simplifies the construction of the instantaneous volatility seasonality pattern operating with the information of the highest resolution (tick-by-tick prices). Second, the autocorrelation function of the number of directional changes computed in physical time stays positive for a notably long period of time. Third, the beginning of the volatility autocorrelation function computed in Θ-time can be approximated by the logarithmic function. The part of the autocorrelation plot after the lag bigger than one week declines linearly.

The difference between the instantaneous volatility seasonality patterns of the traditional FX and emerging Bitcoin markets demonstrates the currency digitisation and globalisation effect. The effect can be considered as the template for the future analogous markets to come.

The insights provided within this paper underline the relevance of the proposed directional-change framework as a valuable alternative to the traditional time-series analysis tools. The independence of directional-change intrinsic time on the frequency of price changes over a period of time makes it an effective tool for capturing periods of changing price activity. Results of the provided research can be used to extend the set of risk management tools constructed to evaluate the statistical properties of traditional and emerging financial markets.

3.A Daily Seasonality

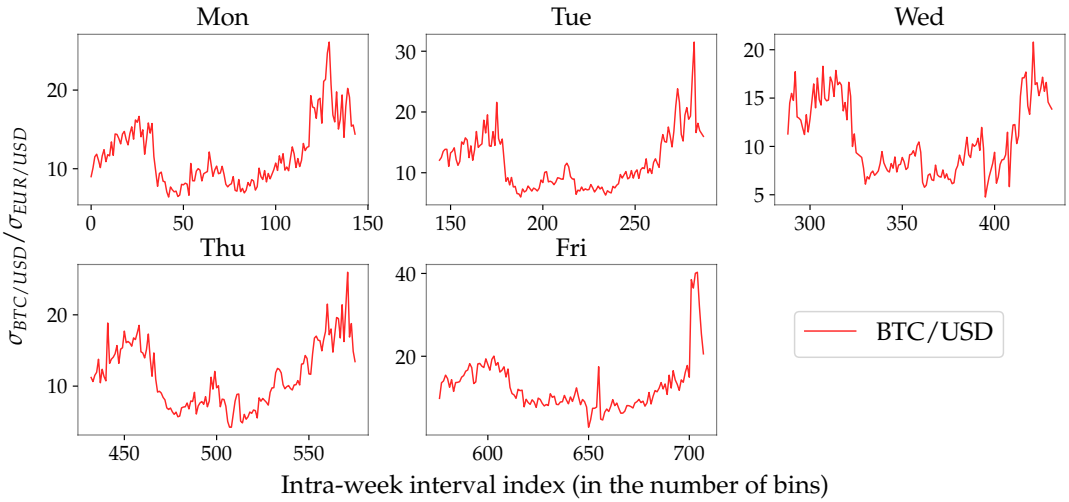

FIGURE 3.15: Daily realised volatility ratio of BTC/USD measured over 10-min time intervals dissecting the entire week into 1008 bins. The volatility is computed according to the "traditional" approach (Equation (3.20)).

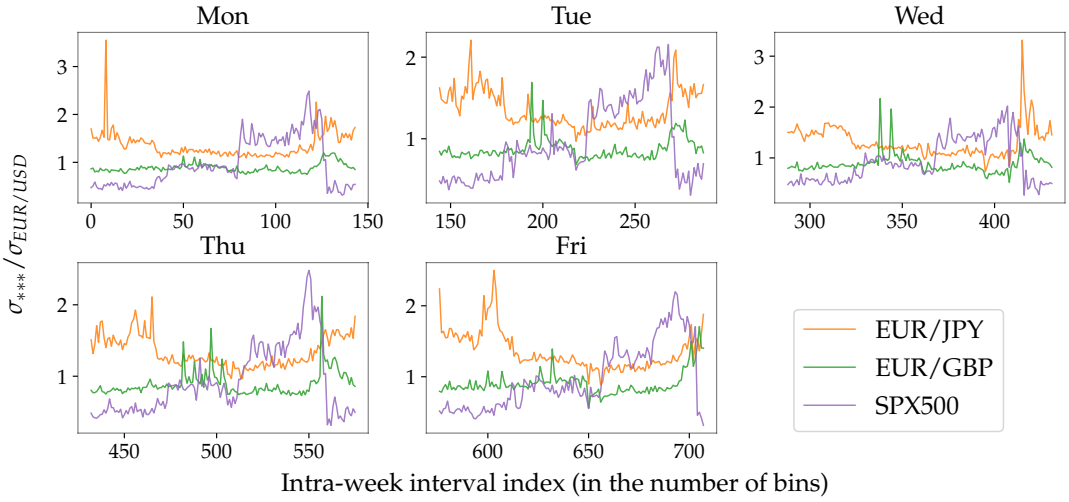

FIGURE 3.16: Daily realised volatility ratio of the given exchange rates (labelled by ***) and EUR/USD. The volatility is computed according to the "traditional" approach (Equation (3.20)).

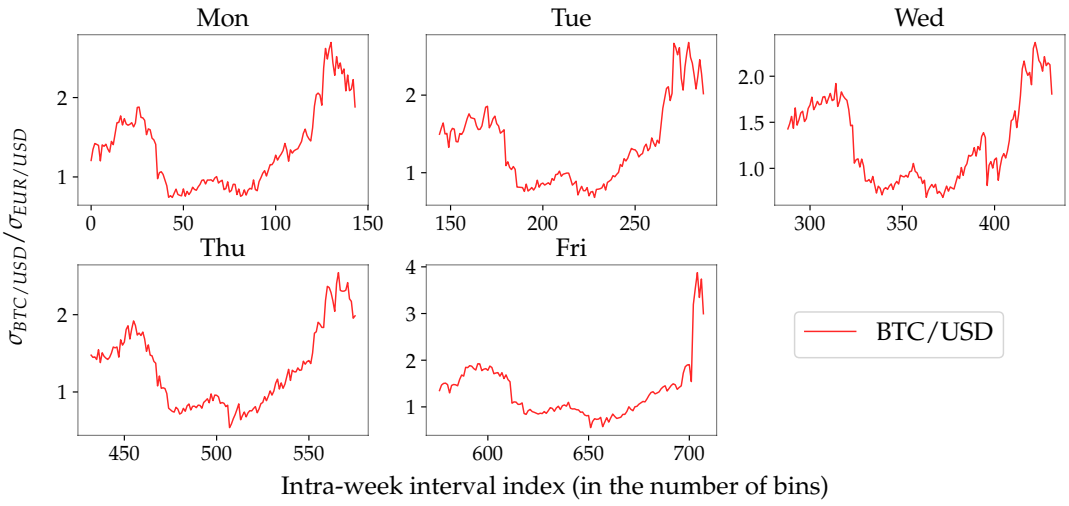

FIGURE 3.17: Daily instantaneous volatility ratio of BTC/USD measured over 10-min time intervals dissecting the entire week into 1008 bins. The volatility is computed according to the novel approach (Equation (3.19)).

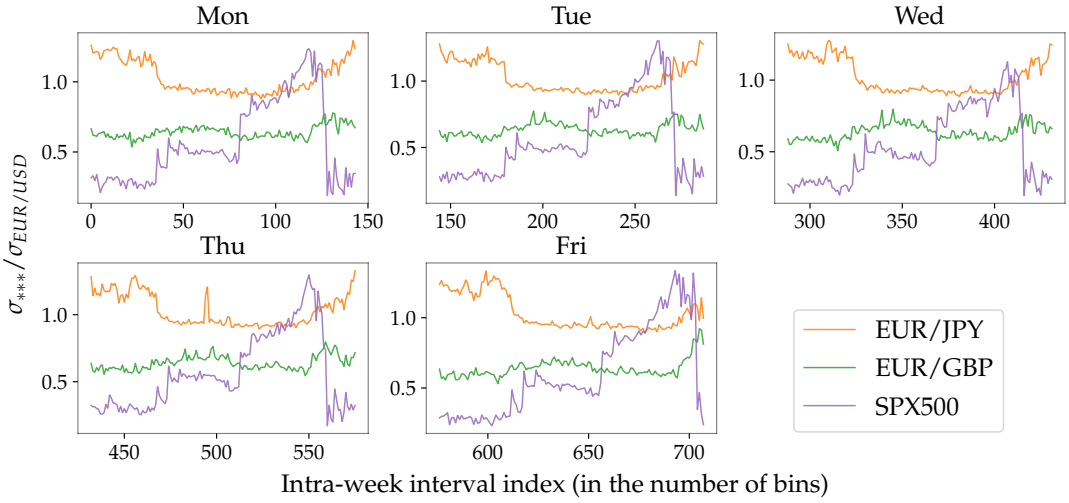

FIGURE 3.18: Daily instantaneous volatility ratio of the given exchange rates (labelled by ***) and EUR/USD. The volatility is computed according to the novel approach (Equation (3.19)).

TABLE 3.4: Daily instantaneous volatility ratio and the weekly standard deviation of two FX (EUR/JPY and EUR/GBP), one crypto (BTC/USD), and one stock (SPX500) exchange rates to EUR/USD. Columns $Ratio_*$ stands for the ratio of the average daily volatility of the corresponding exchange rate and one of EUR/USD. The average value computed over 10-min intervals. Columns std_* contain the standard deviation values of the volatility ratio over the set of 10-min intervals. The subscripts *trad* and *DC* label the measures made using the traditional volatility estimator (Equation (3.20)) and the novel approach (Equation (3.19)) correspondingly. The daily volatility ratios are graphically presented in Figures 3.16 and 3.17.

		Rat_{trad}	std_{trad}	Rat_{DC}	std_{DC}	Rat_{trad}/Rat_{DC}	std_{trad}/std_{DC}
Monday	EUR/JPY	1.35	0.27	1.03	0.12	1.31	2.25
	EUR/GBP	0.89	0.1	0.64	0.04	1.39	2.50
	BTC/USD	11.75	3.99	1.35	0.51	8.70	7.82
	SPX500	0.97	0.51	0.57	0.29	1.70	1.76
Tuesday	EUR/JPY	1.35	0.23	1.02	0.11	1.32	2.09
	EUR/GBP	0.88	0.13	0.63	0.05	1.40	2.60
	BTC/USD	11.7	4.53	1.35	0.52	8.67	8.71
	SPX500	0.95	0.47	0.57	0.3	1.67	1.57
Wednesday	EUR/JPY	1.31	0.3	1.02	0.12	1.28	2.50
	EUR/GBP	0.88	0.19	0.64	0.05	1.38	3.80
	BTC/USD	10.83	3.74	1.29	0.46	8.40	8.13
	SPX500	0.93	0.42	0.53	0.26	1.75	1.62
Thursday	EUR/JPY	1.34	0.22	1.03	0.12	1.30	1.83
	EUR/GBP	0.89	0.18	0.64	0.05	1.39	3.60
	BTC/USD	11.42	4.42	1.29	0.5	8.85	8.84
	SPX500	0.93	0.49	0.57	0.28	1.63	1.75
Friday	EUR/JPY	1.35	0.28	1.03	0.12	1.31	2.33
	EUR/GBP	0.9	0.17	0.64	0.06	1.41	2.83
	BTC/USD	11.81	4.93	1.3	0.54	9.08	9.13
	SPX500	0.98	0.46	0.61	0.31	1.61	1.48

4

Intrinsic Time Directional-Change Methodology in Higher Dimensions

---

The key to growth is the introduction of higher dimensions of consciousness into our awareness

— Lao Tzu

Vladimir Petrov, Anton Golub, and Richard Olsen

A version of this paper has been submitted to *Econometrics* (ISSN 2225-1146).

I have presented it at:

- Robust Techniques in Quantitative Finance, September 2018, Oxford, UK;
- Conference on Complex Systems 2018, September 2018, Thessaloniki, Greece;
- 4th Symposium on Quantitative Finance and Risk Analysis, June 2018, Mykonos, Greece.

Abstract

We extend the intrinsic time directional-change methodology to multidimensional space. The methodology is explored in the context of currencies where the currencies are orthogonal dimensions. The intrinsic time ticks whenever the price reverses from the local pick by a certain percentage. We generalise the concept of the price direction to the space of many dimensions. Scaling laws which were reported for one-dimensional time series are now reproduced in the multidimensional space. We report the increased systematic curvature in the fitted Forex scaling law data. The increase in the curvature size is associated with dimensionality growth. The novel methodology can be used as a method to estimate multidimensional volatility. The paper provides various ideas for practical applications of the multidimensional directional-change methodology.

4.1 Introduction

Foreign exchange (FX) is a complex system. Companies and individuals interact with each other at FX markets by exchanging national currencies. The total exchanged daily volume is measured in trillions of dollars[1] and is approximately a quarter of the entire USA GDP[2]. Such vast number indicates high market activity. That activity happens in the globalised financial world which can be considered as an interconnected system. Political movements, social trends, and media reports have an international impact in such a system (Gilpin and Gilpin 2001). Political and economical events relevant to a particular currency can occur at any moment and any geographical location. Media instantly transmit raw and preprocessed information about the events in par with rumours across the world. All national currencies can encounter a certain level of influence caused by any particular scheduled or an unexpected piece of news (Bauwens, Omrane, and Giot 2005). There are observations that currency markets still absorb news several days following the announcement (Evans and Lyons 2005). The financial market interconnectedness and the delayed information propagation suggest that monitoring of only a part of the complex system does not guarantee the absolute understanding of its behaviour. The constant supervision of multiple currency exchange rates should be performed in order to capture the information from the constantly evolving markets.

Development of multiple exchange rates can be interpreted as the evolution of a multidimensional system. Various research works have been performed in order to investigate the statistical properties of similar systems (see Canelas, Neves, and Horta (2013), Stöber and Czado (2014), Li, Yang, and Li (2017), Gidea and Katz (2018), and He, Shang, and Xiong (2018), among others). The preponderance of the research papers on the multidimensional financial data considers the market as a system developing in physical time. Physical time assumes measuring intervals between financial events in years, days, or minutes. It is not always discussed that the equidistant periods, typically employed for the market analysis, are directly linked to the physical rotation of the cosmic bodies. For instance, periodicity of days, so commonly used to close positions or correct indexes, is defined by the rotation of the Earth around its axis. The round dance of seasons, in turn, is the result of the Earth revolving around the Sun. Furthermore, the international unit of physical time is one second. According to the International System of Units (Taylor and Thompson 2008):

1 According to the Bank for International Settlements, the average daily FX volume in 2016 exceeds five trillion. https://www.bis.org/publ/rpfx16.htm.

2 According to https://www.bea.gov/.

> The second is the duration of 9 192 631 770 periods of the radiation corresponding to the transition between the two hyperfine levels of the ground state of the cesium 133 atom.

Consequently, market regime switches, trading returns, volatility seasonality, and many other financial metrics viewed over predefined intervals in physical time are expected to be linked to the peculiar behaviour of a particular atom. It is hardly presumable that natural disasters, fiscal political decisions, or large business moves deliberate the tiny atom oscillations while deciding when to appear. The market-related activities sovereignty of event-time is pronounced in the following metamorphosis: price curve standstills followed by an accidental extreme activity which rapidly disappears after an irregular period of time. Therefore, referring to the price behaviour over fixed and lengthy time intervals inevitably results in refraining a substantial part of the information related to the market's microstructure (Bauwens and Hautsch 2009). Alternatively, too much noisy data is collected if the intervals are overly short.

Even-driven time frameworks were proposed to consider endogenous exchange rate heartbeat pronounced as the price variability. The concepts advocate the use of the number of performed transactions (Mandelbrot and Taylor 1967), cumulative trading volume (Mandelbrot 1997), and alternating price moves of the certain size (Guillaume et al. 1995) as events. The success of these research works sparked the attention to the event-driven time. In particular, it produced an increasing interest in time independent empirical patterns of high frequency markets (Glattfelder, Dupuis, and Olsen 2011).

The event-driven time framework proposed by Guillaume et al. (1995) considers price moves as the only source of information. Guillaume introduced a new financial time measure: "intrinsic time". The intrinsic time ticks when a price curve experiences a trend reversal of the given size. In other words, the curve performs directional-changes (threshold δ determines the size of the price move until a directional change). The intrinsic time framework dissects chronological collection of prices into an ensemble of directional-change intrinsic events. The set of events can be interpreted as a compilation of interchanging drawups and drawdowns. Size of each drawup and drawdown matches the size of the threshold δ. The threshold and the initial direction of the trend are the only variables needed to begin the dissection procedure.

Many research papers have been written regarding the directional-change intrinsic time. Most of the authors utilised the framework for high frequency markets analysis. We would like to highlight the article of Golub et al. (2014) among others. The authors of the arti-

cle proposed Intrinsic Network (IN) model based on the directional-change intrinsic time framework. The model can be employed to express the evolution of high frequency markets considered from multiple scales. The Intrinsic Network is arranged as an aggregate of directional-change intrinsic events observed at various trends. The authors illustrated how the evolution of the hierarchical network structure can be used as an early warning signal of financial crises. The proposed model is also capable of serving as a liquidity indicator for high frequency markets. The indicator can be equally applied to markets characterised by any scale of volatility. Later, Golub, Glattfelder, and Olsen (2017) employed the proposed Intrinsic Network as a part of an efficient trading algorithm. The algorithm, called "Alpha Engine", does not only produce steady profit but also stabilises markets by providing liquidity. The designed counter-trending algorithm submits orders at the moments of intrinsic events at the given exchange rate. The high performance of the trading method is attributed to the way how different market properties pronounced at various trend scales are efficiently captured in directional-change intrinsic time.

The directional-change intrinsic time framework became a new paradigm in financial data analysis. Its advantages can be summarised as the following:

- the dissection algorithm can be applied to any tick-by-tick time series; no special algorithm tuning is required despite the diverse range of frequency and magnitude of the provided exchange rate returns. The effect is vividly pronounced in Glattfelder, Dupuis, and Olsen (2011) where similar scaling properties were observed after applying the directional-change algorithm to different exchange rates;

- distinct thresholds can be utilised to simultaneously dissect a time series into a collection of directional-changes; information on directional-changes observed at multiple scales can be aggregated to study the statistical probability of the given price trajectories (read about the price "surprise" in Golub et al. (2014));

- volatility of a financial time series impacts the frequency of directional changes; the information on the impact can be used to compute instantaneous volatility (see Petrov, Golub, and Olsen (2019) for an example how the intrinsic time can be utilised to unveil the instantaneous volatility seasonality).

Authors of research articles where the directional-change intrinsic time was employed for high frequency data analysis focused their attention on single time series only. To the limits of our knowledge, the extension of the intrinsic time framework to the multidimensional space has never been proposed. Therefore, this is the first paper suggesting the multidimensional

directional-change intrinsic time framework. The framework is capable of managing multiple exchange rates concurrently.

This paper continues as follows: Section 4.2 provides the basics of the directional-change intrinsic time dissection procedure previously reported for one-dimensional data. Section 4.3 describes the theoretical concepts developed in one-dimensional intrinsic time. We provide the extended version of the directional-change intrinsic time to the multidimensional space in Section 4.4. Section 4.5 outlines how the analytical tools developed for one-dimensional data can be applied in multidimensional space. A set of experiments on two-dimensional processes formed by independent and correlated Brownian motions is described in Section 4.6. Analysis of two-, five-, and 23-dimensional FX exchange rates is illustrated in Section 4.7. Finally, we summarise the major findings of this paper in Section 4.8.

4.2 One-dimensional Directional-Change Intrinsic Time

Figure 4.1 presents an example of five-days long price curve dissected into a collection of directional-changes. The arbitrary chosen fixed directional-change threshold δ specifies the scale of trend changes which are associated with intinsic events. The threshold selected for the given example is displayed in Figure 4.1 at the centre of the frame as a vertical red line. The threshold has to be defined at the beginning of the dissection procedure. It stays constant over time. The direction of the initial trend (mode) can be arbitrary chosen among two states: mode upward or mode downward. The choice of the initial trend has a low impact on the dissection procedure results: the sequence of the directional changes becomes independent of the initial direction choice after two intrinsic events. It is assumed to be downward for the dissection procedure depicted in Figure 4.1.

The start of the dissection procedure in Figure 4.1 is labelled by a star. The first directional-change event occurs when the price moves down by δ from the local extreme: the highest price since the dissection initialisation (the first grey square from the left, tick "1" on the "Intrinsic Events" timeline). The mode alternates (becomes upward) as soon as a new directional-change is registered. At this step, the local extreme is reset: it now indicates the smallest observed price since the latest directional-change. The next intrinsic event is registered when a return of the size δ measured from the local extreme and the latest price unfolds (labelled as tick "2" on the "Intrinsic Events" timeline). The trend mode alternates again, the local extreme becomes reset, and the dissection process continues. The part of the price trajectory between previous directional-change and the latest local extreme observed before the new directional change is called overshoot (see, for example, the dashed line between events number 2 and

3). The initial price curve becomes split into a set of intervals. All intervals belong to one of two categories: directional-changes (marked by solid lines) and overshoots (dashed lines).

The directional-change threshold δ affects the quantity and the frequency of intrinsic events in a time series of the given length. Various dissection patterns similar to the one on Figure 4.1 emerge depending on the chosen threshold size.

The directional-change intrinsic time proposed by (Guillaume et al. 1995) operates beyond the limits of physical time. Only price changes of particular size affect the periodicity of intrinsic events. That time independence made possible the financial data analysis not constrained by drawbacks of the data filtering associated with the equidistant periods used for the market observations. Guillaume et al. (1997) reported the first scaling-law fully based on price behaviour considered from the directional-change intrinsic time point of view. The scaling law relates the number of directional-changes $N_{DC}(\delta)$ in a given time series to the size of the threshold δ chosen for the dissection:

$$N_{DC}(\delta) = \left(\frac{\delta}{C_{N_{DC}}}\right)^{E_{N_{DC}}}, \tag{4.1}$$

where $E_{N_{DC}}$ and $C_{N_{DC}}$ are the scaling law coefficients[3]. Scaling law (4.1) was shown to be stable for the wide range of FX exchange rates and for a wide variety of time intervals: from 10 minutes to two months. Glattfelder, Dupuis, and Olsen (2011) extended the list of known high frequency FX scaling laws. Several scaling laws revealed by the authors are found using the directional-change intrinsic time concept. All uncovered by the authors dependencies have the form:

$$y = \left(\frac{x}{C_*}\right)^{E_*}. \tag{4.2}$$

Symbol $*$ under scaling coefficients E and C stands for the type of values connected by the function (4.2). For example, the dependence can be built for the number of ticks or the maximum return per a given period of time ($*$ becomes N_{ticks} and Δx_{max}). The discovered by Glattfelder, Dupuis, and Olsen (2011) set of omnipresent statistical properties promised to significantly enhance our ability to interpret and foresee FX prices behaviour.

4.3 Theoretical Background

The analytical and empirical study of the expected number of directional-changes and waiting times has progressed over the years. Petrov, Golub, and Olsen (2019) provided analytical expressions for the expected number of intrinsic events in Brownian motion with volatility

3 The coefficient $E_{N_{DC}}$ is also called the drift exponent.

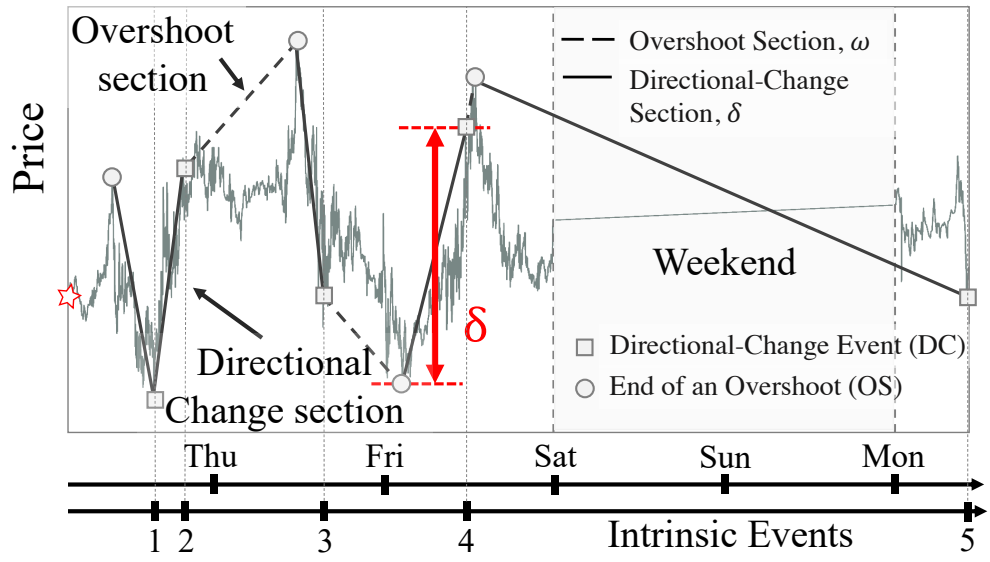

FIGURE 4.1: Example of an exchange rate price curve dissected into a set of directional-changes. The size of the threshold δ, used in the procedure, is shown by the red vertical line. Grey squares and grey circles label directional-change points and the latest local extremes correspondingly; solid and dashed lines are directional-change and overshoot sections. The dissection is initiated at the first available price (marked by a red star at the beginning of the time range).

σ and trend μ. The events are registered using the threshold δ within a time interval of the length T:

$$\mathbb{E}[N(\delta;\mu,\sigma,[0,T])] = \frac{2T\frac{2\mu^2}{\sigma^2}}{e^{-\frac{2\mu}{\sigma^2}\delta} + e^{\frac{2\mu}{\sigma^2}\delta} - 2}. \tag{4.3}$$

Taylor expansion $e^{\pm\frac{2\mu}{\sigma^2}\delta} = 1 \pm \frac{2\mu}{\sigma^2}\delta + \frac{(\frac{2\mu}{\sigma^2}\delta)^2}{2!} + \mathcal{O}(\mu^3)$ can be applied to derive the expected time when the trend $\mu \to 0$ and period T is one year:

$$\mathbb{E}[N(\delta;\sigma)] = \frac{\sigma^2}{\delta^2}. \tag{4.4}$$

Using properties of the renewal point process from Rolski et al. (2009), the expected time of a new directional-change can be defined as a reciprocal to the expected number of directional changes:

$$\mathbb{E}[T(\delta;\mu,\sigma)] = \frac{e^{-\frac{2\mu}{\sigma^2}\delta} + e^{\frac{2\mu}{\sigma^2}\delta} - 2}{2\frac{2\mu^2}{\sigma^2}}. \tag{4.5}$$

Equation (4.4) states that the number of directional-changes registered by the threshold of the size δ increases as the second power of volatility σ. The obtained dependence is closely similar to the empirically observed scaling law reported in Guillaume et al. (1997) and confirmed by Glattfelder, Dupuis, and Olsen (2011) (law ob in the article, "Directional change count"). That similarity confirms close to the Brownian motion evolution of FX exchange rates.

In this work, we contribute to the theoretical knowledge on one-dimensional directional-change intrinsic time. We combine equations (4.1) and (4.4) in order to demonstrate the connection of the volatility and the scaling law coefficient $C_{N_{DC}}$ of Directional change count scaling law:

$$\mathbb{E}[N(\delta;\sigma)] = \frac{\sigma^2}{\delta^2} = \left(\frac{\delta}{\sigma}\right)^{-2} \Longrightarrow E_{N_{DC}} = -2, \;\; C_{N_{DC}} = \sigma. \tag{4.6}$$

Equation (4.6) states that the scaling coefficient $E_{N_{DC}}$ should tend to be equal to -2 and the coefficient $C_{N_{DC}}$ represents the volatility value of the studied stochastic process. The latter builds the bridge between properties of scaling laws revealed in the intrinsic time and volatility of the process typically measured in physical time. One can find a confirmation of the bridging by referring to the list of tables provided in Glattfelder, Dupuis, and Olsen (2011). Table A1 named "Directional change count, law (0b)" contains scaling coefficients $C_{N_{DC}}$ for a series of FX exchange rates. An attentive reader might find the presented coefficients to be relatively close to the volatility of the selected exchange rates[4].

We confirm the connection of the Direction Change Count scaling law coefficient $C_{N_{DC}}$ and the volatility of the studied process. The confirmation is done by comparing the scaling law coefficient with volatilises of the exchange rates used in our tests. We also propose to consider the scaling coefficient $C_{N_{DC}}$ as the proxy for the multidimensional volatility. The volatility, the computation of which is independent on the space dimensionality. To the extent of our knowledge, this is the first work where a concept of multidimensional volatility is presented.

4.4 Multidimensional Directional-Change Intrinsic time

This work challenges the extension of the one-dimensional directional-change algorithm to work with multidimensional data. We create a list of criteria which have to be satisfied in order to confirm the validity of the extended approach:

- the multidimensional algorithm, applied to 1D data, should reproduce the same set of intrinsic events generated by the 1D algorithm (convergence);
- the algorithm should work with data sets composed of any number of dimensions (universality);
- risk management and data analysis tools developed in 1D intrinsic time should be equally applicable in the multidimensional space (expansion).

4 We leave the computation part needed to verify the statement to the reader.

Multidimensional space morphology complicates the direct extension of the 1D dissection algorithm. Upward and downward orientations straightforward in the 1D price-time space cannot be unambiguously defined in the space where exchange rates form dimensions. To visualise the problem, the upper part of Figure 4.2 demonstrates a 2D system[5] formed by two orthogonal time series: P_1 and P_2. The 2D price-price space has no point which would unconditionally define the upward and the downward orientations. This is the crucial difference considering that the 1D algorithm (Section 4.2) review whether a new price is located above or below the latest local extreme for every new price tick. Therefore, the local trend orientation and the local extreme definitions should be reconsidered. The "convergence" validation criteria should always be kept in mind.

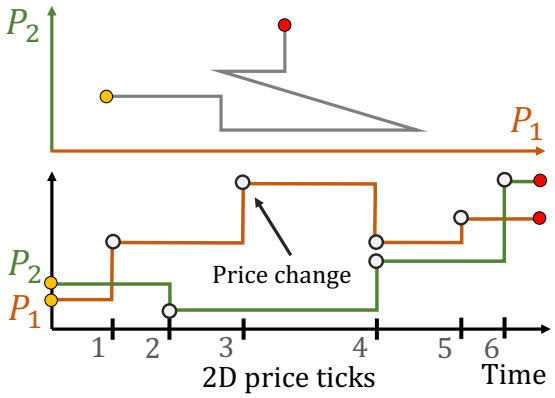

FIGURE 4.2: Upper part: stylised example of price moves in a two-dimensional space formed by orthogonally placed exchange rates P_1 and P_2. Lower part: an example of two time series P_1 and P_2 whose price changes are registered on the same time curve (black strokes).

One point is enough to split a 1D price space. One of the regions stands for all prices below the given point, and another region stands for all prices above. These two sub-spaces are used to classify a newly registered price tick in the original 1D directional-change algorithm (see Figure 4.3a). The classification determine whether the local extreme has to be updated. Similarly, the price trend is defined by whether the price curve tends to go above or below that local extreme. We reformulate the concept of price trend which would work in the space of any dimensionality.

The 1D directional-change dissection procedure operates with such definitions as up and down. However, there is an alternative way of defining the trend in 1D space. The relative location of a pair of prices selected on the historical price curve can serve as the reference for the trend. The required points are the location of the latest to the given moment

5 An example of 3D price moves in the space formed by real FX exchange rates can be see in Figure 4.16.

directional-change (S_{DC}, DC stands for "directional-change") and the local extreme preceding that directional-change (S^p_{ext}, p stands for "previous"). The mode depends on the direction of the vector, which starts from the previous extreme price and passes through the latest directional-change point. We call such a vector as "directional vector" and label it by $\vec{D}$. The latest local extreme S_{ext} will serve as "transition point". Every new prices which appears on the opposite side of the 1D space from S^p_{ext} with respect to the transition point is the new extreme.

The new vector-based orientation definition allows the extension of the 1D dissection procedure to the multidimensional space. Following the logic of the entire space split in two equal parts, a line can split a 2D space. The local extreme update can be defined by considering in what sub-space the new price is located with respect to a line. Two points have to be selected in order to split a 2D space into two sub-spaces (according to the point–line–plane postulate). The line, going through the latest local extreme and orthogonal to the vector $\vec{D}$, splits the 2D space into two regions (Figure 4.3b). We call the line "transition border".

The transition border defines whether a new price updates the local extreme in 2D: a new price is a new extreme if the price and the latest directional-change are located on opposite sides of the transition border. Following the logic of the space split into two equal parts by a transition point in 1D and by a transition border in 2D, the line gets extended to a surface in three- or higher- dimensional space. The surface is orthogonal to the directional vector $\vec{D}$ and includes the latest local extreme (Figure 4.3c). Without the loss of generality, we will call the transition point/border/surface as "transition border".

The trend mode, equal to "upward" or "downward" in 1D, losses the orientation meaning in higher dimensions. We assign values ± 1 to the mode which alters after each directional change.

We note that the chose of the distance metric does not impact results of the experiments due to the equivalence of metrics in higher dimensions. We selected Euclidean metric to compare two points $\mathbf{p} = (p_1, p_2, \ldots, p_n)$ and $\mathbf{q} = (q_1, q_2, \ldots, q_n)$ where p_i and q_i are coordinate along corresponding axis i:

$$d(\mathbf{p}, \mathbf{q}) = \sqrt{(q_1 - p_1)^2 + (q_2 - p_2)^2 + \ldots + (q_n - p_n)^2} = \sqrt{\sum_{i=1}^{n} (q_i - p_i)^2}. \tag{4.7}$$

The original 1D directional-change algorithm operates with relative distances. Therefore, we define the n-dimensional Euclidean distance as:

$$d\left(\mathbf{p}, \mathbf{q}\right) = \sqrt{\sum_{i=1}^{n} \left(\frac{q_i - p_i}{p_i}\right)^2}. \tag{4.8}$$

A directional-change happens if the following two criteria are satisfied:

1. the new price is not a new local extreme;
2. the shortest distance between the new price and the current transition border is bigger than or equal to the threshold δ.

The associated with the directional-change event overshoot part of the price curve is defined as the shortest distance between a directional-change and the transition border preceding the following event.

The second item in the list can be optimised by introducing two new concepts of the multidimensional dissection procedure. First, there is an "escape point/border/surface". The escape point/border/surface is parallel to and always located at the distance δ from the transiting border. The distance is measured towards the beginning of the directional vector. As in the case of the transition border, we will use "escape border" whenever we talk about the escape point/border/surface. Two rules from the list 2 can be substituted by the following one:

> a directional-change happens when price curve crosses the escape border.

Second, we call the space between the transition and the escape borders as the "transition corridor". The transition corridor defines a part of the space where the price can freely fluctuate without triggering a new directional-change or updating the local extreme. In one-dimensional case, the transition corridor is equivalent to the price fluctuations between S_{ext} and $S_{ext}(1 \pm \delta)$. Figure 4.3a visualises a 1D space where new and updated directional-change terms are applied. The figure demonstrates a directional vector $\vec{D}$ (red vector), the latest directional-change (black square), preceding local extreme (downward triangle), "transition point" (empty circle), "escape point" and transition corridor.

4.4.1 Dissection Example

An example of the multidimensional directional-change dissection procedure applied in 2D space is provided in Figure 4.4. For the demonstration purposes, the threshold δ has been defined in absolute terms.

First (Figure 4.4a), the initial directional vector $\vec{D}$ has to be specified given only one price ("Start price" on the figure). The vector can be defined in the following way: one should wait until the moment when the price moves away from the initially given point to the distance δ. That is, the price should escape the circle of radius δ with the centre at the initial price (red

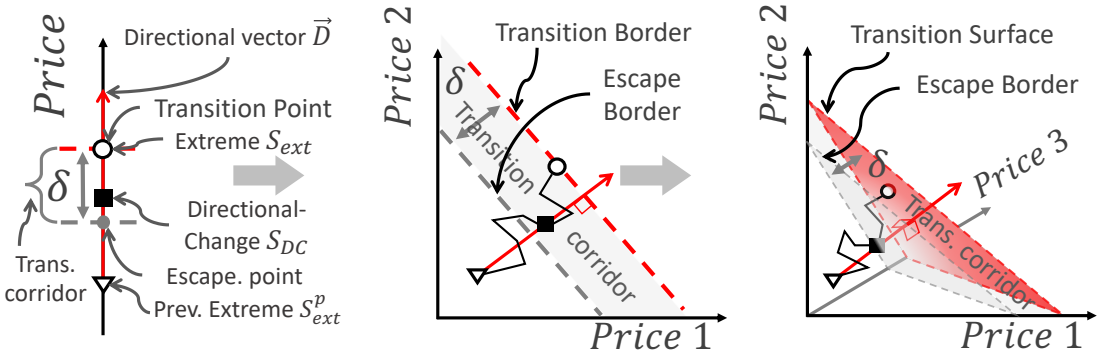

FIGURE 4.3: Components and the evolution of the directional-change intrinsic time concept in **(a)** 1D, **(b)** 2D, and **(c)** 3D spaces. Price moves are represented by the solid black broken lines in sub-figures **(b)** and **(c)**. Solid squares ■ stand for the latest DC price (S_{DC}), empty circles ○ are the latest extremes (S_{ext}), downward triangles ▽ mark the preceding the directional-change local extremes (S^p_{ext}). Red dashed line labels the transition point in 1D space, transition border in 2D space, and transition surface in 3D space. Grey dashed line marks the escape point, escape line, and escape surface.

dashed line in Figure 4.4a defines the border of the circle). We call the price crossing the circle as the first directional change (S_{DC}, labelled by a full black square). The centre of the circle (the start price) becomes the preceding to the directional-change local extreme (S^p_{ext}, labelled by a reversed empty triangle).

Sub-figure 4.4b shows how the latest directional-change and the preceding local extreme define the directional vector (red vector $\vec{D}$). The vector and the latest local extreme determine the transition border (red dashed line). The line determines two regions of the 2D space. We call by "Overshoot region" the area, entering which the price becomes a new extreme. "Directional-Change" is the region, inside of which the next directional-change intrinsic event will be registered.

The price trajectory between a couple of consecutive intrinsic events is presented in Figure 4.4c. There are two noticeable parts of the price evolution. First, the price updated the transition border (and the local extreme) by crossing it twice. The transition border was adjusted (as well as the escape border) after every local extreme update. The latest local extreme (S_{ext}) (white circle) coincides with the price which updated the transition border for the last time. Second, the price left the transition corridor by crossing the escape border. A new directional-change becomes registered right after the escape. At that point, the length of the overshoot part (ω_1) of the price curve can be measured.

The mode alternates after a new directional-change. The directional vector gets redefines considering new S_{DC} and S^p_{ext} (see Figure 4.4d). The 2D space is split by the new transition border. Figures 4.4e and 4.4f demonstrate a piece of the price curve evolution and one more directional-change intrinsic event. As in the 1D case, the whole price curve becomes dissected into a collection of directional-changes and overshoots (solid and dashed lines in Figure 4.4g).

We provide a pseudo-code of the multidimensional directional-change dissection algorithm in Appendix 4.E. Some of the tools used for the given research can be found in the author's GitHub repository https://github.com/VladUZH/VlPetrov.

4.4.2 Algorithm Coherence

According to the set of validation criteria (Section 4.4), the proposed multidimensional directional-change algorithm should be coherent with the original 1D dissection procedure. In other words, the set or directional-changes returned by the multidimensional version of the algorithm applied to the 1D time series should coincide with the set of events returned by the 1D algorithm applied to the same data. In addition, scaling laws based on the directional-change events should coincide in both cases too. A series of tests was performed in order to validate the coherence.

Returns dS_t of the artificially simulated time series used for the validation experiment are based on the Geometrical Brownian Motion (GBM) with parameters μ (trend) and σ (volatility):

$$dS_t = \mu S_t dt + \sigma S_t dW_t, \tag{4.9}$$

Parameters used in the test are: $S_0 = 1.0$, $\mu = 0$, $\sigma = 0.2$. There were 200 000 000 elementary returns generated.

The set of returns was run through the original 1D and the multidimensional algorithms. A collection of directional-change thresholds of various sizes was applied. The thresholds range from $\delta = 0.01\%$ to $\delta = 4.0\%$. They are equally distributed over 50 intervals in the log-space. First, price-time coordinates of each intrinsic event were registered. The coordinates confirm that both dissection methods return exactly the same set of directional-changes. Second, the average overshoot length $\langle \omega(\delta) \rangle$ and the total number of directional changes $N_{DC}(\delta)$ were computed for every threshold δ. Dependencies $\langle \omega(\delta) \rangle$ and $N_{DC}(\delta)$ (Overshoot and Directional change count scaling laws) were build in the log-log space[6]. As in the work of Glattfelder,

6 We note that the same procedure will be applied to reveal scaling laws in all further sections unless otherwise is specified.

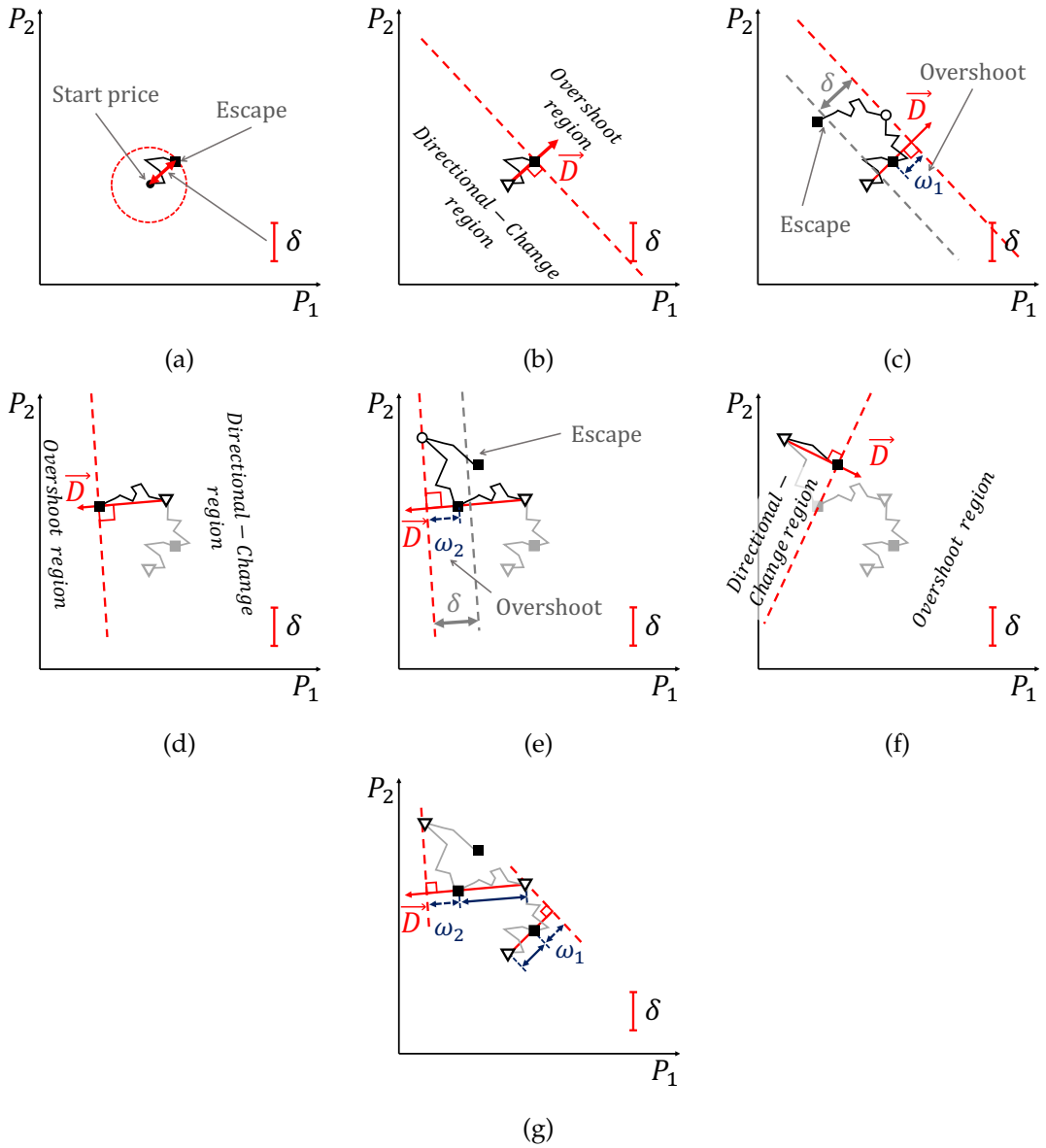

Figure 4.4: Example of a 2D price curve (P_1, P_2) dissected into a collection of directional-change intrinsic events. The selected threshold δ is expressed in absolute terms. The size of the threshold is shown on each subplot. **(a)** Initialisation of the dissection procedure: the price curve escapes a circle with the centre at the initially given price (black circle •) and with the radius δ. **(b)** The first directional vector ($\vec{D}$) is defined as a vector starting from the previous extreme (S^p_{ext}) (empty triangle ▽) and going through the latest directional-change point S_{DC} (black square ■). The transition border (red dashed line) defined as the straight line orthogonal to the directional vector and going through the latest extreme (white circle ○, currently coincides with the directional-change point). The border splits the 2D space into the Overshoot and the Directional-Change regions. **(c)** The transition border changes every time when the price crosses it. The distance between the transition and the escape borders is equal to the threshold δ. A new directional-change happens when the price escapes the transition corridor crossing the escape border. **(d)** The directional vector as well as the transition border are redefined considering the location of the latest directional-change and the preceding local extreme. The updated previous extreme and the newest directional-change point determine the directional vector. **(e)** Another intrinsic event is observed when the price escapes the transition corridor. **(f)** Redefined directional vector and the transition border. **(g)** Solid dark-blue lines are the directional-change parts of the price trajectory (their size is $\geq \delta$). Dashed dark-blue lines are overshoot sections $\omega_i \geq 0$ where i is the index of the corresponding directional-change.

Dupuis, and Olsen (2011), a linear relationship between the variables y ($\langle\omega(\delta)\rangle$ or $N_{DC}(\delta)$) and x (δ) in the log-log space was assumed. Scaling parameters C_* and E_* were derived through the parameters A and B of the best fit $y = A + Bx$:

$$E = B, \quad C = \exp(-A/B). \tag{4.10}$$

Scaling parameters of the Directional change count and the Overshoot scaling laws (laws (c) and (q) in Glattfelder, Dupuis, and Olsen (2011)) coincide for both algorithms. Figure 4.5 demonstrates the scaling laws computed applying the multidimensional version of the directional-change algorithm to the 1D time series.

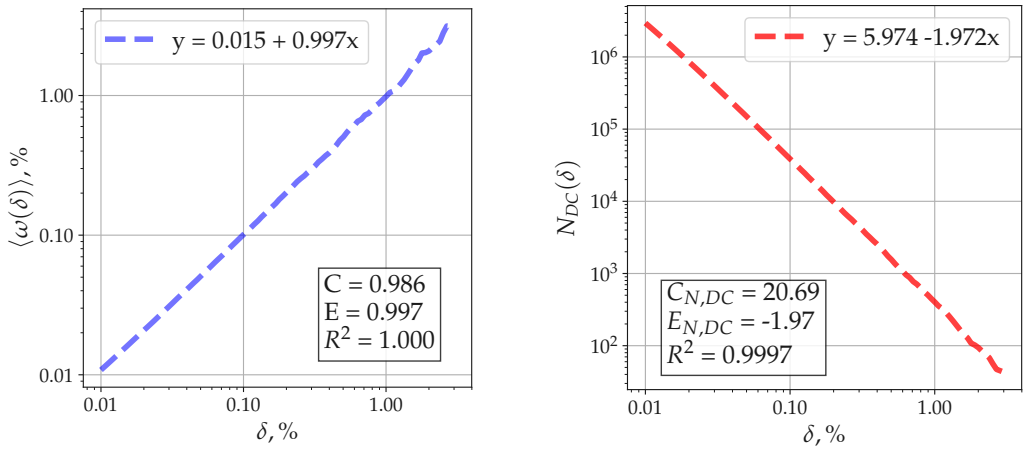

(a) (b)

FIGURE 4.5: **(a)** Overshoot and **(b)** Directional change count scaling laws found using the multidimensional directional-change algorithm (Section 4.4 and Appendix 4.E) applied to a simulated 1D GBM time series. Parameters of the generated time series are: $S_0 = 1.0$, $\mu = 0$, $\sigma = 0.2$. There are 200 000 000 returns in the data set.

In Section 4.3 we noticed that the scaling coefficient $C_{N_{DC}}$ of the Directional change count scaling law should coincide with volatility of the studied process and $E_{N_{DC}}$ should tend to -2. Value $C_{N_{DC}} = 20.69$ in Figure 4.5b is indeed close to the value of the assumed volatility 20%. Coefficient $E_{N_{DC}} = -1.97 \approx -2$ confirms the theory.

4.5 Extension of 1D Approaches

In this section, we show how equations (4.3) and (4.5) defining the expected waiting time until the next directional-change and the total number of intrinsic events in 1D space can be employed in n-dimensional space. Multidimensional processes, used in the section, are

composed of 1D Brownian motions with volatility σ_i. We assume complete independence of the processes forming the multidimensional space.

4.5.1 2D Space

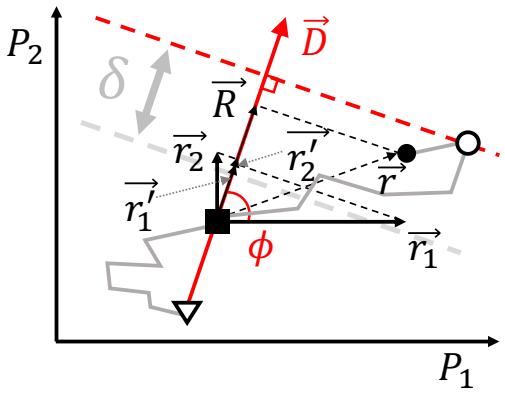

FIGURE 4.6: An illustration of the 2D space $(P_1(\sigma_1), P_2(\sigma_2))$.

According to the extended definition of the directional-change intrinsic time algorithm (Section 4.4), there is always a transition border which splits the space into two regions. Vector $\vec{D}$ passing through the latest directional-change and starting from the preceding local extreme represents the direction of the shortest path to the transition border. In Figure 4.6, vector $\vec{r}$ labels the distance between the current price (black circle) and the latest directional-change in 2D. Only the component of $\vec{r}$ parallel to the directional vector $\vec{D}$ contributes to the change in the distance between the current price and the transition border. The price can freely fluctuate along the border (inside the transition corridor) without triggering a new intrinsic event. Therefore, properties of price moves along the vector $\vec{D}$ (we label the corresponding process by R) is the only information needed to employ equations (4.3) and (4.5) to describe the evolution of the 2D process given that particular vector. We note, that the equations work only for the fixed directional vector. They do not yet describe the evolution of $\vec{D}$ in the entire 2D space.

Properties of the process R can be found using properties of processes P_1 and P_2 forming the 2D space. The degree to which they contribute to the evolution of the process R is defined by the relative location of the directional vector $\vec{D}$. The location of the vector $\vec{D}$ is determine by the angle $\phi \in [0, 2\pi)$ measured between the positive direction of axis P_1 and the vector itself.

If P_1 and P_2 are independent and identically distributed random variables (iid) than their projections r'_1 and r'_2 on $\vec{D}$ are iid too. In this case, the volatility of the process R:

$$\sigma_R(\sigma_{r'_1}, \sigma_{r'_2}) = \sqrt{\sigma^2_{r'_1} + \sigma^2_{r'_2}}. \tag{4.11}$$

In turn, volatilities $\sigma_{r'_1}$ and $\sigma_{r'_2}$ of projections are:

$$\begin{aligned} \sigma_{r'_1}(\sigma_1; \phi) &= \sigma_1 \cos\phi, \\ \sigma_{r'_2}(\sigma_2; \phi) &= \sigma_2 \sin\phi, \end{aligned} \tag{4.12}$$

which leads to:

$$\sigma_R(\sigma_1, \sigma_2; \phi) \equiv \sigma_{\parallel}(\sigma_1, \sigma_2; \phi) = \sqrt{(\sigma_1 \cos\phi)^2 + (\sigma_2 \sin\phi)^2}. \tag{4.13}$$

We use the notation $\sigma_{\parallel}$ to highlight that the composed volatility is the volatility of the process evolving parallel to the directional vector $\vec{D}$.

The volatility of the process R is independent of the angle ϕ if $\sigma_1 = \sigma_2 = \sigma$ (equation (4.13)). That fact allows interpreting the evolution of 2D process in the directional-change intrinsic time as the evolution of 1D process with volatility σ. The mandatory requirement: the processes, forming the 2D space, have to be iid, have no trend component, and should be equally volatile.

Figure 4.7a demonstrates σ_R as a function of the angle ϕ in 2D space. Three sets of volatilities σ_1 and σ_2 are presented. The smallest and the largest volatility values of the process R can be observed at the angle $\phi = 0$ (along x-axis) and $\phi = \pi/2$ (along y-axis). The values are equal to the volatility of the processes evolving along the corresponding axis.

Equation (4.13) was derived assuming independence of the processes forming the space. However, FX exchange rates are rarely entirely independent. The equation has to be adapted in order to be used for real practical implications.

If $\rho_{1,2}$ is the correlation coefficient of processes P_1 and P_2, then the variance of the process R:

$$\begin{aligned} \mathrm{Var}(R) &= \mathrm{Var}(r'_1) + \mathrm{Var}(r'_2) + 2\mathrm{Cov}(r'_1, r'_2) = \\ &= \cos^2\phi \mathrm{Var}(P_1) + \sin^2\phi \mathrm{Var}(P_2) + 2\rho_{1,2}\cos\phi\sin\phi\sqrt{\mathrm{Var}(P_1)\mathrm{Var}(P_2)}. \end{aligned} \tag{4.14}$$

Volatility σ_R can be defined using the variance and considering that for a process x $\sigma^2(x) = \mathrm{Var}(x)$:

$$\sigma_R = \sqrt{\sigma^2_{r'_1} + \sigma^2_{r'_2} + 2\mathrm{Cov}(r'_1, r'_2)} = \sqrt{\cos^2\phi\sigma_1^2 + \sin^2\phi\sigma_2^2 + 2\rho_{1,2}\cos\phi\sin\phi\sigma_1\sigma_2}. \tag{4.15}$$

Equation (4.15) connects volatilities of the processes forming the 2D space (σ_1, σ_2), their correlation coefficient ($\rho_{1,2}$), and the angular coordinates of the directional vector $\vec{D}$ (ϕ) with the

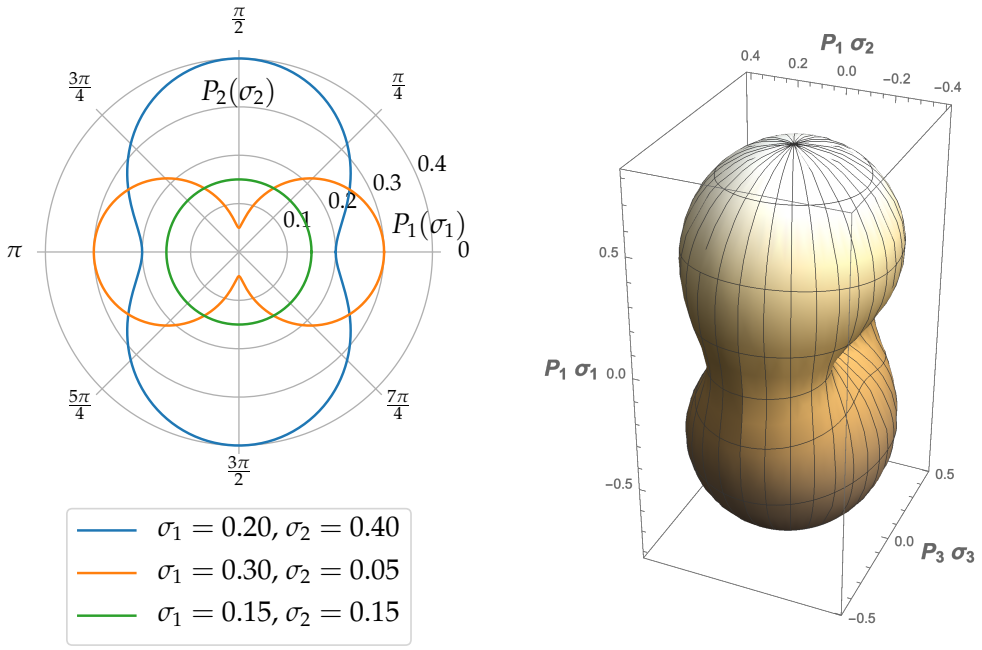

(a) (b)

FIGURE 4.7: **(a)** Volatility surface of the process R evolving along the directional vector $\vec{D}$ (σ_R in equation (4.13)). Three combinations of σ_1 and σ_2 are displayed. Volatilities of the processes forming the 2D space are shown under the plot. **(b)** Volatility σ_R in 3D space formed by processes $P_1(\sigma_1 = 0.8)$, $P_2(\sigma_2 = 0.45)$, and $P_3(\sigma_3 = 0.1)$.

volatility of the process R (σ_R) evolving along the vector. The expressed volatility σ_R can serve as an input for analytical equations from Section 4.3. For example, the expected waiting time for a directional-change to unfold in 2D space:

$$\mathbb{E}[T(\delta, \rho_{1,2}, \sigma_1, \sigma_2; \phi)] = \frac{\delta^2}{\cos^2\phi\sigma_1^2 + \sin^2\phi\sigma_2^2 + 2\rho_{1,2}\cos\phi\sin\phi\sigma_1\sigma_2}. \tag{4.16}$$

The expected number of directional-changes, correspondingly:

$$\mathbb{E}[N(\delta, \rho_{1,2}, \sigma_1, \sigma_2, [0,T]; \phi)] = \frac{T(\cos^2\phi\sigma_1^2 + \sin^2\phi\sigma_2^2 + 2\rho_{1,2}\cos\phi\sin\phi\sigma_1\sigma_2)}{\delta^2}. \tag{4.17}$$

Total number of directional-changes as a function of the angle ϕ is shown in Figure 4.8. The case of uncorrelated processes P_1 and P_2 is presented in subplot 4.8a when non-zero correlation case is shown in subplot 4.8b. Number of events across 2π space is sensitive to the relative values σ_1/σ_2 (conditional zero correlation coefficient). The difference between the largest and the smallest number of directional-changes is 2.8 times in case of $\sigma_1 = 15\%$ and $\sigma_2 = 25\%$ (blue curve in Figure 4.8a). The difference growth to 49.0 in case of $\sigma_1 = 35\%$ and $\sigma_2 = 5\%$ (orange curve in Figure 4.8a). That difference indicates that the multidimensional directional-change intrinsic time will tick more often along axis where the corresponding 1D

exchange rate has the largest volatility. The high sensitivity of the curve shape to the volatility ratio can be used to register the volatility difference of real independent exchange rates.

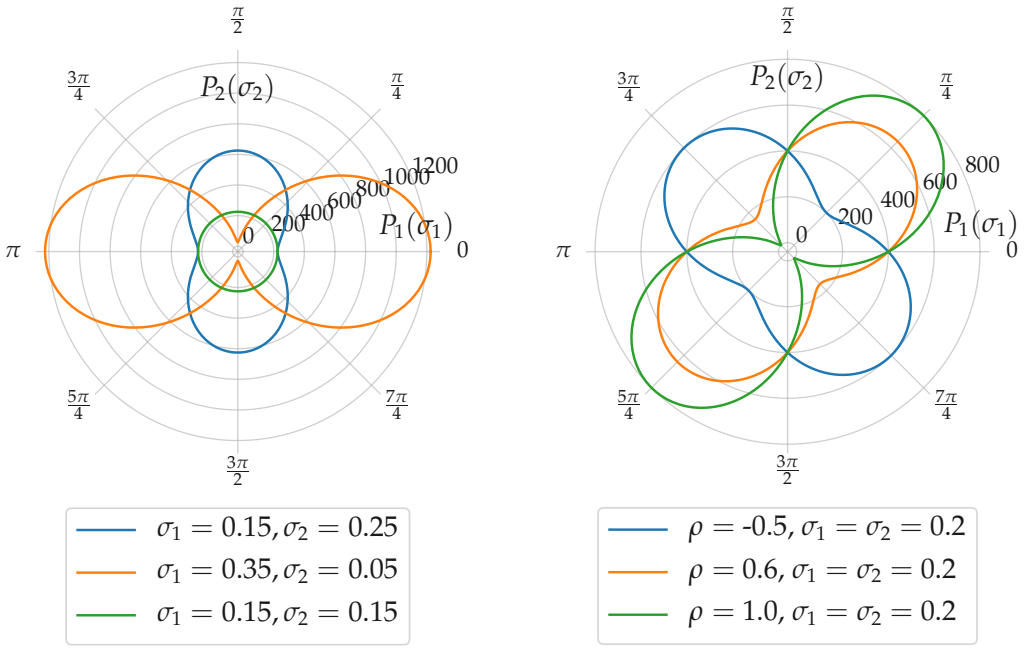

FIGURE 4.8: Total number of directional-changes in 2D space given the directional vector $\vec{D}$ defined by the angle ϕ (equation (4.17)). **(a)** Iid P_1 and P_2 ($\rho_{1,2} = 0$), different volatility components ($\sigma_1 \neq \sigma_2$). **(b)** Processes P_1 and P_2 have non-zero correlation coefficient ($\rho_{1,2} \neq 0$), volatilities of the processes are fixed and equal to each other ($\sigma_1 = \sigma_2 = 20\%$). The directional-change threshold used in both cases is $\delta = 1\%$.

Number of directional-changes curves shown in Figure 4.8b are build for the processes P_1 and P_2 with equal volatilities and non-zero correlation coefficient. The curves have stretched shape comparing to the circular contour character to the uncorrelated time series ($\sigma_1 = \sigma_2 = 15\%$ in Figure 4.8a). The direction of the stretching depends on the sign of the correlation coefficient. Positive correlation values induce a decrease in the number of events along $\phi = 3/4\pi$ while inducing an increase along $\phi = \pi/4$. The count becomes zero along the angle $\phi = 3/4\pi$ if the processes are perfectly correlated ($\rho_{1,2} = 1.0$, green curve in Figure 4.8b). This phenomenon shows how the multidimensional directional-change intrinsic time can be used to visualise the correlation coefficient between exchange rates forming a 2D space. In Section 4.7.2, we will show how the number of directional-changes, measured for 2D FX exchange rates, depicts the "footprint" of the changing correlation factor.

Expected waiting time curve is based on the reciprocal to the total number of directional-changes equation (4.16). The function is depicted in Figure 4.18 available in Appendix 4.C.

4.5.2 3D and Higher Dimensions

Coordinates of a point in a space of dimensionality higher than two can be expressed as components of an "n-sphere". In an n-sphere, location a point is defined by one radial coordinate r and $n-1$ angular coordinates $\phi_1, \phi_2, \ldots, \phi_{n-1}$. The radial coordinate defines the shortest distance from the centre of the sphere to the point. Each of the first $n-2$ angular coordinates range over $[0, \pi)$. The radial coordinate with the index n ranges over $[0, 2\pi)$.

In the 2D space, directional vector $\vec{D}$ defines the shortest distance to the transition border. Similar, the directional vector in the space of higher dimensions defines the shortest distance to the transition surface (see Figure 4.3c). The vector is fixed in the space (its coordinates do not change over time) between two consecutive directional-changes. Properties of the process R evolving along the vector $\vec{D}$ define the expected waiting time and the expected number of directional changes along the vector. Evolution of each of the processes P_i, forming the multidimensional space, contributes to the evolution of the process R. The contributions depend on the angular coordinate of the directional vector.

Volatility of the process R is composed of volatilities $\sigma_1, \sigma_2, \ldots, \sigma_n$ of the processes forming the space. Similar to the volatility in 2D space (equation (4.11)), volatility in higher dimensions can be expressed in the following way:

$$\sigma_R(\sigma_{r'_1}, \ldots, \sigma_{r'_n}) = \sqrt{\sigma^2_{r'_1} + \sigma^2_{r'_2} + \ldots + \sigma^2_{r'_n}}. \tag{4.18}$$

Each component $\sigma_{r'_i}, i \in [1, n]$ is the volatility of of each exchange rate's projection on the directional vector $\vec{D}$. The volatilities depend on the angular coordinates ϕ_i and volatilities $\sigma_1, \sigma_2, \ldots, \sigma_n$:

$$\begin{aligned}
\sigma_{r'_1}(\sigma_1; \phi_1) &= \sigma_1 \cos\phi_1, \\
\sigma_{r'_2}(\sigma_2; \phi_1, \phi_2) &= \sigma_2 \sin\phi_1 \cos\phi_2, \\
\sigma_{r'_3}(\sigma_3; \phi_1, \phi_2, \phi_3) &= \sigma_3 \sin\phi_1 \sin\phi_2 \cos\phi_3, \\
&\ldots \\
\sigma_{r'_{n-1}}(\sigma_{n-1}; \phi_1, \ldots, \phi_{n-1}) &= \sigma_{n-1} \sin\phi_1, \ldots \sin\phi_{n-2} \cos\phi_{n-1}, \\
\sigma_{r'_n}(\sigma_n; \phi_1, \ldots, \phi_{n-1}) &= \sigma_n \sin\phi_1, \ldots \sin\phi_{n-2} \sin\phi_{n-1}.
\end{aligned} \tag{4.19}$$

Figure 4.7b demonstrates volatility of the process R evolving along the directional vector $\vec{D}$ as the function of angles $\phi_1 \in [0, \pi)$ and $\phi_2 \in [0, 2\pi)$ in 3D space. The space is formed by independent processes $P_i(\sigma_i), i \in [1, 3]$.

In the case when processes P_i forming the multidimensional space are characterised by non-zero correlation factors $\rho_{i,j}$, the volatility of the process R becomes:

$$\sigma_R(\sigma_{r'_1}, \ldots, \sigma_{r'_n}) = \sqrt{\sum_{i=1}^{N} \sigma_{r'_i}^2 + 2 \sum_{i \neq j}^{N} \rho_{i \neq j} \sigma_{r'_i}^2 \sigma_{r'_j}^2}, \tag{4.20}$$

where volatilities $\sigma_{r'_i}$ are defined in equation (4.19).

Expected number of directional changes and the waiting time can be computed for any directional vector $\vec{D}$ given in the space of dimensionality higher than two. The procedure is equivalent to the one described in Section 4.5.1. Equations (4.3)-(4.5) take the volatility of the process R (equations (4.18) and (4.20)) evolving along the directional vector as an input. The multidimensional process is indistinguishable from the 1D case if all components of the space are iid and are equally volatile.

It is non-trivial to interpret the curves of the expected waiting time and the total number of directional-changes build for a time series of dimensionality higher than two. Visualisation of a 3D space is complicated and 4D and higher dimensions can be built only as projections on lower-dimensional spaces. However, the scaling laws based on directional-change intrinsic time can be easily drawn. Therefore, the following section will discuss various interpretations of scaling law parameters in multidimensional data.

4.6 Experiments

4.6.1 Expansion Validation Criteria

The following experiment is dedicated to the expansion validation criteria (Section 4.1). The validity of the multidimensional directional-change approach will be confirmed if the Overshoot and Directional change count scaling laws will be found in time series of dimensionality higher than one. 16 independent Monte Carlo (MC) simulations were performed to test the criteria. GBM time series composed of 10 000 000 points were generated for each simulation. The number of dimensions in the generated time series varies from one to 16. All processes $P_i, i \in [1, n]$ forming the n-dimensional space have zero trend. Their annual volatility is 20%. Zero cross-correlation coefficients were assumed in order to simulate the evolution of independent markets.

Overshoot and Directional change count scaling laws were computed for all constructed multidimensional time series. All corresponding plots placed on the same frame are presented in Figures 4.9a and 4.9b. The figures demonstrate linear dependencies. The observa-

tion confirms the expansion property of the multidimensional directional-change algorithm.

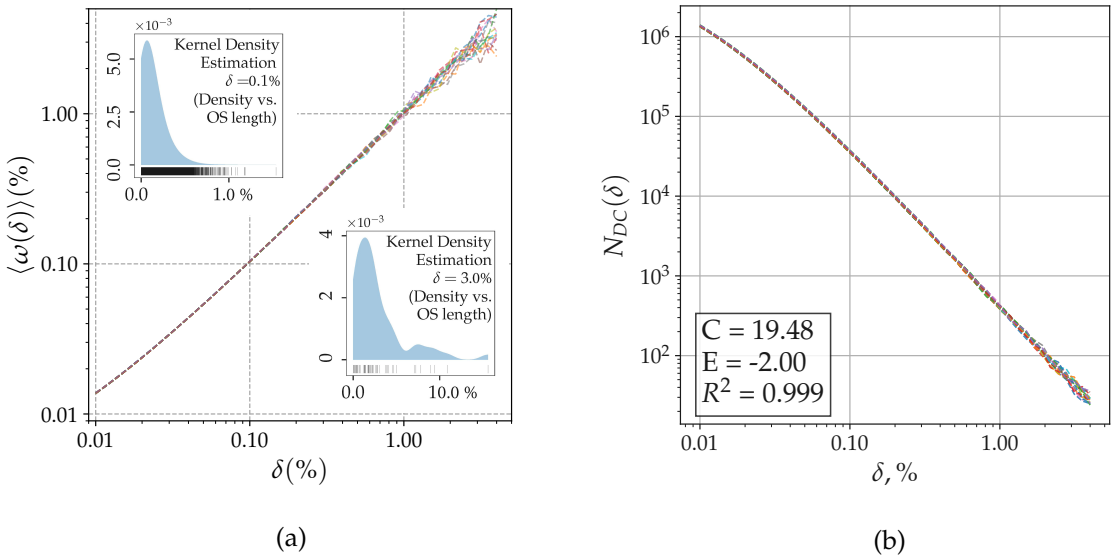

FIGURE 4.9: **(a)** Average overshoot length $\langle\omega(\delta)\rangle$ (Overshoot scaling law) and **(b)** total number of directional changes (Directional change count scaling law) as functions of the threshold δ. The scaling law is computed by applying the multidimensional directional-change intrinsic time algorithm to GBM data. The dimensionality of the data ranges from one to 16. Each time series contains 10 000 000 points. All 1D time series P_i forming each multidimensional space have no trend and have the annualised volatility $\sigma = 20\%$. The kernel density functions displayed in the insets of subplot (a) are built using the Gaussian kernel. The selected parameters for the kernels: threshold $\delta = 0.1\%$, bandwidth 0.001, approximately 26 000 observations (upper left inset); threshold $\delta = 3.0\%$, bandwidth 0.008, 54 observations (bottom right inset).

Scaling coefficients, presented on Figure 4.9b, correspond to the average scaling coefficients computed for all 16 time series. Value $C_{N_{DC}} = 19.48$ is close to the value of the assumed GBM volatility (20%). Obtained coefficient $E_{N_{DC}} = -2$ is in line with the theory too.

4.6.2 Correlation Coefficient Impact

Exchange rates often have non-zero correlation coefficients (row ρ^{trad} in Table 4.2 contains coefficient of five EUR exchange rates). In this section, we test how the scaling factor of Overshoot and Directional change count scaling laws change as the non-zero correlation becomes introduced.

2D GBM time series were produced to perform the test. 1D components P_1 and P_2 of the generated time series have the correlation coefficient $\rho_{1,2}$. Several coefficients $\rho_{1,2}$ were selected

to produce (a) fully correlated ($\rho_{1,2} = 1.0$) and (b) partially positively[7] correlated time series ($\rho_{1,2} \in [0.2, 0.8]$, step $\Delta\rho = 0.2$). The selected range of the correlation coefficients and the step $\Delta\rho = 0.2$ resulted in a set of five 2D time series. Scaling coefficients of an additional uncorrelated 2D time series were used as a reference.

Gaussian random variables P_1 and P_2 were derived from the normal distribution $N(0, \sigma^2)$. The correlation $\rho_{1,2}$ is defined as:

$$\rho_{1,2} = \frac{\langle (P_1 - \langle P_1 \rangle)(P_2 - \langle P_2 \rangle) \rangle}{\sigma^2}. \tag{4.21}$$

Two independent random variables P_1 and P_3 were first generated to produce the random variable P_2 characterised by the given correlation coefficient:

$$P_2 = \rho_{1,2} P_1 + \sqrt{1 - \rho_{1,2}^2} P_3. \tag{4.22}$$

Each 2D data set used in the test contains 100 000 000 price changes. The data time span is equivalent to one year. Such large number of ticks per annum was selected in order to mimic high frequency market dynamic. Volatilities $\sigma_{i=1,2} = 20\%$. A set of directional-change thresholds δ was applied to the generated 2D time series. The average overshoot length $\langle \omega(\delta) \rangle$ and the total number of directional changes $N_{DC}(\delta)$ observed during the evolution of the given time series were computed. Results of the experiments are presented as plots $\langle \omega(\delta) \rangle$ and $N_{DC}(\delta)$ in Figure 4.10.

All $\langle \omega(\delta) \rangle$ dependencies computed for every correlation coefficient $\rho_{1,2}$ (Figure 4.10a) are linear and indistinguishable. The Overshoot scaling law coefficient $C = 1.0$ coincides with the scaling coefficient observed in 1D space. Minimum and maximum values of the coefficient E are 0.93 ($\rho = 0.0$) and 1.16 ($\rho = 1.0$) correspondingly. We highlight that the scaling coefficient E represents the slope of the linear approximation in the log-log space. Thus, the slope of the plot growths together with the increasing correlation coefficient. Overall, the deviation of the scaling coefficients registered for time series with a non-zero $\rho_{1,2}$ is insignificant. The observation confirms the robustness of the multidimensional directional-change algorithm with regards to the correlation.

The impact of the correlation coefficient on the properties of the process R can be used to explain the observed robustness. The correlation impacts the volatility size σ_R. The size increases or decreases depending on the angle ϕ the directional vector forms with the x-axis (see Figures 4.6 where the directional vector is visualised and 4.7a where the theoretical volatility surface in a 2D space is presented). Overshoot scaling law states that the average

7 Negative correlation coefficients were omitted due to the results symmetry.

overshoot length is equal to the corresponding threshold δ independently on the size of the threshold and the volatility of the observed process. Therefore, a variation of the volatility size σ_R caused by the varying $\rho_{1,2}$ does not affect coefficients of the Overshoot scaling law. The angular coordinate ϕ of the vector $\vec{D}$ has no impact too. The effect is stable in any space of dimensionality higher than two.

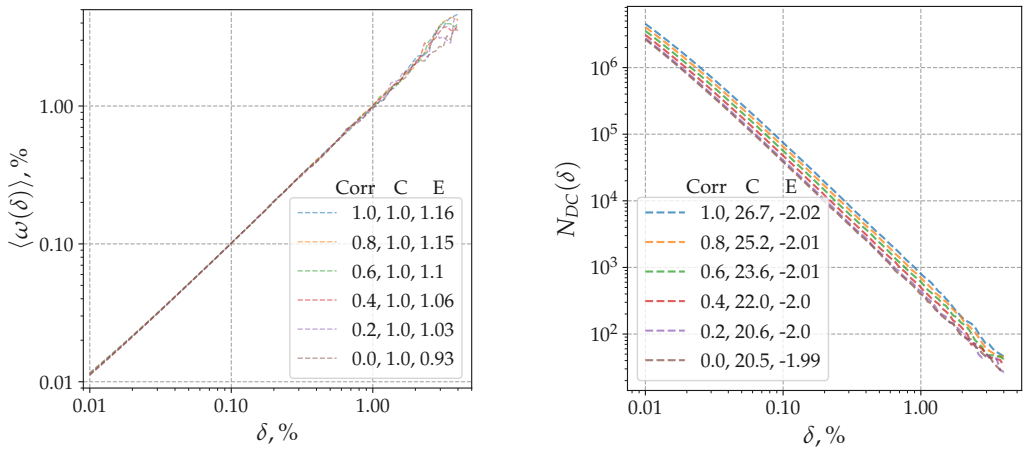

(a) (b)

FIGURE 4.10: **(a)** Average overshoot length $\langle\omega(\delta)\rangle$ as a function of the threshold δ (Overshoot scaling law). The dependence is computed for six 2D GBM time series. Components of each 2D time series have positive correlation coefficients ranging from $\rho = 0.0$ to $\rho = 1.0$ with the step $\Delta\rho = 0.2$. Trend $\mu_{i=1,2} = 0$, volatility $\sigma_{i=1,2} = 20\%$. There are 100 000 000 points composing each time series. **(b)** Total number of directional changes $N_{DC}(\delta)$ observed within the generated time series as the function of threshold δ (Directional change count scaling law). The correlation coefficients as well as the scaling law parameters $C_{N,DC}$ and $E_{N,DC}$ of equation (4.1) are presented in the picture.

Directional change count scaling laws build for correlated 2D GBM are displayed in Figure 4.10b. In contrast to the Overshoot scaling law constructed for the same data (see Figure 4.10a), the presented $N_{DC}(\delta)$ curves do not coincide with each other. The observed lines separation occurs due to the impact of the correlation coefficient $\rho_{1,2}$ on volatility σ_R. The volatility is the crucial factor affecting the waiting time until the next directional change (equation (4.5)). Higher volatility induces faster price escape from the transition corridor. The latter results as the higher number of directional changes observed within the given period of time. For example, a 2D process formed by two perfectly correlated processes $P_1(\sigma)$ and $P_2(\sigma)$ ($\rho = 1.0$) is characterised by constant price moves along the diagonal $\phi = \pi/4$. In this case, volatility σ_R is equal to volatility σ multiplied by $\sqrt{2}$ (equation (4.13)).

A total number of directional-changes observed within the fixed period of time along $\vec{D}$ can be computed using the correlation coefficient $\rho_{1,2}$ of processes forming the space. We highlight that the statement does not apply to the vectors $\vec{D}$ evolving across the 2π space. A deeper investigation has to be performed in order to describe the evolution not restricted by the angle ϕ. Appendix 4.D provides insides on how the flow of the directional-change intrinsic time in multidimensional spaces can be interpreted as one-step Markov chain. Thoroughly constructed transition probability matrix is essential for the further theoretical analysis. A more comprehensive study is expected to be performed in future research works.

4.7 Multidimensional FX Market

Glattfelder, Dupuis, and Olsen (2011) provided a comprehensive overview of scaling laws observed in 1D high frequency FX data. Some of the scaling laws were found by applying the directional-change algorithm. In this section, we exercise extended multidimensional version of the algorithm using 2D space formed by orthogonally placed FX exchange rates. The goal is to confirm the presence of Overshoot and Directional change count scaling laws in high-dimensional FX markets. Employed in the experiment tick-by-tick data was obtained from *JForex* trading platform. The platform is developed by the Swiss bank and marketplace *Ducascopy*, which provides various types of market data in the highest resolution[8].

4.7.1 Ticks in Multidimensional Space

Each new price tick should be used as an input for the 1D directional-change dissection procedure. Two FX 1D exchange rates structure the 2D space. The exchange rates form axis x and y. They can experience price changes in different moments of time. Therefore, coordinates of a point in 2D space might not change simultaneously. New rules of defining price ticks in multidimensional space have to be introduced.

There are multiple ways of interpreting price changes in multidimensional space formed by constantly evolving 1D exchange rates. For example, one exchange rate can be selected as a leader when the second as a follower. Elementary price changes of the leader induce a new signal for the algorithms whenever the latest to the moment tick of the follower should be taken. Another approach suggests taking the cumulative return computed over a fixed period of time (a minute, a day, a week). Authors of the current research work are convinced that

8 https://www.dukascopy.com/swiss/english/forex/jforex/.

every elementary price change of each of the exchange rates bears a particular part of the information on the current market activity. Therefore, in our work:

> a tick occurs when the price of at least one exchange rate forming the multidimensional space changes.

At the bottom part of Figure 4.2, one can see an example of two exchange rates P_1 and P_2 placed on the same timeline. In this example, prices P_1 and P_2 experienced four and three changes correspondingly (labelled by empty circles). Only one couple of the changes occurred at the same moment of time (the tick number four). The total number of ticks in the 2D time series (upper part of Figure 4.2) is equal to six. According to the rule described above, all six price changes should be used as an input for the multidimensional directional-change intrinsic time algorithm.

4.7.2 2D FX EUR Exchange Rates

Five EUR exchange rates were selected for the first test: EURAUD, EURUSD, EURJPY, EURGBP, and EURCHF. The covered time interval is five years: from January 1st 2011 to January 1st 2016. The number of ticks ranges from 69 689 587 (EURCHF) to 137 956 164 (EURAUD). The 10 time series were connected in pairs to form 10 2D data sets.

Section 4.5 showed how volatilities of exchange rates forming a 2D space and their correlation factors impact the number of directional changes and the expected waiting time along the given directional vector. We eliminate the volatility impact by normalising all returns of 1D processes forming the space on their annualised volatility. The normalisation is needed to concentrate the attention on the correlation factor of real exchange rates. The volatility used for the normalisation is computed in the "traditional" way:

$$R_t = \ln(S_t / S_{t-1}), \quad R_{avg} = \frac{\sum_{t=1}^{n} R_t}{n}, \quad \sigma_{annual}^{trad} = \sqrt{\frac{\sum_{t=1}^{n} \left(R_t - R_{avg}\right)^2}{n-1}}, \tag{4.23}$$

where S_t are closing prices at day t and n is the number of days in a calendar year.

The close resemblance of real returns dS_t and the normal distributions were assumed in order to perform the volatility normalisation:

$$dS_t = \sigma dW_t. \tag{4.24}$$

The normalised exchange rates then:

$$dS_t^{norm} = \frac{dS_t}{\sigma}. \tag{4.25}$$

Such normalisation of returns makes volatilities of all exchange rates equivalent to 100%. The increased volatility (compared to the non-normalised volatility) requires the increase of the directional-change thresholds used to reveal scaling laws. Each of the thresholds was increased by the reciprocal to the currency average volatility of the exchange rates forming the space ($\sigma_{aver} = 10.72\%$).

In addition to the normalised volatility, each of the 1D exchange rates was also normalised on the first entry of the historical set S_t:

$$S_t^{norm} = \frac{S_t}{S_0}. \tag{4.26}$$

That part of the normalisation is necessary in order to better represent price moves on the coordinate plane: elementary price changes in any direction become visually equivalent.

The multidimensional directional-change algorithm was applied to the 2D time series composed of EUR exchange rates. Overshoot and Directional change count scaling laws were computed for each of the 10 2D datasets. Figures 4.11 and 4.12 present the obtained results.

Glattfelder, Dupuis, and Olsen (2011) reported a slight curvature of some of the scaling laws build using 1D FX data. The authors employed the quadratic model $y = A + Bx + Cx^2$ in order to measure the systematic curvature. The curvature was expressed as the difference between the coefficient of determination (r-squared) of the quadratic and the linear models: $R_q^2 - R_l^2$. The paper reported that the quadratic model yields the marginally improved fit only for GBM data. The difference for Overshoot and Directional change count scaling laws reported in the paper ranges from -9.706×10^{-6} (EURAUD) to 7.059×10^{-3} (EURGBP) and -2.733×10^{-6} (GBPJPY) to 1.031×10^{-3} (EURUSD) correspondingly. The differences are considered insignificant. We replicate the curvature test for higher dimensions. The goal of the test is to verify whether and how the curvature pattern changes conditional the increased space dimensionality.

First, we replicated the original 1D curvature test from Glattfelder, Dupuis, and Olsen (2011) considering EUR data used in our work. Results of the experiment are presented in Table 4.1 (rows $R_{q,OS}^2 - R_{l,OS}^2$ and $R_{q,N_{DC}}^2 - R_{l,N_{DC}}^2$). The obtained differences computed for the Overshoot scaling law ranges from 2.776×10^{-7} (EURGBP) to 8.970×10^{-4} (EURJPY) when the one for the Directional change count is from 1.531×10^{-4} (EURCHF) to 8.328×10^{-4} (EURJPY). The observed values are expectedly low.

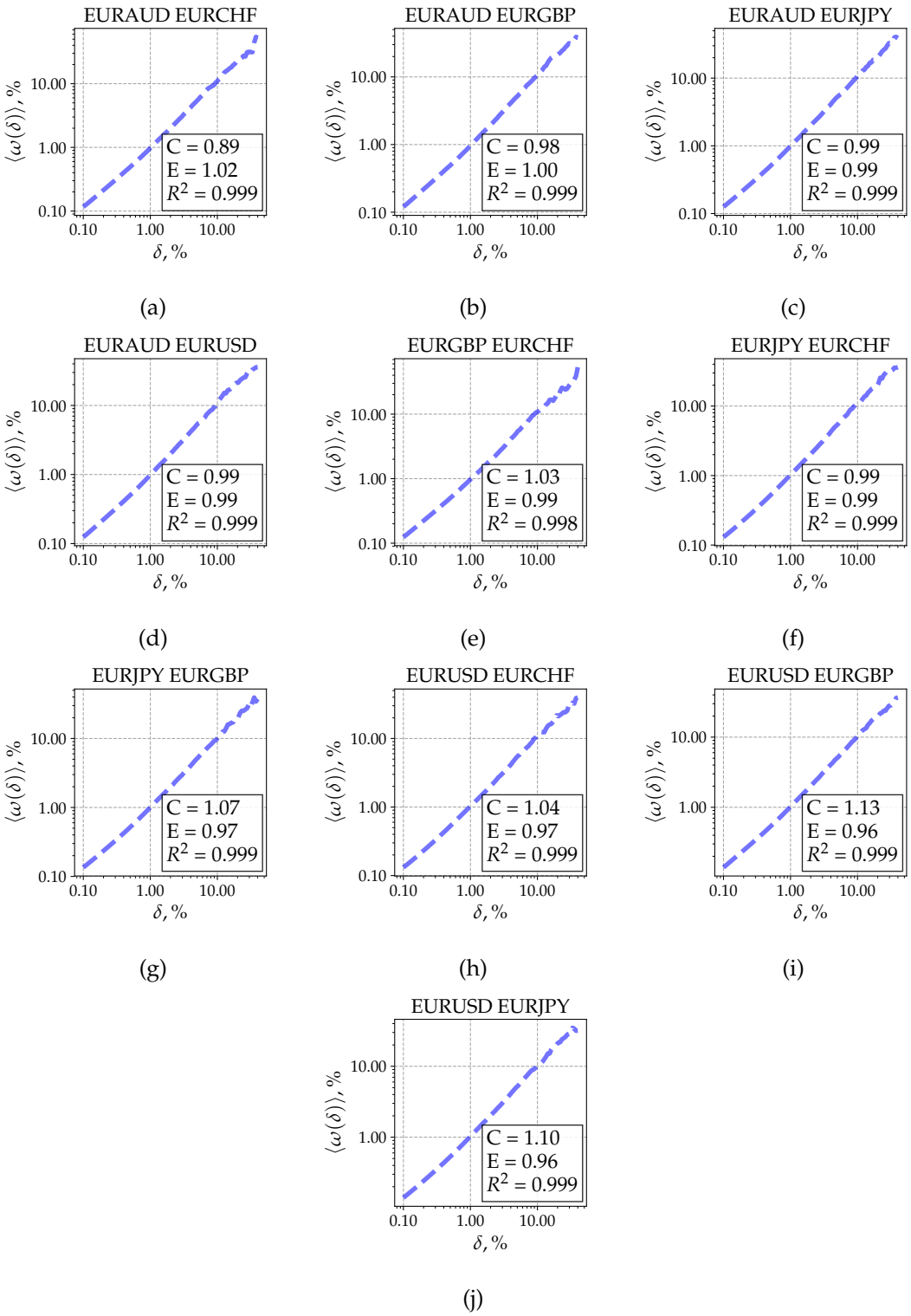

FIGURE 4.11: Overshoot scaling laws observed by applying the multidimensional directional-change intrinsic time dissection procedure to 2D FX time series. EUR is the base currency for all 1D exchange rates. Returns of the tested exchange rates are normalised on the corresponding annualised volatility (equation (4.25)). All prices are also normalised on the first price of the given price set (equation (4.26)). Scaling law coefficients displayed in the figure are computed through the coefficients of the linear fit $y = A + Bx$ drawn through the entire range of δ values.

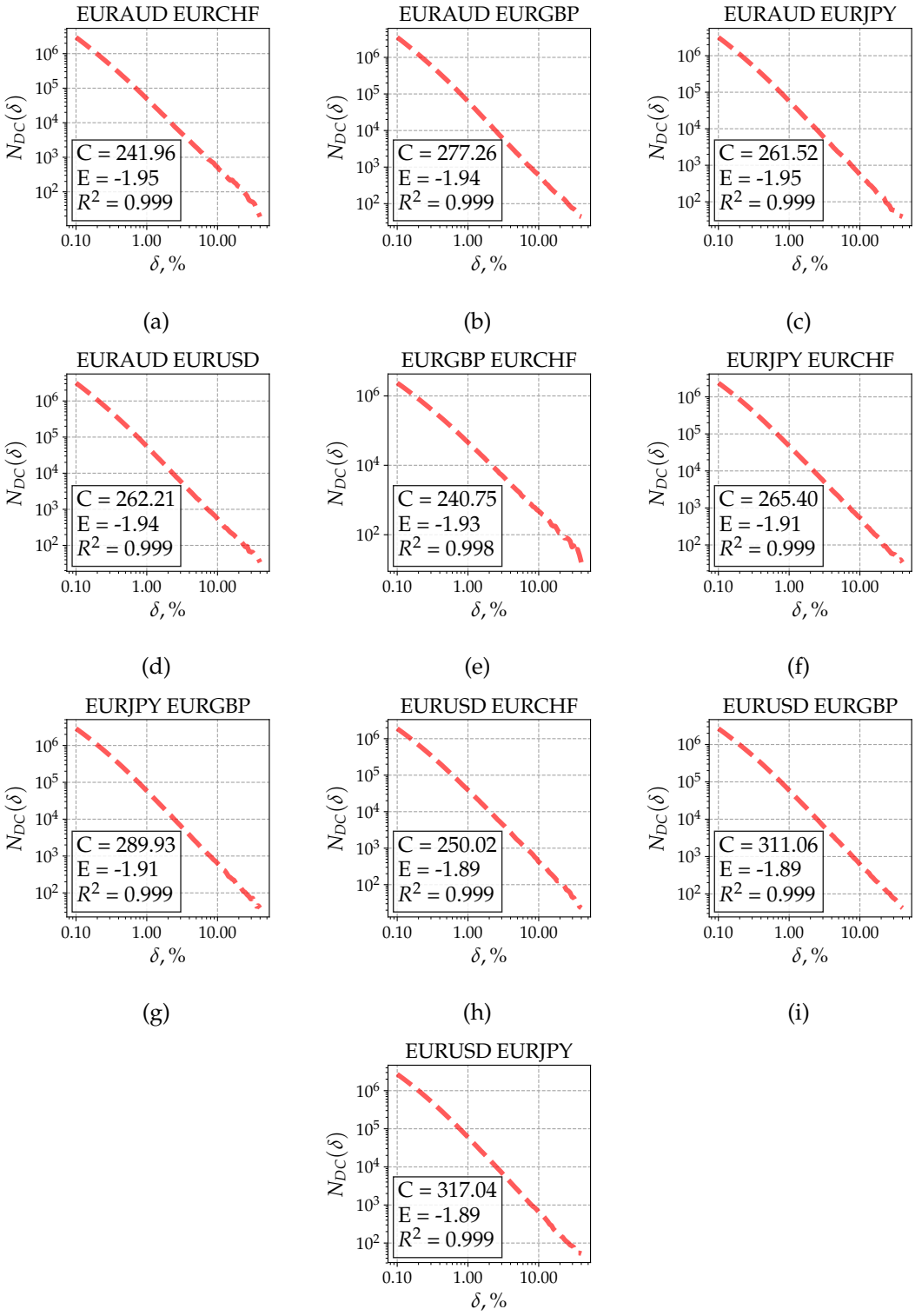

FIGURE 4.12: Directional change count scaling laws observed by applying the multidimensional directional-change intrinsic time dissection procedure to 2D FX time series. EUR is the base currency for all 1D exchange rates. Returns of the tested exchange rates are normalised on the corresponding annualised volatility (equation (4.25)). All prices are also normalised on the first price of the given price set (equation (4.26)). Scaling law coefficients displayed in the figure are computed through the coefficients of the linear fit $y = A + Bx$ drawn through the entire range of δ values.

TABLE 4.1: Scaling coefficients of the Overshoot (E_{OS}, C_{OS}) and Directional change count ($E_{N_{DC}}$, $C_{N_{DC}}$) scaling laws computed for the FX data (Figure 4.17). $R^2_{l,*=OS,N_{DC}}$ and $R^2_{q,*=OS,N_{DC}}$ stand for the linear and the quadratic log-log curve approximation models. σ^{trad}_{annaul} is calculated by applying the "traditional" volatility estimation technique (equation (4.23)). $\sigma^{C_{N_{DC}}}_{annaul}$ is the multidimensional volatility value (see 4.6).

	EURJPY	EURUSD	EURCHF	EURAUD	EURGBP	Curr. aver.
E_{OS}	0.98	0.96	1.00	1.02	0.96	0.98
C_{OS}	1.04	1.09	0.92	0.91	1.19.	1.03
$R^2_{l,OS}$	0.999	0.999	0.998	0.999	0.998	0.999
$R^2_{q,OS} - R^2_{l,OS}$	8.970×10^{-4}	4.778×10^{-4}	7.791×10^{-4}	7.574×10^{-4}	2.776×10^{-7}	5.823×10^{-4}
$E_{N_{DC}}$	-1.90	-1.89	-1.87	-1.96	-1.95	-1.91
$C_{N_{DC}}$	251.12	234.01	188.66	232.13	239.24	229.03
$R^2_{l,N_{DC}}$	0.999	0.999	0.999	0.999	0.999	0.999
$R^2_{q,N_{DC}} - R^2_{l,N_{DC}}$	8.328×10^{-4}	7.973×10^{-4}	1.531×10^{-4}	2.307×10^{-4}	3.790×10^{-4}	4.786×10^{-4}
σ^{trad}_{annaul}, %	12.10	10.80	12.30	10.50	7.90	10.72
$\sigma^{C_{N_{DC}}}_{annaul}$, %	13.60	11.30	10.40	10.90	8.50	10.94
$\sigma^{trad}_{annaul} - \sigma^{C_{N_{DC}}}_{annaul}$, %	-1.50	-0.50	1.90	-0.40	-0.60	-0.22

Second, we applied the same curvature measurement technique to scaling laws of 2D EUR exchange rates. The difference between the coefficients of determination for the Overshoot curves stays below 7.077×10^{-4}. The difference computed for the Directional change count rises up to 1.361×10^{-3} (EURGBP-EURCHF pair). The value is 1.63 times bigger than the largest difference computed in the 1D case. Its currency average is 8.357×10^{-4}. It is close to the highest difference observed for the 1D data. The detected phenomenon does not guaranty but suggests a hypothesis that the scaling laws build for the EUR data of higher dimensionality is characterised by larger curvature. Time series in even higher dimensions have to be tested in order to confirm or reject the hypothesis. The following sections will discuss the tests in details.

Statistical information on the constructed 2D time series and properties of the corresponding scaling laws are presented in Table 4.2. The table contains scaling parameters E^{2D}_{OS}, C^{2D}_{OS} for the Overshoot and $E^{2D}_{N_{DC}}$, $C^{2D}_{N_{DC}}$ for the Directional change count scaling laws. It also lists the average annualised volatility $\langle \sigma^{trad}_{annual} \rangle$ of 1D exchange rates forming the space. Parameters ρ^{trad} in Table 4.2 represent the correlation of exchange rates forming the 2D space:

$$\rho^{trad} = \frac{\mathrm{Cov}(R_{t,x}, R_{t,y})}{\sigma^{trad}_{annual,x} \sigma^{trad}_{annual,y}}, \quad \mathrm{Cov}(R_{t,x}, R_{t,y})) = \frac{\sum_{t=1}^{n} \left(R_{t,x} - \overline{R_{t,x}}\right) \left(R_{t,y} - \overline{R_{t,y}}\right)}{n-1}, \tag{4.27}$$

where $\overline{R_{t,*=x,y}}$ is the average return.

Table 4.2: Statistics of EURXXX-EURYYY 2D exchange rates where XXX and YYY stand for JPY, USD, CHF, AUD, and GBP. Columns' names are formed by the combination of the quoted currencies *XXX-*YYY where the sign * stands for EUR. E^{2D}_{OS}, C^{2D}_{OS}, $E^{2D}_{N_{DC}}$, $C^{2D}_{N_{DC}}$ are the parameters of Overshoot and Directional change count scaling laws (Figures 4.11 and 4.12). $R^2_{l,OS}$ and $R^2_{l,N_{DC}}$ are the R^2 statistics of the linear approximations drawn thought the entire range of values δ. $\langle \sigma^{trad}_{annual} \rangle$ is the average annual volatility of EURXXX and EURYYY exchange rates forming the 2D space computed using the traditional approach (equation (4.23)). $\sigma^{C_{N_{DC}}}_{annual}$ is the annualised 2D volatility computed using the scaling laws parameter $C^{2D}_{N_{DC}}$. ρ^{trad} is the correlation coefficient of exchange rates EURXXX and EURYYY calculated using daily closing prices (equation (4.27)).

	*AUD-*CHF	*AUD-*GBP	*AUD-*JPY	*AUD-*USD	*GBP-*CHF	*JPY-*CHF	*JPY-*GBP	*USD-*CHF	*USD-*GBP	*USD-*JPY	Curr. aver.
E^{2D}_{OS}	1.02	1.00	0.99	0.99	0.99	0.99	0.97	0.97	0.96	0.96	0.98
C^{2D}_{OS}	0.89	0.98	0.99	0.99	1.03	0.99	1.07	1.04	1.13	1.10	1.02
$R^2_{l,OS}$	0.999	0.999	0.999	0.999	0.998	0.999	0.999	0.999	0.999	0.999	0.999
$R^2_{q,OS} - R^2_{l,OS}$	5.3×10^{-4}	4.3×10^{-4}	5.8×10^{-4}	3.2×10^{-4}	5.1×10^{-4}	3.2×10^{-4}	7.0×10^{-4}	2.3×10^{-4}	4.6×10^{-4}	4.4×10^{-4}	4.5×10^{-4}
$E^{2D}_{N_{DC}}$	-1.95	-1.94	-1.95	-1.94	-1.93	-1.91	-1.91	-1.89	-1.89	-1.89	-1.92
$C^{2D}_{N_{DC}}$	241.96	277.26	261.52	262.21	240.75	265.40	289.93	250.02	311.06	317.04	271.72
$R^2_{l,N_{DC}}$	0.999	0.999	0.999	0.999	0.998	0.999	0.999	0.999	0.999	0.999	0.999
$R^2_{q,N_{DC}} - R^2_{l,N_{DC}}$	6.1×10^{-4}	2.6×10^{-4}	7.1×10^{-4}	3.7×10^{-4}	1.3×10^{-3}	9.5×10^{-4}	9.4×10^{-4}	1.2×10^{-3}	9.8×10^{-4}	9.1×10^{-4}	8.3×10^{-4}
$\langle \sigma^{trad}_{annual} \rangle$, %	11.40	9.20	11.30	10.65	10.10	12.20	10.00	11.55	9.35	11.45	10.72
$\sigma^{C_{N_{DC}}}_{annual}$, %	12.34	11.41	13.22	12.49	10.87	14.48	12.97	12.91	13.01	16.23	12.99
ρ^{trad}	0.11	0.43	0.27	0.31	0.15	0.24	0.42	0.31	0.5	0.48	0.32

Table 4.2 contains values of the multidimensional volatility ($\sigma_{annual}^{C_{N_{DC}}}$). The volatility is computed through the scaling coefficient $C_{N_{DC}}$ of the Directional change count scaling law. We note that five years of data were used and that each of 1D exchange rates was preliminary normalised on its annual volatility. Therefore, the scaling coefficient $C_{N_{DC}}$ was multiplied by the currency average volatility, and the result was divided by $\sqrt{5}$.

As it was shown in Section 4.5.1, the shape of the curve built for the total number of directional changes in 2π space depends on the correlation factor of used exchange rates. In this section, we present the curves built for the selected set of 2D EUR exchange rates. Values for the curves were computed in the following way: each of the 1D exchange rates forming the corresponding 2D space was normalised on the annualised volatility and the initial price; a threshold $\delta = 0.94\%$ was selected to run the multidimensional directional-change dissection procedure; angular coordinates ϕ of each directional vector $\vec{D}$ were recorded; the total number of intrinsic events was computed for all directional vectors observed in the intervals $[(i-1)\Delta\phi, i\Delta\phi]$ where $\Delta\phi = 12^\circ$ and $i \in [1, 30]$.

The total number of directional-changes registered for the 2D EUR exchange rates as a function of angle ϕ is shown in Figure 4.13. The curves do not resemble the smooth shapes of the curves based on the analytical equation (4.17) and have unstable patterns. The values vary significantly over the range of selected intervals $\Delta\phi$.

Periodically varying correlation factor $\rho_{1,2}$ is the aspect which can influence the distribution of the number of directional changes across the 2π space. We verify the hypothesis by calculating the rolling window correlation coefficient. Correlations $\rho_{1,2}$ are indeed unstable over time for all selected exchange rates. For example, exchange rates EURJPY and EURAUD have the minimum and the maximum correlation coefficients equal to $\rho_{1,2}^{min} = -0.30$ and $\rho_{1,2}^{max} = 0.72$ (difference 1.02). That correlation instability results in the total number of intrinsic events pattern presented in Figure 4.13. Therefore, the directional-change intrinsic time applied to 2D data captures the "footprint" of the correlation factor evolution. Results of the experiment where the rolling window is 100 days are presented in Figure 4.22.

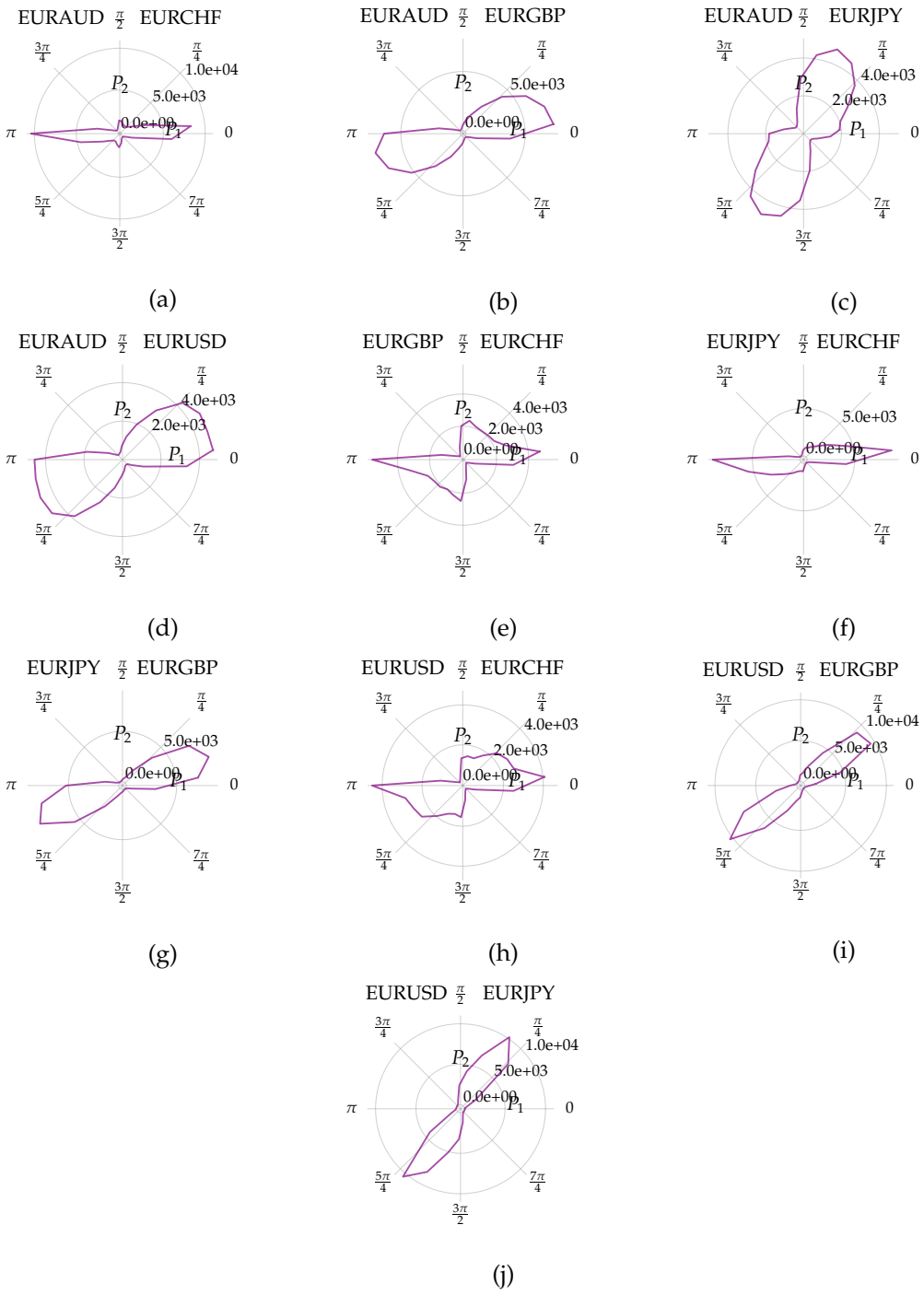

FIGURE 4.13: Total number of directional change registered in the interval $\Delta\phi$ in 2D space formed by FX exchange rates. The interval size is $\Delta\phi = 12°$. 30 intervals in total. The selected directional-change threshold is $\delta = 0.94\%$. 1D exchange rates forming the space were preliminary normalised on their volatility and the initial price.

4.7.3 5D FX EUR exchange rates

The higher number of exchange rates bears more information about the state and the evolution of a particular market. In this section, we investigate the intrinsic time properties of 5D

EUR time series. The same exchange rates used in Section 4.7.2 have been employed to form the space. Price ticks have been registered as described in Section 4.7.1. All 1D time series were preliminary normalised on the corresponding annualised volatility and the first price in the given time series (see Section 4.7.2 for details on the normalisation techniques).

Overshoot and Directional change count scaling laws were computed using the composed 5D data. The corresponding plots are presented in Figures 4.14a and 4.14b. The Overshoot scaling law (Figure 4.14a) has the scaling parameters $E = 1.02$ and $C = 0.97$. The coefficients are close to the empirical and theoretical values found for 1D space (see Glattfelder, Dupuis, and Olsen (2011) and Golub et al. (2014)). We measure the curvature of the law by comparing coefficients of determination R^2 computed for the linear $y = A + Bx$ and quadratic $y = A + Bx + Cx^2$ models: $R^2_{q,OS} - R^2_{l,OS} = 8.765 \times 10^{-4}$. The values are comparable to the values computed for 1D EUR exchange rates (see Table 4.1).

The Directional change count scaling law revealed for 5D FX data is characterised by clearly pronounced curvature (Figure 4.14b). The curvature can be seen as the difference between the empirical curve and the linear fit (red line) build thought the range of thresholds $\delta > 1.0\%$. The chosen range corresponds to the straightest part of the $N_{DC}(\delta)$ curve. The line is shown for the visualisation purposes only: quadratic and linear approximation models are drawn through the entire range of the thresholds δ. The difference between the coefficients of determination $R^2_{q,N_{DC}} - R^2_{l,N_{DC}} = 1.792 \times 10^{-3}$. The difference is 1.31 times bigger than the maximum analogous value registered in the case of 2D EUR exchange rates (1.361×10^{-3}). The evidence of the weak pattern, related to the synchronous curvature increase together with the dimensionality rise, becomes stronger.

Scaling law coefficient $C_{N_{DC}}$ from Figure 4.14b can be used to compute the multidimensional volatility of the constructed 5D EUR space. Volatility $\sigma^{C_{N_{DC}}}_{annual} = 388.32/10.72\%/\sqrt{5} = 16.20\%$. The value is noticeable bigger than the currency average (10.72%) or than the largest volatility value among all five exchange rates (13.60%, EURJPY).

4.7.4 23D FX

Previous sections described the directional-change intrinsic time data analysis in gradually increased dimensions: from 1D to 2D and to 5D. In this section, we extend the number of dimensions to 23. The 23D time series is comprised of the following FX exchange rates:

AUD/JPY, AUD/NZD, AUD/USD, CAD/JPY, CHF/JPY, EUR/AUD, EUR/CAD, EUR/CHF, EUR/GBP, EUR/JPY, EUR/NZD, EUR/USD, GBP/AUD, GBP/CAD,

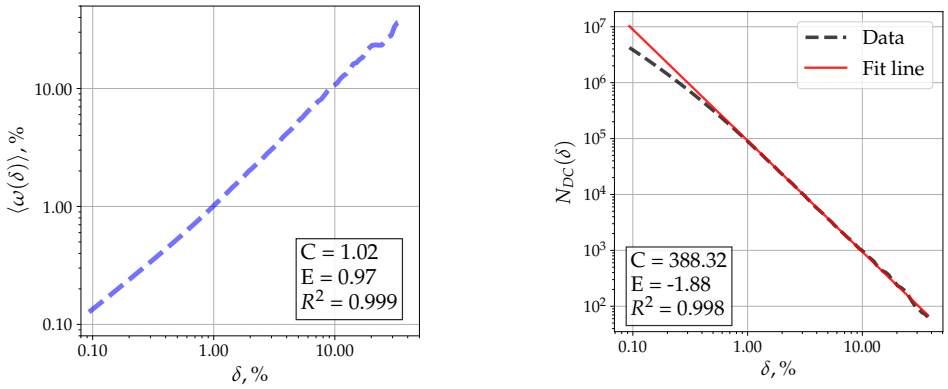

(a) (b)

FIGURE 4.14: **(a)** Overshoot and **(b)** Directional change count scaling laws observed in 5D space formed by EUR exchange rates. Scaling parameters C and E shown in Figure **(a)** correspond to the linear approximation $y = A + Bx$ drawn through the entire range of values δ, and **(b)** to the linear approximation build in the region $\delta > 1.0\%$.

GBP/CHF, GBP/JPY, GBP/USD, NZD/CAD, NZD/JPY, NZD/USD, USD/CAD, USD/CHF, USD/JPY.

The considered time range is Jan 1st 2011 to Jan 1st 2016. The smallest and the largest number of ticks among all selected exchange rates is 74 038 306 (EUR/CHF) and 169 405 060 (GBP/JPY). The cumulative number of ticks in all exchange rates forming the comprised 23D time series is about three billion: 2 774 533 294 ticks precisely. Assuming 252 trading days per year, the average number of ticks per a second is 25.5[9].

As in the previous section, every 1D component of the multidimensional space was preliminary normalised on the corresponding volatility and the first price. The multidimensional directional-change intrinsic time algorithm was applied to the constructed 23D time series. The set of the directional-change thresholds δ was adjusted on the currency average volatility (10.3%) in order to better manage the normalised returns.

Overshoot and Directional change count scaling laws were constructed based on the series of directional-changes registered in the 23D space. Both scaling laws are presented in Figures 4.15a and 4.15b. The increase of the Overshoot scaling law coefficient C compared to the coefficient observed in 5D (1.16 versus 1.02) is attributed to the FX stylised facts better pronounced in higher dimensions. That is, the fat-tailed distribution of returns stylised fact reported for 1D FX exchange rates is the most vivid in the area of short time intervals (see, for example,

9 This large amount of data demonstrates the impossibility of using manual techniques to perform simultaneous analysis of multiple high frequency markets. Fortunately, the computation power of modern computers is sufficiently high to duly deal with the bombarding frequency of data streamed in real time.

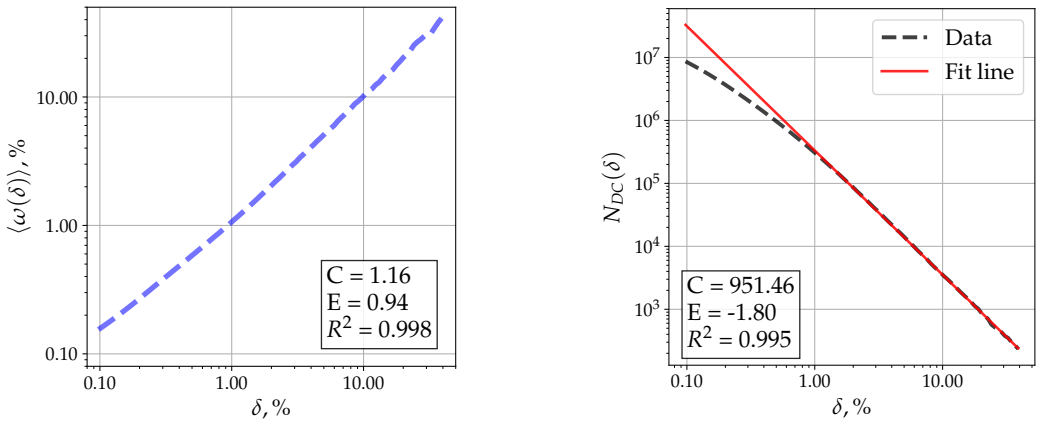

(a) (b)

FIGURE 4.15: **(a)** Overshoot and **(b)** Directional change count scaling laws observed in 23D space formed by EUR exchange rates. Scaling parameters C and E shown in Figure **(a)** correspond to the linear approximation $y = A + Bx$ drawn through the entire range of values δ, and **(b)** to the linear approximation build in the region $\delta > 1.0\%$.

Michel M Dacorogna et al. (2001)). The effect disappears when the returns are calculated over days, weeks and longer periods. The latter is known as the aggregational Gaussianity (Antypas, Koundouri, and Kourogenis 2013). Small directional-change thresholds are associated with high frequency of the intrinsic time ticks. They can be considered as the equivalent of frequently measured price returns over equidistant time intervals. Therefore, the increased Overshoot scaling law coefficient C together with the increased curvature of the scaling law plot ($R^2_{q,OS} - R^2_{l,OS} = 1.5 \times 10^{-3}$) are in line with the two stylised facts: fat-tailed returns and the aggregational Gaussianity.

The curvature of the Directional change count scaling law was shown to be increasing together with the growing number of dimensions (see Sections 4.7.2 and 4.7.3). The curvature computed in the 23D space formed by FX exchange rates confirms the observed tendency. The difference between the coefficients of determination of the Directional change count scaling law growths up to $R^2_{q,N_{DC}} - R^2_{l,N_{DC}} = 4.3 \times 10^{-3}$. The number is 2.4 times bigger than the value found for the 5D case (Section 4.7.3) and 3.16 times bigger than the value for the 2D exchange rates (Section 4.7.2). That empirical observation reinforces the hypothesis: the rising curvature of Directional change count scaling law is associated with the increased dimensionality. The observation can be utilised to highlight FX stylised facts.

Similar to the procedure described in Section 4.7.3, we employ the scaling law coefficient $C_{N_{DC}}$ from Figure 4.15b to compute the multidimensional volatility of the 23D FX data. Volatility $\sigma^{C_{N_{DC}}}_{annual} = 951.46/10.30\%/\sqrt{5} = 41.31\%$. The value four times exceeds the currency average

(10.30%) and is 3.13 times larger than the biggest volatility among all 23 exchange rates. We leave the discussion of the multidimensional intrinsic time volatility estimator and its potential applications to the future research.

4.8 Concluding Remarks

We extend the directional-change intrinsic time framework to the multidimensional space. We show that the extended framework can be used to perform the endogenous price curve analysis of multiple Forex exchange rates. The framework is designed to capture information from the space where orthogonally arranged exchange rates form dimensions.

We generalise the directional-change intrinsic time price curve dissection rules initially developed for the work on one-dimensional data. The absence of the monosemantic and straightforward definition of the up and down notions in the space of higher dimensions complicated the generalisation. We introduce a new "directional vector" concept which allows to circumvent the predicament. The vector starts from the local extreme registered before the trend directional change and passes through the point where the change occurred. Such a vector can be found in any space despite its dimensionality.

The proposed multidimensional directional-change algorithm can efficiently cope with any space morphology. A point, used as a reference for the size of a price move in one-dimensional price space, becomes translated into a line in two- and into a surface in three- and higher dimensions. The matters can be used as references for local price picks and lows in the space of any dimensionality.

The multidimensional framework extends the range of areas where the directional-change intrinsic time can be applied. We show how the analytical equations derived for the one-dimensional data analysis in the intrinsic time can be employed in the multidimensional case. This inheritance ability of the extended algorithm suggests that the risk management, market-making or trading algorithms where the one-dimensional intrinsic time has been involved can now be extended to perform in the space of higher dimensionality.

The extended algorithm was employed to perform an empirical analysis of Forex exchange rates. We outline the observed uneven distribution of directional vectors across the two-dimensional space formed by two Forex exchange rates. That is an interesting observation considering that the distribution is uniform in the case of the Monte Carlo simulation where the exchange rate volatilities are alike. We demonstrate that the varying volatilities of the Forex returns provoke the uneven distribution. A similar contribution is demonstrated for the correlation coefficients: the distribution becomes more irregular with the rise of the ab-

solute correlation coefficient value. We illustrate how the latter can be utilised to unveil the "footprint" of the correlation fluctuating over time.

We report that scaling laws based on the directional-change intrinsic time and so far found in one-dimensional time series are also present in the higher-dimensional Forex data. The laws connect the number of directional changes and the average overshoot length with the size of the trend change (Directional change count and Overshoot laws). We determine a connection between the properties of the first scaling law and the volatility of the examined process. The connection has been further employed as the novel approach of evaluating the volatility of the multidimensional exchange rates. The multidimensional volatility concept proposed in the paper has no alternative in the traditional literature. The concept will be further investigated in forthcoming research works.

Linear and quadratic models were tested as the fitting curves for the Overshoot and Directional change count scaling laws. We considered one-, two-, five-, and 23-dimensional Forex data to track the curvature change associated with the dimensionality increase if any. The curvature was measured as the difference between the coefficients of determination (r-squared) corresponding to the linear and quadratic scaling law data fit in the log-log space. The series of experiments demonstrated the constant increase in the difference between the coefficients of determination. The difference growth together with the increase in the number of exchange rates forming the space. We attribute the phenomenon to the fat-tailed distribution of returns and the aggregational Gaussianity stylised facts of the Forex market. The latter implies that the curvature of the scaling laws can be used as the indicator of the market's deviation from the fully stochastic process.

The multidimensional directional-change algorithm processed dozens of price changes per second. Every change was regarded in the context of the evolution of one inseparable matter: the entire market. The information retrieved from such evolution can serve as an input for various risk management tools. The supreme origin of the information suggests a higher degree of the quality one should expect from the risk management performed using the intrinsic time properties. For instance, the market making adapted to work in the multidimensional intrinsic time can benefit from automatically switching its activity to the components of the space where the volatility is higher. Low liquidity markets, in turn, will inevitably profit from such market making.

The omnipresent interdependence of the steadily evolving world of finance has been continuously growing. We believe that the proposed multidimensional directional-change intrinsic time framework is going to attract more attention to the risk management research

domain. The framework will serve as a base for Pleiades of new research activities targeting the supreme market analysis. The activities should address a wide range of questions related to the extension of the conventional risk management instruments to the multidimensional space.

4.A 3D Price Move

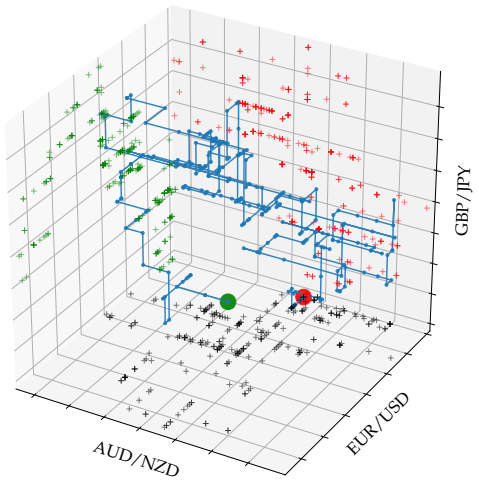

FIGURE 4.16: Real price moves in the three-dimensional space. Tick-by-tick data of the following exchange rates form the space: AUD/NZD, EUR/USD, and GBP/JPY. The presented data sample covers 15-minutes time interval from 21:00 to 21:15 on July 22nd 2012. There are 452 price changes registered within the interval. Elementary price changes, are presented by the blue broken line. Projections of each point onto two-dimensional surfaces are marked by green, red, and blue crosses. The green and red circles label the beginning and the end of the price trajectory correspondingly.

4.B 1D EUR Scaling Laws

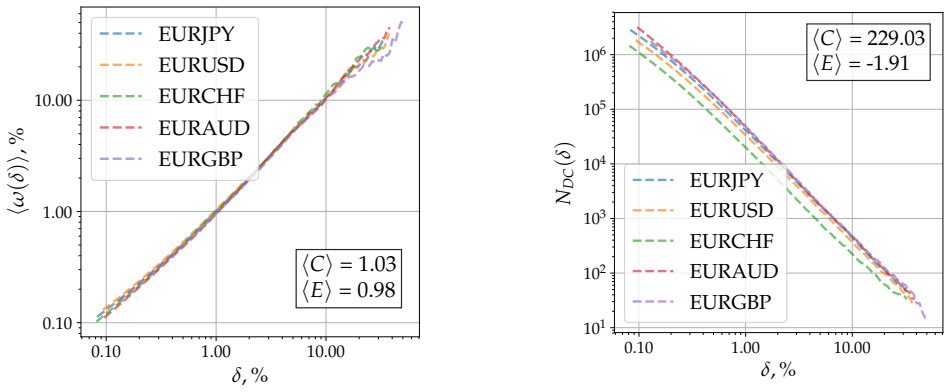

(a) (b)

FIGURE 4.17: **(a)** A set of Overshoot and **(b)** Directional change count scaling laws build for 1D EUR exchange rates. Values $\langle C \rangle$ and $\langle E \rangle$ stand for the average scaling law parameters of the linear approximations build through the entire range of values δ. Comparative statistic of the corresponding exchange rates is provided in Table 4.1.

4.C Expected Waiting Time

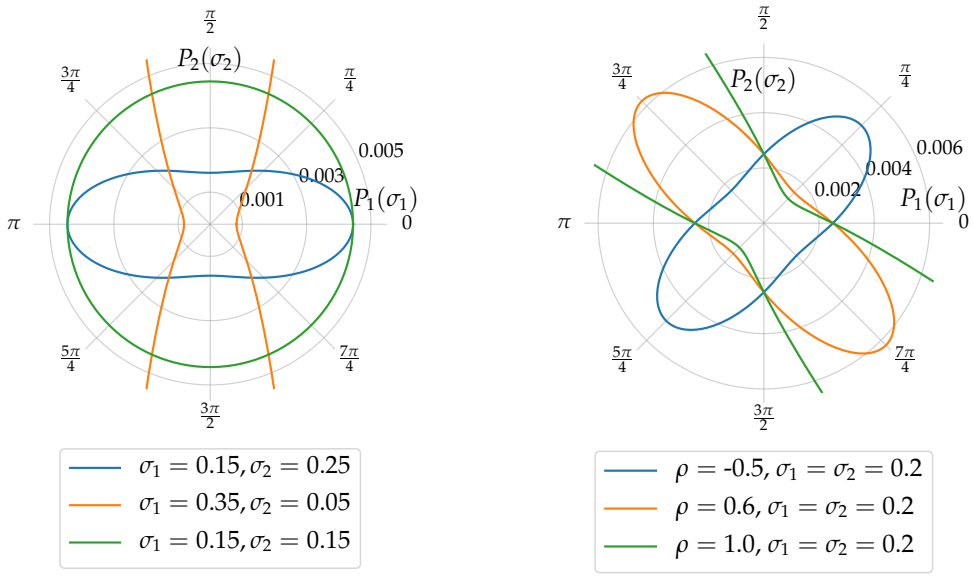

(a) (b)

FIGURE 4.18: Expected waiting time (in years) for a directional-change intrinsic event to unfold in 2D space given the directional vector $\vec{D}$ defined by the angle ϕ (equation (4.16)). **(a)** Iid P_1 and P_2 ($\rho_{1,2} = 0$), different volatility components ($\sigma_1 \neq \sigma_2$). **(b)** Processes P_1 and P_2 have non-zero correlation coefficient ($\rho_{1,2} \neq 0$), volatilities of the processes are fixed and equal to each other ($\sigma_1 = \sigma_2 = 20\%$). The directional-change threshold used in both cases is $\delta = 1\%$. The difference between the largest and the smallest waiting times is 2.8 times in the case of $\sigma_1 = 15\%$ and $\sigma_2 = 25\%$ (blue curve). The difference growths to 49.0 in the case of $\sigma_1 = 35\%$ and $\sigma_2 = 5\%$ (orange curve).

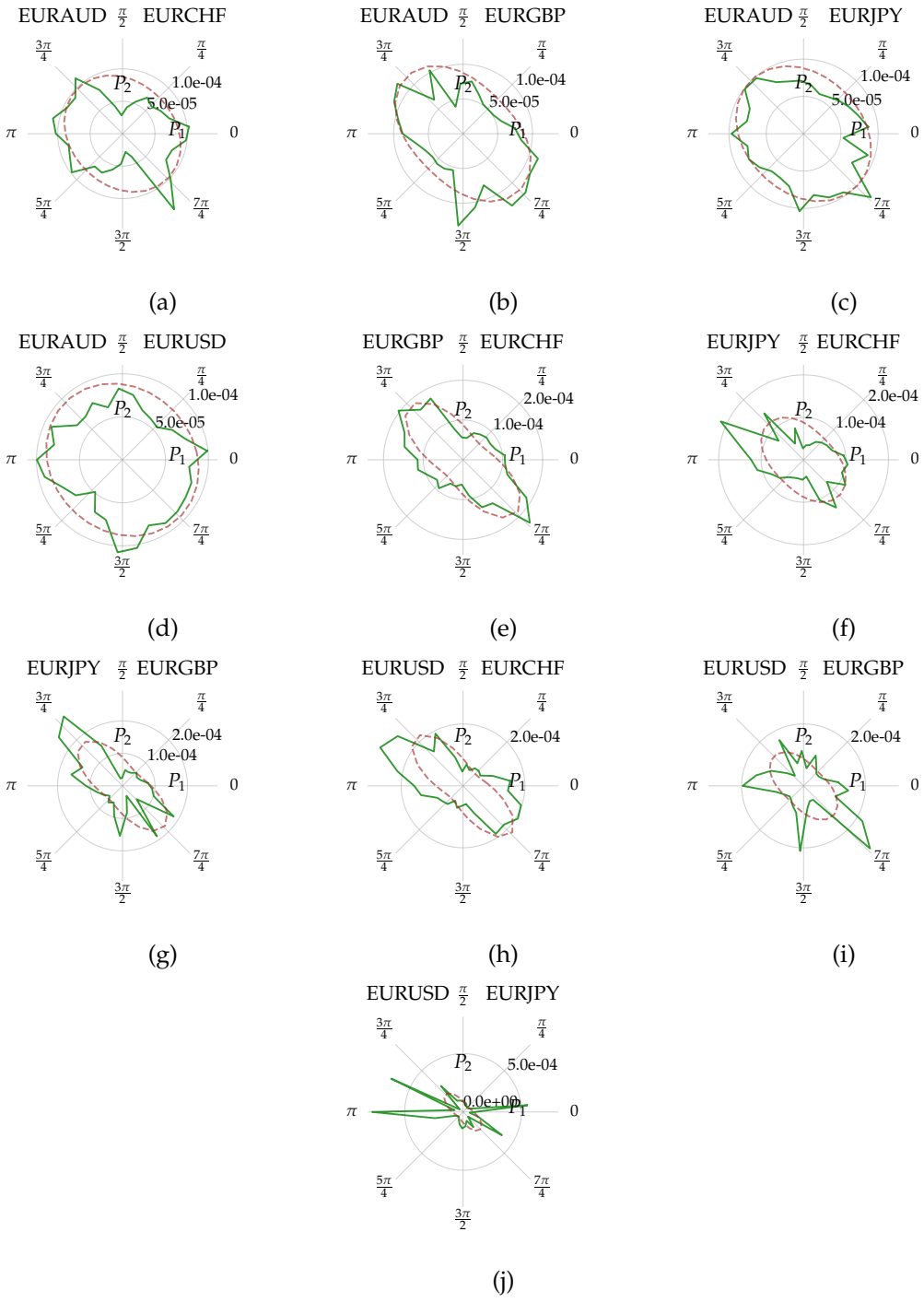

FIGURE 4.19: Average waiting time (in years) until the next directional change to unfold in the interval $\Delta\phi$. FX exchange rates form the 2D space. The interval size is $\Delta\phi = 12°$. There are 30 intervals in total. The selected directional-change threshold is $\delta = 0.94\%$. 1D exchange rates forming the space were preliminary normalised on their volatility and the initial price. Brown dashed lines are approximations of the curves by function (4.16). Parameter $\rho_{1,2}$ is the fitting parameter of the approximation. The fitting expectedly does not succeed in capturing the granted patterns.

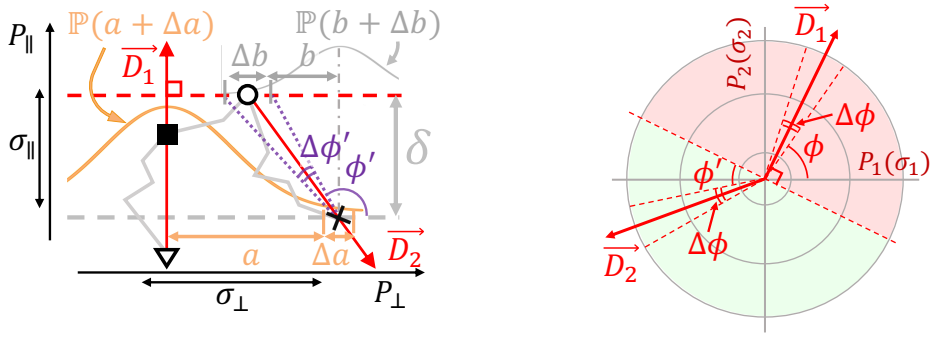

(a) (b)

FIGURE 4.20: **(a)** Visual representation of the price deviating from the directional vector (red vertical vector) while escaping the transition corridor. The corridor is formed by the transition border (red dashed line) and the parallel line (grey dashed line) at the distance δ towards the previous local extreme (flipped triangle). The grey broken lines show three potential price trajectories. The latest transition border of all three price paths is the same. Empty circles mark the latest extreme values observed before the new directional-change. The points where the price curves escape the transition corridor are marked by grey crosses on the grey dashed line. One of the escapes points is shown inside of the interval Δa located at the distance a from the directional vector. The orange bell-shaped curve depicts the probability curve or price deviating from the directional vector by a certain distance. $\sigma_\parallel$ and $\sigma_\perp$ are the parallel and perpendicular to the directional vector volatility components of the 2D price moves. **(b)** Directional vectors $\vec{D}_1$ and $\vec{D}_2$ in 2D space formed by processes $P_1(\sigma_1)$ and $P_2(\sigma_2)$. Green and red backgrounds stand for the sections of the space where the vector $\vec{D}_2$ can and cannot occur conditionally the position of the vector $\vec{D}_1$. Coordinates of the vectors are defined by the angle ϕ measured from the positive direction of the x-axis.

4.D Evolution of Directional Vector as Markov Chain

Price moves in a 2D space can represented by two components: one component parallel to the directional vector $\vec{D}$ and one perpendicular to it ($P_\parallel(\sigma_\parallel)$ and $P_\perp(\sigma_\perp)$). Volatility of the parallel component is described by equation (4.13). Volatility of the perpendicular one is:

$$\sigma_\perp(\sigma_1, \sigma_2; \phi) = \sqrt{(\sigma_1 \sin\phi)^2 + (\sigma_2 \cos\phi)^2}. \tag{4.28}$$

Probability of observing the price escaping the transition corridor (triggering a new directional-change intrinsic event) in the interval Δa located at the distance a from the directional vector $\vec{D}$ (see Figure 4.20a):

$$\mathbb{P}(a, \Delta a, \sigma_\perp, \sigma_\parallel) = \int_0^\infty \int_a^{a+\Delta a} \frac{1}{\sigma_\perp \sqrt{2\pi t}} e^{-\frac{1}{2}\left(\frac{x-\mu}{\sigma_\perp \sqrt{t}}\right)^2} \sum_{k=-\infty}^{\infty} \frac{2h(1+4k)}{\sigma_\parallel \sqrt{2\pi t^{3/2}}} e^{-\frac{h^2(1+4k)^2}{2t\sigma_\parallel^2}} dx dt. \tag{4.29}$$

Equation (4.29) is built using the assumption that the evolution of the price move along the transition border can be described as an evolution of a normal Brownian motion. The probability density of the normal distribution:

$$f(x|\mu,\sigma^2,t) = \frac{1}{\sigma\sqrt{2\pi t}} e^{-\frac{1}{2}\left(\frac{x-\mu}{\sigma\sqrt{t}}\right)^2}. \tag{4.30}$$

The waiting time until the next directional-change, in turn, depends on the evolution of the process along the directional vector $\vec{D}$. The process will trigger a new directional-change as soon as it makes a drawdown (considering the case presented in Figure 4.20a) of the size δ. The waiting time of a drawdown, in turn, has been fount to be equal to the first exit time. The probability density functions (PDF) of the first exit time for an interval of the size h:

$$p_{\tau_h}(t) = \sum_{k=-\infty}^{\infty} \frac{2h(1+4k)}{\sigma\sqrt{2\pi t^{3/2}}} e^{-\frac{h^2(1+4k)^2}{2t\sigma^2}}. \tag{4.31}$$

Equation (4.29) was validated by a Monte Carlo (MC) simulation. Perpendicular and parallel volatility components were selected to be equal to each other: $\sigma_\perp = \sigma_\parallel = 10\%$. Three independent directional-change thresholds were applied in the experiments: $\delta = \{1\%, 2.5\%, 5\%\}$. In each MC simulation, the location of the price escaping the transition corridor was registered. The location was computed with respect to the x-coordinate of the latest directional-change. Results of the experiments are presented as the probability $\mathbb{P}(a + \Delta a)$ and the cumulative probability $F_X(a + \Delta a)$ in Figures 4.21a and 4.21b.

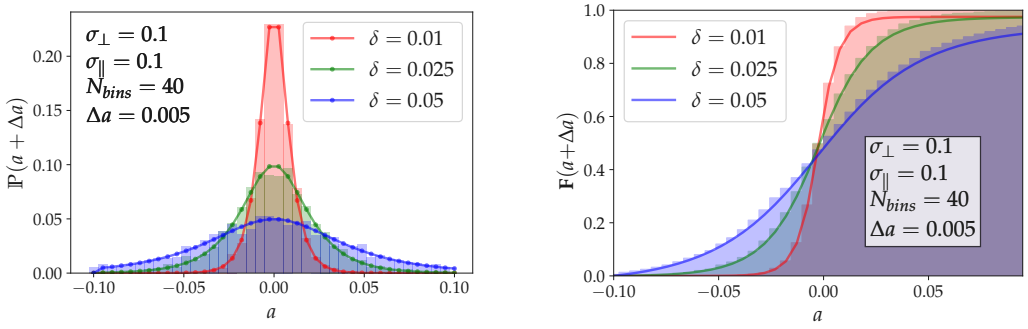

(a) (b)

FIGURE 4.21: **(a)** Monte Carlo simulation and the probability distribution function (4.29) of a directional-change intrinsic event registered in the interval $[a, a + \Delta a]$. The interval is located along the escape border (see Figure 4.20a). The Monte Carlo simulation consisted of 3 000 repetitions. Parameters of the 2D Brownian motions used for the simulation are presented on the picture. There are 100 000 steps in each simulation. x-axis is split in 40 bins of length $\Delta a = 0.005$.

We used the Kolmogorov-Smirnov test[10] to confirm the null-hypothesis that the observed empirical MC distribution is drawn from equation (4.29). Low Kolmogorov–Smirnov statistic values D_n confirm the null hypothesis: $D_n = \{0.176, 0.048, 0.007\}$ for $\delta = \{0.01, 0.025, 0.05\}$.

Position of the directional vector after a new event depends on two factors. Coordinates of the point where the price escapes the transition corridor is the first factor. The coordinates of the point where the price curve crosses the transition border for the last time (see Figure 4.20a) is the second factor. The probability of the former is conditional on the expected time of a total move (a directional-change plus an overshoot). The dependence is expressed by equation (4.29). The probability of the latter is conditional on the expected time of a directional-change to unfold. It can be derived taking into account the fact that the expected time of the overshoot section is twice longer than the expected time of the corresponding directional-change (see Glattfelder, Dupuis, and Olsen (2011)). Therefore, the waiting time is the only difference between the probability of observing the price escaping the transition corridor in the interval Δa located at the distance a from the directional vector and the probability of the latest transition border update happening in the interval Δb located at the distance b from the point where the price escapes the corridor. The same logic used to derive equation (4.29) can be employed to derive the probability $\mathbf{P}(b + \Delta b)$. The time parameter t in the equation (4.30) should be scaled by the factor $2/3$ in order to account for the fact that the overshoot trajectory lasts two-thirds of the total move time. The adjustment leads to the following equation:

$$\mathbb{P}(b, \Delta b, \sigma_\perp, \sigma_\parallel) = \int_0^\infty \int_a^{a+\Delta a} \frac{1}{\sigma_\perp \sqrt{2\pi \frac{2}{3} t}} e^{-\frac{1}{2}\left(\frac{x-\mu}{\sigma_\perp \sqrt{t}}\right)^2} \sum_{k=-\infty}^{\infty} \frac{2h(1+4k)}{\sigma_\parallel \sqrt{2\pi} t^{3/2}} e^{-\frac{h^2(1+4k)^2}{2t\sigma_\parallel^2}} dx dt. \tag{4.32}$$

Location of the vector $\vec{D_2}$ in the 2D space is defined by the angle ϕ'. The angle is formed by the directional vector $\vec{D_2}$ and the positive direction of the x-axis (Figure 4.20a). The size of the angle varies from 0 to π and depends on the location of the latest extreme (the latest transition border update) relative to the point where the price escapes the transition corridor (the interval $[b, b + \Delta b]$). Every angle ϕ' can be expressed in terms of the coordinate x of the latest extreme update and the size of the transition corridor δ:

$$\phi'(x, \delta) = \begin{cases} \arctan\left(\frac{\delta}{x}\right) & \text{for} \quad x > 0 \\ \frac{\pi}{2} & \text{for} \quad x = 0 \\ \pi - |\arctan\left(\frac{\delta}{x}\right)| & \text{for} \quad x < 0 \end{cases} . \tag{4.33}$$

10 $D_n = \sup_a |F_n(a) - F(a)|$ where the n is the number of observations, $F(a)$ is the cumulative density function, and $F_n(a)$ is the set of empirical observations.

Using equation (4.33), one can derive the angle ϕ' relative to the location b and $b + \Delta b$ as well as the interval $\Delta\phi'(b, \Delta b, \delta) = \phi'(b + \Delta b, \delta) - \phi'(b, \delta)$.

Probability of the vector $\vec{D}_2$ being observed in the interval $[\phi', \phi' + \Delta\phi']$ can be converted to the probability of the vector escaping the transition corridor at the particular interval Δb. The equation converting angular coordinates ϕ' and $\Delta\phi'$ into b and Δb should be used to perform the calculation:

$$b(\phi' + \Delta\phi', \delta) = \frac{\delta}{\tan(\phi' + \Delta\phi')}, \tag{4.34}$$

$$\Delta b(\phi', \Delta\phi', \delta) = \frac{\delta}{\tan(\phi')} - b(\phi' + \Delta\phi', \delta). \tag{4.35}$$

The evolution of the directional vector can be presented as the evolution of the vector across the 2π space split in intervals $\Delta\phi$. The number of such intervals is $N_{\Delta\phi} = 2\pi/\Delta\phi \in \mathbb{R}$. We assign unique indexes to each section. The indexes span from one to $N_{\Delta\phi}$. The location of the directional vector is expressed as $\vec{D} \in \Delta\phi_i$.

Location of the vector $\vec{D}_1$ defines properties of the process evolving along the particular directional vector. The process determines the speed and the frequency of directional changes along the given vector. Therefore, the location of the directional vector $\vec{D}_2$ depends on the location of $\vec{D}_1$:

$$\mathbb{P}\left(\vec{D}_2 \in \Delta\phi_k \mid \vec{D}_1 \in \Delta\phi_m\right) \forall k, m \in \left[1, N_{\Delta\phi}\right]. \tag{4.36}$$

The moves of the directional vector are independent of the historical directional vectors but the latest one. The independence suggests that the evolution of the vector is one-step Markov chain. The one-step right stochastic transition probability matrix:

$$\mathbf{P}^{(1)} = \left\| \begin{array}{ccc} \mathbb{P}\left(\vec{D}_2 \in \Delta\phi_1 \mid \vec{D}_1 \in \Delta\phi_1\right) & \dots & \mathbb{P}\left(\vec{D}_2 \in \Delta\phi_{N_{\Delta\phi}} \mid \vec{D}_1 \in \Delta\phi_1\right) \\ \vdots & \ddots & \vdots \\ \mathbb{P}\left(\vec{D}_2 \in \Delta\phi_1 \mid \vec{D}_1 \in \Delta\phi_{N_{\Delta\phi}}\right) & \dots & \mathbb{P}\left(\vec{D}_2 \in \Delta\phi_{N_{\Delta\phi}} \mid \vec{D}_1 \in \Delta\phi_{N_{\Delta\phi}}\right) \end{array} \right\| \tag{4.37}$$

Each entry of the transition probability matrix can be defined using equation (4.32). The range under the integral over dx is defined through equations (4.34) and (4.35). The ijth entry of the matrix $\mathbf{P}^{(n)}$ gives the probability that the Markov chain, starting from the state $\vec{D}_1 \in \Delta\phi_i$, will come to the state $\vec{D}_n \in \Delta\phi_j$ after n directional changes.

The initial distribution of the directional vector $\vec{D}_1$ is defined as the probability vector $\mathbf{u}$. The probability that the chain ends in the state $\vec{D}_n \in \Delta\phi_i$ after n directional-changes is the ith entry of the vector $\mathbf{u}^{(n)}$:

$$\mathbf{u}^{(n)} = \mathbf{u}\mathbf{P}^{(n)}. \tag{4.38}$$

The transition probability matrix (4.37) in par with equation (4.38) have significant predictive power. First, knowing the observed number of directional vectors across the 2D space one can estimate volatilises of the processes forming the space. Second, it is possible to retrieve correlation coefficients conditional the observed distribution of the directional vectors and known volatilities. Third, substantial deviation of the observed directional vector distribution from the analytical predictions can be interpreted as market shocks pronounced at the high-dimensional levels.

Results, presented in this section, concern the evolution of the directional vector in 2D space. The same logic, developed above, can be applied to the space of any dimensionality using angular coordinated of the directional vector (equations (4.18) and (4.19)).

4.E Pseudocode of Multidimensional Dissection Algorithm

The algorithm returns 1 if a directional-change event is registered at the price S_{tick}. Otherwise, it returns 0. $Dist(S_i, S_j)$ is the Euclidean distance between prices S_i and S_j. $Ext\,(Vec, S_{tick})$ method computes coordinates of the transition border using the directional vector Vec (vector $\vec{D}$ in Section 4.4.1) and the point S_{tick}. $DiffSides(Ext, S^p_{ext}, S_{tick}))$ returns *true* if the previous extreme S^p_{ext} and the latest price S_{tick} are on different sides of the transition border Ext. L_{OS} stands for the length of the overshoot section. The initial values of the *first price* and the *initialised* variables are *true* and *false* correspondingly. $NDim$ is the space dimensionality.

Algorithm 2: Multidimensional Runner

procedure RunnerM(S_{tick}, δ)
  if *not initialized* **then**
    if *first price* **then**
      $S^p_{ext} \leftarrow S_{tick}$
      first price $\leftarrow$ *false*
    if $Dist(S_{tick}, S^p_{ext}) \geq \delta$ **then**
      $S_{DC} \leftarrow S_{tick}$
      $Vec \leftarrow \overbrace{S^p_{ext} S_{DC}}$
      $Ext \leftarrow Ext\,(Vec, S_{tick})$
      initialized $\leftarrow$ *true*
      return 1
  else
    if $DiffSides(Ext, S^p_{ext}, S_{tick})$ **then**
      $Ext \leftarrow Ext(Vec, S_{tick})$
      $S_{ext} \leftarrow S_{tick}$
      return 0
    else if $Dist(S_{tick}, Ext) \geq \delta$ **then**
      $L_{OS} \leftarrow Dist(Ext, S_{DC})$
      $S_{DC} \leftarrow S_{tick}$
      $S^p_{ext} \leftarrow S_{ext}$
      $Vec \leftarrow \overbrace{S^p_{ext}, S_{DC}}$
      $Ext \leftarrow Ext(Vec, S_{tick})$
      return 1

ALGORITHM 3: Euclidean distance between two points

1: **procedure** DIST(S_1, S_2)
2: $sum = 0$
3: **for** $i \leftarrow 0$, i++, while $i < NDim$ **do**
4: $sum \leftarrow sum + ((S_2[i] - S_1[i])/S_1[i])^2$
5: **return** $\sqrt{sum}$

ALGORITHM 4: Checks whether points S_1 and S_2 are on different sides of the transition border Ext

1: **procedure** DIFFSIDES(Ext, S_1, S_2)
2: $a = 0$
3: $b = 0$
4: **for** $i \leftarrow 0$, i++, while $i < NDim$ **do**
5: $a \leftarrow a + Ext[i] * S_1[i]$
6: $b \leftarrow a + Ext[i] * S_2[i]$
7: $a \leftarrow a + Ext[NDim - 1]$
8: $b \leftarrow b + Ext[NDim - 1]$
9: **if** $a * b < 0$ **then**
10: **return** $true$
11: **else**
12: **return** $false$

ALGORITHM 5: Computes the directional vector

1: **procedure** VEC(S^p_{ext}, S_{DC})
2: **for** $i \leftarrow 0$, i++, while $i < NDim$ **do**
3: $Vec[i] \leftarrow S_{DC} - S^p_{ext}$
4: **return** Vec

Algorithm 6: Computes the transition border

1: **procedure** BordCoef(Vec, S_{tick})
2: $dummy \leftarrow 0$
3: **for** $i \leftarrow 0$, $i{+}{+}$, while $i < NDim$ **do**
4: $Ext\,[i] \leftarrow Vec\,[i]$
5: $dummy \leftarrow dummy + Vec\,[i] * S_{tick}\,[i]$
6: $Ext\,[NDim - 1] \leftarrow -dummy$
7: **return** Ext

4.F Correlation coefficients of EUR exchange rates

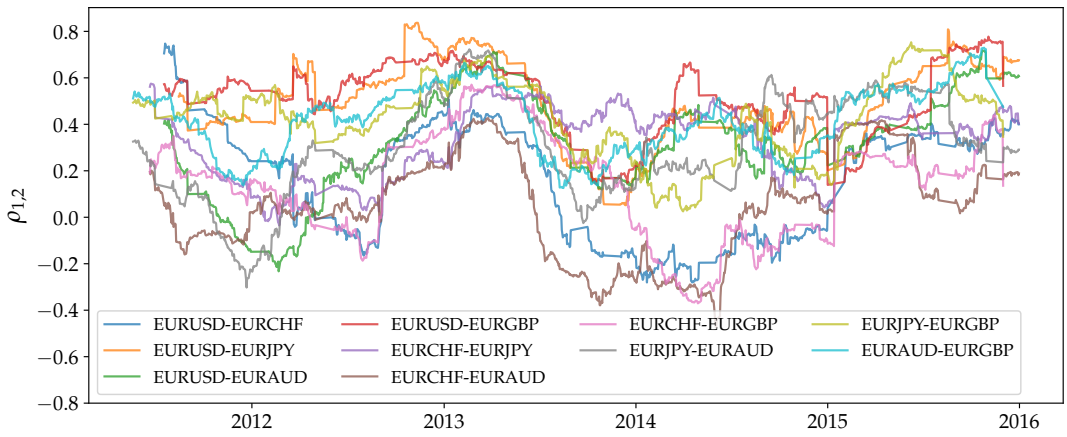

FIGURE 4.22: Correlation coefficient $\rho_{1,2}$ of EUR exchange rates as a function of time. The correlation is computed using daily returns and the rolling window. The length the of rolling window is 100 days.

Bibliography

Abdymomunov, Azamat, and James Morley. 2011. "Time variation of CAPM betas across market volatility regimes." *Applied Financial Economics* 21 (19): 1463.

Ait-Sahalia, Yacine, Per A Mykland, and Lan Zhang. 2005. "How often to sample a continuous-time process in the presence of market microstructure noise." *The review of financial studies* 18 (2): 351.

A1, Yacine, Robert Kimmel, et al. 2007. "Maximum likelihood estimation of stochastic volatility models." *Journal of financial economics* 83 (2): 413.

Allais, Maurice. 1974. "The psychological rate of interest." *Journal of Money, Credit and Banking* 6 (3): 285.

Aloud, Monira, Maria Fasli, Edward Tsang, Alexander Dupuis, and Richard Olsen. 2017. "Modeling the High-Frequency FX Market: An Agent-Based Approach." *Computational Intelligence* 33 (4): 771.

Andersen, Torben G, and Jesper Lund. 1997. "Estimating continuous-time stochastic volatility models of the short-term interest rate." *Journal of econometrics* 77 (2): 343.

Andreoni, James, and Charles Sprenger. 2012a. "Estimating time preferences from convex budgets." *American Economic Review* 102 (7): 3333.

———. 2012b. "Risk preferences are not time preferences." *American Economic Review* 102 (7): 3357·

Andriani, Pierpaolo, and Bill McKelvey. 2007. "Beyond Gaussian averages: redirecting international business and management research toward extreme events and power laws." *Journal of International Business Studies* 38 (7): 1212.

Ang, Andrew, and Joseph Chen. 2007. "CAPM over the long run: 1926–2001." *Journal of Empirical Finance* 14 (1): 1.

Antypas, Antonios, Phoebe Koundouri, and Nikolaos Kourogenis. 2013. "Aggregational Gaussianity and barely infinite variance in financial returns." *Journal of Empirical Finance* 20:102.

Arneodo, Alain, Jean-Philippe Bouchaud, Rama Cont, Jean-François Muzy, Marc Potters, and Didier Sornette. 1996. "Comment on"Turbulent cascades in foreign exchange markets"." *arXiv preprint cond-mat/9607120.*

Asmussen, Søren, and Hansjörg Albrecher. 2010. *Ruin probabilities.* World Scientific Publishing Co Pte Ltd.

Bakhach, Amer, Venkata Chinthalapati, Edward Tsang, and Abdul El Sayed. 2018. "Intelligent dynamic backlash agent: A trading strategy based on the directional change framework." *Algorithms* 11 (11): 171.

Ballocchi, Giuseppe, Michel M Dacorogna, Carl M Hopman, Ulrich A Müller, and Richard B Olsen. 1999. "The intraday multivariate structure of the Eurofutures markets." *Journal of Empirical Finance* 6 (5): 479.

Bandt, Chstoph, and Faten Shiha. 2007. "Order patterns in time series." *Journal of Time Series Analysis* 28 (5): 646.

Barndorff-Nielsen, Ole E, and Neil Shephard. 2002. "Econometric analysis of realized volatility and its use in estimating stochastic volatility models." *Journal of the Royal Statistical Society: Series B (Statistical Methodology)* 64 (2): 253.

Basu, Sanjoy. 1977. "Investment performance of common stocks in relation to their price-earnings ratios: A test of the efficient market hypothesis." *The journal of Finance* 32 (3): 663.

Bauwens, Luc, and Nikolaus Hautsch. 2009. "Modelling financial high frequency data using point processes." In *Handbook of financial time series*, 953. Springer.

Bauwens, Luc, Walid Ben Omrane, and Pierre Giot. 2005. "News announcements, market activity and volatility in the euro/dollar foreign exchange market." *Journal of International Money and Finance* 24 (7): 1108.

Begušić, Stjepan, Zvonko Kostanjčar, H Eugene Stanley, and Boris Podobnik. 2018. "Scaling properties of extreme price fluctuations in Bitcoin markets." *Physica A: Statistical Mechanics and its Applications* 510:400.

Bessembinder, Hendrik. 1994. "Bid-ask spreads in the interbank foreign exchange markets." *Journal of Financial economics* 35 (3): 317.

BIS. 2016. *Triennial central bank survey: Foreign exchange turnover in April 2016.*

Bisig, Thomas, Alexandre Dupuis, Vito Impagliazzo, and Richard B Olsen. 2012. "The scale of market quakes." *Quantitative Finance* 12 (4): 501.

Black, Fischer, and Myron Scholes. 1973. "The pricing of options and corporate liabilities." *Journal of political economy* 81 (3): 637.

Blattberg, Robert C, and Nicholas J Gonedes. 1974. "A comparison of the stable and student distributions as statistical models for stock prices." *The journal of business* 47 (2): 244.

Boland, Lawrence A. 1978. "Time in economics vs economics in time: The'Hayek Problem'." *Canadian Journal of Economics:* 240.

Bollerslev, Tim, and Ian Domowitz. 1993. "Trading patterns and prices in the interbank foreign exchange market." *The Journal of Finance* 48 (4): 1421.

Bollerslev, Tim, and Michael Melvin. 1994. "Bid—ask spreads and volatility in the foreign exchange market: An empirical analysis." *Journal of International Economics* 36 (3): 355.

Bouchaud, Jean-Philippe. 2001. "Power laws in economics and finance: some ideas from physics."

———. 2010. "Price impact." *Encyclopedia of quantitative finance.*

Brown, Stephen J, and Jerold B Warner. 1985. "Using daily stock returns: The case of event studies." *Journal of financial economics* 14 (1): 3.

Campbell, John Y, Stefano Giglio, Christopher Polk, and Robert Turley. 2018. "An intertemporal CAPM with stochastic volatility." *Journal of Financial Economics* 128 (2): 207.

Canelas, António, Rui Neves, and Nuno Horta. 2013. "Multi-dimensional pattern discovery in financial time series using SAX-GA With extended robustness." In *Proceedings of the 15th annual conference companion on Genetic and evolutionary computation*, 179. ACM.

Carr, Peter, Hongzhong Zhang, and Olympia Hadjiliadis. 2011. "Maximum drawdown insurance." *International Journal of Theoretical and Applied Finance* 14 (8): 1195.

Cassel, Gustav, Joseph McCabe, et al. 1923. "Theory of social economy."

Chakraborti, Anirban, Ioane Muni Toke, Marco Patriarca, and Frédéric Abergel. 2009. "Econophysics: Empirical facts and agent-based models." *arXiv preprint arXiv:0909.1974.*

Chekhlov, Alexei, Stanislav Uryasev, and Michael Zabarankin. 2005. "Drawdown measure in portfolio optimization." *International Journal of Theoretical and Applied Finance* 8 (1): 13.

Cheung, Yin-Wong, and Menzie David Chinn. 2001. "Currency traders and exchange rate dynamics: a survey of the US market." *Journal of international money and finance* 20 (4): 439.

Cho, D Chinhyung, and Edward W Frees. 1988. "Estimating the volatility of discrete stock prices." *The Journal of Finance* 43 (2): 451.

Chordia, Tarun, Richard Roll, and Avanidhar Subrahmanyam. 2001. "Market liquidity and trading activity." *The journal of finance* 56 (2): 501.

Christie, Andrew A. 1982. "The stochastic behavior of common stock variances: Value, leverage and interest rate effects." *Journal of financial Economics* 10 (4): 407.

Cohen, Lauren, Karl B Diether, and Christopher J Malloy. 2007. "Supply and demand shifts in the shorting market." *The Journal of Finance* 62 (5): 2061.

Cont, Rama. 2001. "Empirical properties of asset returns: stylized facts and statistical issues."

———. 2011. "Statistical modeling of high-frequency financial data." *IEEE Signal Processing Magazine* 28 (5): 16.

Cont, Rama, Marc Potters, and Jean-Philippe Bouchaud. 1997. "Scaling in stock market data: stable laws and beyond." *Scale invariance and beyond* 7:75.

Corsi, Fulvio, Gilles Zumbach, Ulrich A Muller, and Michel M Dacorogna. 2001. "Consistent high-precision volatility from high-frequency data." *Economic Notes* 30 (2): 183.

Cotter, John. 2005. "Tail behaviour of the euro." *Applied Economics* 37 (7): 827.

Dacorogna, Michael M, Ulrich A Müller, Robert J Nagler, Richard B Olsen, and Olivier V Pictet. 1993. "A geographical model for the daily and weekly seasonal volatility in the foreign exchange market." *Journal of International Money and Finance* 12 (4): 413.

Dacorogna, Michel M, Ulrich A Müller, Olivier V Pictet, and Casper G De Vries. 2001. "Extremal forex returns in extremely large data sets." *Extremes* 4 (2): 105.

Danielsson, Jon, and Casper G de Vries. 1997. "Tail index and quantile estimation with very high frequency data." *Journal of empirical Finance* 4 (2-3): 241.

Dassios, Angelos, and Jia Wei Lim. 2018. "An efficient algorithm for simulating the drawdown stopping time and the running maximum of a Brownian motion." *Methodology and Computing in Applied Probability* 20 (1): 189.

De Bondt, Werner FM, and Richard H Thaler. 1987. "Further evidence on investor overreaction and stock market seasonality." *The Journal of finance* 42 (3): 557.

Debreu, Gerard. 1987. *Theory of value: An axiomatic analysis of economic equilibrium.* 17. Yale University Press.

Delage, Vivien, Christian Brandlhuber, Karl Tuyls, and Gerhard Weiss. 2010. "Multi-Agent based simulation of FOREX exchange market." *Maastricht University, Department of Knowledge Engineering, the Netherlands Teramark Technologies GmbH, Munich, Germany.*

Di Matteo, Tiziana. 2007. "Multi-scaling in finance." *Quantitative finance* 7 (1): 21.

Di Matteo, Tiziana, Tomaso Aste, and Michel M Dacorogna. 2005. "Long-term memories of developed and emerging markets: Using the scaling analysis to characterize their stage of development." *Journal of Banking & Finance* 29 (4): 827.

Diamond, Peter A, and Jerry A Hausman. 1994. "Contingent valuation: is some number better than no number?" *Journal of economic perspectives* 8 (4): 45.

Dyhrberg, Anne H, Sean Foley, and Jiri Svec. 2018. "How investible is Bitcoin? Analyzing the liquidity and transaction costs of Bitcoin markets." *Economics Letters* 171:140.

Dyhrberg, Anne Haubo. 2016. "Bitcoin, gold and the dollar–A GARCH volatility analysis." *Finance Research Letters* 16:85.

Easley, David, Marcos M López De Prado, and Maureen O'Hara. 2012. "The volume clock: Insights into the high-frequency paradigm." *The Journal of Portfolio Management* 39 (1): 19.

Ederington, Louis H, and Jae Ha Lee. 1993. "How markets process information: News releases and volatility." *The Journal of Finance* 48 (4): 1161.

Ehrentreich, Norman. 2007. *Agent-based modeling: The Santa Fe Institute artificial stock market model revisited.* Vol. 602. Springer Science & Business Media.

Einstein, Albert. 1905. "Zur elektrodynamik bewegter körper." *Annalen der physik* 322 (10): 891.

———. 1915. "The field equations of gravitation." *Sitzungsber. Preuss. Akad. Wiss. Berlin (Math. Phys.)* 1915:844.

Elder, Alexander. 2014. *The new trading for a living: psychology, discipline, trading tools and systems, risk control, trade management.* John Wiley & Sons.

Eross, Andrea, Frank Mcgroarty, Andrew Urquhart, and Simon Wolfe. 2017. "The Intraday Dynamics of Bitcoin." *SSRN Elecronic Journal*, no. August: 1.

Evans, Martin DD, and Richard K Lyons. 2005. "Do currency markets absorb news quickly?" *Journal of International Money and Finance* 24 (2): 197.

Fama, Eugene F. 1970. "Efficient capital markets: A review of theory and empirical work." *The journal of Finance* 25 (2): 383.

Fama, Eugene F, and Kenneth R French. 1992. "The cross-section of expected stock returns." *the Journal of Finance* 47 (2): 427.

———. 1993. "Common risk factors in the returns on stocks and bonds." *Journal of financial economics* 33 (1): 3.

———. 1996. "Multifactor explanations of asset pricing anomalies." *The journal of finance* 51 (1): 55.

———. 1997. "Industry costs of equity." *Journal of financial economics* 43 (2): 153.

———. 2006. "The value premium and the CAPM." *The Journal of Finance* 61 (5): 2163.

Fang, Lily, Chunmei Lin, and Yuping Shao. 2018. "School holidays and stock market seasonality." *Financial Management* 47 (1): 131.

Farmer, J Doyne, Fabrizio Lillo, et al. 2004. "On the origin of power-law tails in price fluctuations." *Quantitative Finance* 4 (1): 7.

Frank, Murray Z., and Ali Sanati. 2018. "How does the stock market absorb shocks?" *Journal of Financial Economics* 129 (1): 136.

Franklin, Benjamin. 1750. *Advice to a young tradesman.* Vol. 1748. Philadelphia.

Frederick, Shane, George Loewenstein, and Ted O'donoghue. 2002. "Time discounting and time preference: A critical review." *Journal of economic literature* 40 (2): 351.

French, Kenneth R, and Richard Roll. 1986. "Stock return variances: The arrival of information and the reaction of traders." *Journal of financial economics* 17 (1): 5.

Gabaix, Xavier, Parameswaran Gopikrishnan, Vasiliki Plerou, and H Eugene Stanley. 2003. "A theory of power-law distributions in financial market fluctuations." *Nature* 423 (6937): 267.

Galluccio, Stefano, Guido Caldarelli, Matteo Marsili, and Y-C Zhang. 1997. "Scaling in currency exchange." *Physica A: Statistical Mechanics and its Applications* 245 (3): 423.

Gençay, Ramazan, Michel Dacorogna, Ulrich A Muller, Olivier Pictet, and Richard Olsen. 2001. *An introduction to high-frequency finance.* Academic press.

Georgescu-Roegen, Nicholas. 1993. "The entropy law and the economic problem." *Valuing the Earth: Economics, ecology, ethics:* 75.

Ghashghaie, Shoaleh, Wolfgang Breymann, Joachim Peinke, Peter Talkner, Yadollah Dodge, et al. 1996. "Turbulent cascades in foreign exchange markets." *Nature* 381 (6585): 767.

Gidea, Marian, and Yuri Katz. 2018. "Topological data analysis of financial time series: Landscapes of crashes." *Physica A: Statistical Mechanics and its Applications* 491:820.

Gilpin, Robert, and Jean M Gilpin. 2001. *Global political economy: Understanding the international economic order.* Princeton University Press.

Glattfelder, James. 2019. *INFORMATION-CONSCIOUSNESS-REALITY: How a New Understanding of the Universe Can Help Answer... Age-old Questions of Existence.* SPRINGER.

Glattfelder, JB, A Dupuis, and RB Olsen. 2011. "Patterns in high-frequency FX data: discovery of 12 empirical scaling laws." *Quantitative Finance* 11 (4): 599.

Golub, Anton, Gregor Chliamovitch, Alexandre Dupuis, and Bastien Chopard. 2014. "Multi-scale representation of high frequency market liquidity." *Available at SSRN 2393428.*

Golub, Anton, James Glattfelder, and Richard B Olsen. 2017. "The Alpha Engine: Designing an Automated Trading Algorithm."

Goodhart, Charles, Takatoshi Ito, and Richard Payne. 1996. "One day in June 1993: a study of the working of the Reuters 2000-2 electronic foreign exchange trading system." In *The microstructure of foreign exchange markets,* 107. University of Chicago Press.

Gossen, Hermann Heinrich. 1854. *The laws of human relations: and the rules of human action derived therefrom, translated by RC Blitz.*

Gottlieb, Gary, and Avner Kalay. 1985. "Implications of the discreteness of observed stock prices." *The Journal of Finance* 40 (1): 135.

Grossman, Sanford J, and Zhongquan Zhou. 1993. "Optimal investment strategies for controlling drawdowns." *Mathematical finance* 3 (3): 241.

Guillaume, Dominique M, Michel M Dacorogna, Rakhal R Davé, Ulrich A Müller, Richard B Olsen, and Olivier V Pictet. 1997. "From the bird's eye to the microscope: A survey of new stylized facts of the intra-daily foreign exchange markets." *Finance and stochastics* 1 (2): 95.

Guillaume, Dominique M, Olivier V Pictet, Ulrich A Müller, and Michel M Dacorogna. 1995. "Unveiling nonlinearities through time scale transformations." *Preprint Olsen group OVP. 1994-06* 26.

Gultekin, Mustafa N, and N Bulent Gultekin. 1983. "Stock market seasonality: International evidence." *Journal of financial economics* 12 (4): 469.

Hadjiliadis, Olympia, and Jan Večeř. 2006. "Drawdowns preceding rallies in the Brownian motion model." *Quantitative Finance* 6 (5): 403.

Haferkorn, Martin, and Josué Manuel Quintana Diaz. 2014. "Seasonality and interconnectivity within cryptocurrencies-an analysis on the basis of Bitcoin, Litecoin and Namecoin." In *International Workshop on Enterprise Applications and Services in the Finance Industry*, 106. Springer.

Hansen, Peter R, and Asger Lunde. 2006. "Realized variance and market microstructure noise." *Journal of Business & Economic Statistics* 24 (2): 127.

Harris, Larry. 2003. *Trading and exchanges: Market microstructure for practitioners.* Oxford University Press, USA.

Hartmann, Philipp. 1999. "Trading volumes and transaction costs in the foreign exchange market: evidence from daily dollar–yen spot data." *Journal of Banking & Finance* 23 (5): 801.

Hasbrouck, Joel. 1991. "Measuring the information content of stock trades." *The Journal of Finance* 46 (1): 179.

———. 2018. "High-frequency quoting: Short-term volatility in bids and offers." *Journal of Financial and Quantitative Analysis* 53 (2): 613.

Hausman, Jerry A, Andrew W Lo, and A Craig MacKinlay. 1992. "An ordered probit analysis of transaction stock prices." *Journal of financial economics* 31 (3): 319.

He, Jiayi, Pengjian Shang, and Hui Xiong. 2018. "Multidimensional scaling analysis of financial time series based on modified cross-sample entropy methods." *Physica A: Statistical Mechanics and its Applications:* -.

Hicks, J. 1946. "Value and Capital–2nd Edition."

Huberman, Gur, and Werner Stanzl. 2004. "Price Manipulation and Quasi-Arbitrage." *Econometrica* 72 (4): 1247.

Ito, Takatoshi, and Yuko Hashimoto. 2006. "Intraday seasonality in activities of the foreign exchange markets: Evidence from the electronic broking system." *Journal of the Japanese and International Economies* 20 (4): 637.

Jagannathan, Ravi, and Zhenyu Wang. 1996. "The conditional CAPM and the cross-section of expected returns." *The Journal of finance* 51 (1): 3.

Jarrow, Robert A, and Philip Protter. 2012. "A dysfunctional role of high frequency trading in electronic markets." *International Journal of Theoretical and Applied Finance* 15 (03): 1250022.

JE de Vries, Jon Erik, and Halvor Aarhus Aalborg. 2017. "What can explain the price, volatility and traded volume of Bitcoin?" Master's thesis, University of Stavanger, Norway.

Jondeau, Eric, and Michael Rockinger. 2003. "Testing for differences in the tails of stock-market returns." *Journal of Empirical Finance* 10 (5): 559.

Joulin, Armand, Augustin Lefevre, Daniel Grunberg, and Jean-Philippe Bouchaud. 2008. "Stock price jumps: news and volume play a minor role." *arXiv preprint arXiv:0803.1769*.

Kablan, Abdalla, and Wing Lon Ng. 2011. "Intraday high-frequency FX trading with adaptive neuro-fuzzy inference systems." *International Journal of Financial Markets and Derivatives* 2 (1-2): 68.

Kaldor, Nicholas. 1961. "Capital accumulation and economic growth." In *The theory of capital*, 177. Springer.

Kaya, Orçun, Jan Schildbach, and Deutsche Bank Ag. 2016. "High-frequency trading." *Reaching the limits, Automated trader magazine* 41:23.

Keim, Donald B. 1983. "Size-related anomalies and stock return seasonality: Further empirical evidence." *Journal of financial economics* 12 (1): 13.

Kelly Jr, John L. 2011. "A new interpretation of information rate." In *The Kelly Capital Growth Investment Criterion: Theory and Practice*, 25. World Scientific.

Kempf, Alexander, and Olaf Korn. 1999. "Market depth and order size." *Journal of Financial Markets* 2 (1): 29.

Klein, Judy L, and Dave Klein. 1997. *Statistical visions in time: a history of time series analysis, 1662-1938*. Cambridge University Press.

Koning, Nico, Daniel T Cassidy, and Rachid Ouyed. 2018. "Extended Model of Stock Price Behaviour." *Journal of Mathematical Finance* 8 (1): 1.

Kozhan, Roman, and Mark Salmon. 2012. "The information content of a limit order book: The case of an FX market." *Journal of Financial Markets* 15 (1): 1.

Krugman, Paul. 2010. "The theory of interstellar trade." *Economic Inquiry* 48 (4): 1119.

Kullmann, L, J Töyli, J Kertesz, A Kanto, and K Kaski. 1999. "Characteristic times in stock market indices." *Physica A: Statistical Mechanics and its Applications* 269 (1): 98.

Kyle, Albert S. 1985. "Continuous auctions and insider trading." *Econometrica: Journal of the Econometric Society:* 1315.

Landriault, David, Bin Li, and Hongzhong Zhang. 2015. "On the frequency of drawdowns for brownian motion processes." *Journal of Applied Probability* 52 (1): 191.

LeBaron, Blake. 2006. "Agent-based computational finance." *Handbook of computational economics* 2:1187.

Lettau, Martin, and Sydney Ludvigson. 2001. "Resurrecting the (C) CAPM: A cross-sectional test when risk premia are time-varying." *Journal of political economy* 109 (6): 1238.

Lewellen, Jonathan, and Stefan Nagel. 2006. "The conditional CAPM does not explain asset-pricing anomalies." *Journal of financial economics* 82 (2): 289.

Li, Ying, Donghui Yang, and Xiaobin Li. 2017. "Multidimensional Time Series Analysis of Financial Markets Based on the Complex Network Approach." *Journal of Mathematical Finance* 7 (3): 734.

Lillo, Fabrizio, J Doyne Farmer, and Rosario N Mantegna. 2003. "Econophysics: Master curve for price-impact function." *Nature* 421 (6919): 129.

Liu, Ruiping, Zhichao Shao, Guodong Wei, and Wei Wang. 2017. "GARCH Model With Fat-Tailed Distributions and Bitcoin Exchange Rate Returns." *Journal of Accounting, Business and Finance Research* 1 (1): 71.

Lundberg, Filip. 1909. "Uber die Theorie der Ruck-versicherung." In *Trans VI International Congress Actuaries,* 877.

Mancino, Maria Elvira, Maria Cristina Recchioni, and Simona Sanfelici. 2017. "Estimation of Instantaneous Volatility." In *Fourier-Malliavin Volatility Estimation,* 31. Springer.

Mandelbrot, Benoit B. 1997. "The variation of certain speculative prices": 371.

Mandelbrot, Benoit B, and Richard L Hudson. 2010. *The (mis) behaviour of markets: a fractal view of risk, ruin and reward.* Profile books.

Mandelbrot, Benoit, and Howard M Taylor. 1967. "On the distribution of stock price differences." *Operations research* 15 (6): 1057.

Mantegna, Rosario N, and H Eugene Stanley. 1995. "Scaling behaviour in the dynamics of an economic index." *Nature* 376 (6535): 46.

Marshall, A. 1961. *Principles of Economics.* Palgrave Macmillan UK.

Marshall, Alfred. 1890. *Principles of economics. Vol. 1.*

Marx, Karl. 1875. *Le capital.* Vol. 1. Lachâtre.

Menger, Carl. 1871. "Principles of Economics, translated by James Dingwall and Bert F." *Hoselitz with an introduction by FA Hayek (New York and London, New York University Press), first published.*

Menkhoff, Lukas, Lucio Sarno, Maik Schmeling, and Andreas Schrimpf. 2012. "Carry trades and global foreign exchange volatility." *The Journal of Finance* 67 (2): 681.

Mijatović, Aleksandar, and Martijn R Pistorius. 2012. "On the drawdown of completely asymmetric Lévy processes." *Stochastic Processes and their Applications* 122 (11): 3812.

Moreva, Ekaterina, Giorgio Brida, Marco Gramegna, Vittorio Giovannetti, Lorenzo Maccone, and Marco Genovese. 2014. "Time from quantum entanglement: an experimental illustration." *Physical Review A* 89 (5): 052122.

Morgan, Mary S, et al. 1990. *The history of econometric ideas.* Cambridge University Press.

Mossin, Jan. 1966. "Equilibrium in a capital asset market." *Econometrica: Journal of the econometric society:* 768.

Müller, Ulrich A, Michel M Dacorogna, Rakhal D Davé, Richard B Olsen, Olivier V Pictet, and Jacob E von Weizsäcker. 1997. "Volatilities of different time resolutions—analyzing the dynamics of market components." *Journal of Empirical Finance* 4 (2-3): 213.

Müller, Ulrich A, Michel M Dacorogna, Rakhal D Davé, Olivier V Pictet, Richard B Olsen, and J Robert Ward. 1993. "Fractals and intrinsic time: A challenge to econometricians." *Unpublished manuscript, Olsen & Associates, Zürich.*

Müller, Ulrich A, Michel M Dacorogna, Richard B Olsen, Olivier V Pictet, Matthias Schwarz, and Claude Morgenegg. 1990. "Statistical study of foreign exchange rates, empirical evidence of a price change scaling law, and intraday analysis." *Journal of Banking & Finance* 14 (6): 1189.

Muth, John F. 1961. "Rational expectations and the theory of price movements." *Econometrica: Journal of the Econometric Society:* 315.

NACIRI, Nawfal, and Mohamed TKIOUAT. 2016. "Economic Agent Based Models." *International Journal of Applied Engineering Research* 11 (8): 5492.

Nakamoto, Satoshi. 2008. "Bitcoin: A peer-to-peer electronic cash system."

Osborne, Maury FM. 1959. "Brownian motion in the stock market." *Operations research* 7 (2): 145.

Pagan, Adrian. 1996. "The econometrics of financial markets." *Journal of empirical finance* 3 (1): 15.

Page, Don N, and William K Wootters. 1983. "Evolution without evolution: Dynamics described by stationary observables." *Physical Review D* 27 (12): 2885.

Petrov, Vladimir, Anton Golub, and Richard Olsen. 2018. "Instantaneous Volatility Estimator Based on Directional-Change Intrinsic Time." Working Paper, University of Zurich.

———. 2019. "Instantaneous Volatility Seasonality of High-Frequency Markets in Directional-Change Intrinsic Time." *Journal of Risk and Financial Management* 12 (2): 54.

Ponsford, Matthew P. 2015. "A comparative analysis of Bitcoin and other decentralised virtual currencies: legal regulation in the people's republic of China, Canada, and the United States." *HKJ Legal Stud.* 9:29.

Pospisil, Libor, Jan Vecer, and Olympia Hadjiliadis. 2009. "Formulas for stopped diffusion processes with stopping times based on drawdowns and drawups." *Stochastic Processes and their Applications* 119 (8): 2563.

Quesnay, François. 1894. *Tableau Oeconomiqueh [microform].: First Printed in 1758 and Now Reproduced in Facsimile for the British Economic Association.* Macmillan & Company.

Rachev, Svetlozar T, Christian Menn, and Frank J Fabozzi. 2005. *Fat-tailed and skewed asset return distributions: implications for risk management, portfolio selection, and option pricing.* Vol. 139. John Wiley & Sons.

Ricardo, David. 1817. *On the Principles of Political Economy and Taxation: London.*

Robinson, Joan. 1980. "Time in economic theory." *Kyklos* 33 (2): 219.

Rohatinski, Željko. 2017. *Time and Economics: The Concept of Functional Time.* Springer.

Rolski, Tomasz, Hanspeter Schmidli, Volker Schmidt, and Jozef L Teugels. 2009. *Stochastic processes for insurance and finance.* Vol. 505. John Wiley & Sons.

Roy, Souvik, and P Venkateswaran. 2014. "Online payment system using steganography and visual cryptography." In *2014 IEEE Students' Conference on Electrical, Electronics and Computer Science,* 1. IEEE.

Rozeff, Michael S, and William R Kinney Jr. 1976. "Capital market seasonality: The case of stock returns." *Journal of financial economics* 3 (4): 379.

Samanidou, Egle, Elmar Zschischang, Dietrich Stauffer, and Thomas Lux. 2007. "Agent-based models of financial markets." *Reports on Progress in Physics* 70 (3): 409.

Sapuric, Svetlana, and Angelika Kokkinaki. 2014. "Bitcoin Is Volatile! Isn't that Right?" In *International Conference on Business Information Systems,* 255. Springer.

Schuhmacher, Frank, and Martin Eling. 2011. "Sufficient conditions for expected utility to imply drawdown-based performance rankings." *Journal of Banking & Finance* 35 (9): 2311.

Schwert, G William. 1989. "Why does stock market volatility change over time?" *The journal of finance* 44 (5): 1115.

Scott, Louis O. 1987. "Option pricing when the variance changes randomly: Theory, estimation, and an application." *Journal of Financial and Quantitative analysis* 22 (4): 419.

Seif, Mostafa, Paul Docherty, and Abul Shamsuddin. 2017. "Seasonal anomalies in advanced emerging stock markets." *The Quarterly Review of Economics and Finance* 66:169.

Shackle, George Lennox Sharman. 1967. *Time in economics.* North-Holland Publishing Company.

Sharpe, William F. 1964. "Capital asset prices: A theory of market equilibrium under conditions of risk." *The journal of finance* 19 (3): 425.

Shintate, Takuya, and Lukáš Pichl. 2019. "Trend Prediction Classification for High Frequency Bitcoin Time Series with Deep Learning." *Journal of Risk and Financial Management* 12 (1): 17.

Sornette, Didier. 2001. "Fokker–Planck equation of distributions of financial returns and power laws." *Physica A: Statistical Mechanics and its Applications* 290 (1-2): 211.

Stöber, Jakob, and Claudia Czado. 2014. "Regime switches in the dependence structure of multidimensional financial data." *Computational Statistics & Data Analysis* 76:672.

Stock, James H. 1988. "Estimating continuous-time processes subject to time deformation: an application to postwar US GNP." *Journal of the American Statistical Association* 83 (401): 77.

Taylor, BN, and A Thompson. 2008. "The International System of Units (SI)(Special Publication 330)(Gaithersburg, MD: National Institute of Standards and Technology) http://physics. nist. gov/Pubs." *SP330/sp330. pdf.*

Taylor, Howard M. 1975. "A stopped Brownian motion formula." *The Annals of Probability:* 234.

Walras, Leon. 2013. *Elements of pure economics.* Routledge.

Zarowin, Paul. 1990. "Size, seasonality, and stock market overreaction." *Journal of Financial and Quantitative analysis* 25 (1): 113.

Zhang, Hongzhong. 2015. "Occupation times, drawdowns, and drawups for one-dimensional regular diffusions." *Advances in Applied Probability* 47 (1): 210.

Zhang, Hongzhong, and Olympia Hadjiliadis. 2012. "Drawdowns and the speed of market crash." *Methodology and Computing in Applied Probability* 14 (3): 739.

Zhang, Lan, Per A Mykland, and Yacine Aıt-Sahalia. 2005. "A tale of two time scales: Determining integrated volatility with noisy high-frequency data." *Journal of the American Statistical Association* 100 (472): 1394.

Zhou, Bin. 1996. "High-frequency data and volatility in foreign-exchange rates." *Journal of Business & Economic Statistics* 14 (1): 45.

Curriculum Vitae

Personal information

Name	Vladimir Petrov
Date of Birth	December 27, 1991
Place of Birth	Adygea Republic, Russia

Education

2016 – 2019	PhD Candidate Department of Banking & Finance University of Zurich Zurich, Switzerland
2010 – 2016	Master and Bachelor of Physics Moscow State University Moscow, Russia

Employment

March 2019 –	Financial Methodology Research Lykke Corp. Zurich, Switzerland
2015 – 2016	Researcher Russian Academy of Sciences Moscow, Russia
August 2015 - December 2015	Intern CERN Geneva, Switzerland